Seismic Performance Evaluation of a New Inspectable Hybrid Buckling Restrained Brace

A thesis submitted in fulfilment of the requirements for the degree of

DOCTOR OF PHILOSOPHY

by

PALLAB JYOTI DAS

DEPARTMENT OF CIVIL ENGINEERING
INDIAN INSTITUTE OF TECHNOLOGY GUWAHATI
GUWAHATI-781039, ASSAM, INDIA

APRIL, 2022

Dedicated to my

Parents Pronob Kanta Das, Lina Rani Das

&

Brother Pinak Pani Das

DECLARATION

I hereby declare that the work presented in the thesis entitled "**Seismic Performance Evaluation of a New Inspectable Hybrid Buckling Restrained Braces**" in partial fulfillment of the requirement for the award of the degree of Doctor of Philosophy is the outcome of the research work, performed by myself, else stated, under the guidance of Prof. Sajal Kanti Deb.

Any part of this work has not been submitted for the award of any degree, diploma, associate-fellowship, fellowship or its equivalent to any university or institution.

Pallab Jyoti Das
Registration No. 156104032
Department of Civil engineering
Indian Institute of Technology Guwahati

CERTIFICATE

It is certified that the work contained in the thesis entitled "**Seismic Performance Evaluation of a New Inspectable Hybrid Buckling Restrained Braces**" by Mr. Pallab Jyoti Das (156104032), a student in the Department of Civil Engineering, Indian Institute of Technology Guwahati, India, for the award of the degree of Doctor of Philosophy, has been carried out under my supervision and, that this work has not been submitted elsewhere for the degree.

Date:

Sajal Kanti Deb
Professor
Department of Civil Engineering
Indian Institute of Technology Guwahati
Guwahati-781039, India

ACKNOWLEDGEMENT

I want to grab this opportunity to acknowledge the greatness of all those people who helped and support me to complete this thesis. First of all, I want to thank my supervisor, Prof. Sajal Kanti Deb for giving endless important suggestions and critical reviews of my work through his guidance. His endless reassurance, recommendations and co-operation have been a great motivation for me while carrying out my research work. I will always be grateful to him for the knowledge he conveyed from his enormous experience.

Besides my supervisor, I would like to gratefully acknowledge the doctoral committee members, Prof. Anjan Dutta, Dr. Sandip Das and Prof. Debabrata Chakraborty for their valuable recommendations and insightful remarks throughout the course of research activities, which has constantly engaged me towards undertaking a meaningful thesis work.

I would also like to acknowledge the financial support extended by the Public Works Department (PWD), Arunachal Pradesh Government, for carrying out experimental work reported in this research.

I would like to acknowledge the scientific officer, technical superintendents and support staffs of the Department of Civil Engineering namely, Dr. Arun Ch. Borsaikia, Mr. Biswajit Debnath, Mr. Pranab Hazarika, Mr. Saurabh Mudoi, and Mr. Suresh Boro for their valuable time and help during my experiments. Further, special appreciation for the technician and support staff of Central Instrumentation Facility, IIT Guwahati for extending help and support during material testing.

I am truly grateful to my colleague-turned-friends: Monjusha Sarmah, Tori Basar, Subhra Paul and Gopa Das for their contributions towards my dissertation, be it preparing drafts or assisting me in experiments/simulations. Further, I would like to thank my seniors, Dr. Kamal Jyoti Nath and Dr. Sulaem Musaddiq Laskar for their timely advice and valuable suggestions throughout my research.

My time here is one of my favourite memories. I would like to express my heartfelt gratitude to all of my colleagues in the NDT Laboratory: Lavish, Pranjal, Subhadip, Saroj, Kasturi, Bonisha, Prinza and Arpita, for all of the enriching and valuable discussions. My journey might have been less enjoyable if it had not been for this group. Further, I would like to thank my friends back home: Dipanjan, Sanjay, Saurodip, Sumit, Ananya and Tanushree for their time, advice and moral

support during my Ph.D. journey.

Last but not the least, I owe my gratitude towards my parents Mr. Pronob Kanta Das, Mrs. Lina Rani Das, brother Dr. Pinak Pani Das and sister-in-law Sagarika Paul for being the constant guiding and supporting force throughout my journey.

ABSTRACT

High intensity seismic events have a devastating effect on many of the existing civil engineering structures. Previous researchers have documented the damaged and collapsed states of structures which reflects severity of past earthquakes and the need for research in the area of seismic response control has been emphasized. To meet structural demands in high seismic zones, properly designed lateral load-resisting frame systems are required. The structure must have sufficient strength, stiffness and ductility to withstand significantly high inelastic deformations during large earthquakes. Over the years, steel braces have been employed in framed structures to enhance their strengths and stiffnesses. However, unwanted buckling of these braces under compressive loading led researchers to develop buckling restrained braces (BRB). By restraining lateral displacement of the steel core with the help of restraining mechanism, BRBs achieve comparable load carrying capacities in both tension and compression. It enhances the performance of framed structures by providing significant energy dissipation capacity. As a result, BRBs are commonly used as structural fuses for retrofitting of structures vulnerable to seismic actions as well as for high performance seismic design of new structures. A conventional BRB is composed of an axial load carrying steel core, a debonding layer and a mortar-filled steel restrainer to avoid global buckling.

Conventional BRBs are generally more efficient in dissipating energy at higher strain levels. These are designed to ensure safety of the structural elements against severe earthquakes. Therefore, energy dissipation in BRBs at low core strain level, under frequent low to moderate intensity earthquakes, is generally very low as compared to that at high core strain level. Further, there has been no study to date on the use of restrained buckling of core about the weak axis first and subsequently about the strong axis at higher axial core strain level for enhanced stiffness at higher earthquake intensity. The main objective of this research is to develop a novel inspectable hybrid BRB (HyBRB) which addresses the aforementioned limitations of existing BRBs to increase energy dissipation and to reduce residual displacement in the BRB core at higher strain levels. In this study, experimental investigations have been carried out to evaluate seismic performance of the newly developed inspectable HyBRB under cyclic loading.

The HyBRB with a flat core and highly deformable rubber-like infill layers

in between the core and restrainers, is expected to achieve enhanced energy dissipation capacity in a wide range of axial core strain levels. A simplified design procedure is presented for fabrication of the components of HyBRB. Procedure for estimation of critical loads corresponding to restrained buckling modes of the core is discussed. Total eight HyBRBs are fabricated and tested for their performance assessment. The specimens are classified into two categories: (a) HyBRB-A and (b) HyBRB-B, based on the infill material used for fabrication. HyBRB-A utilizes neoprene rubber, while, HyBRB-B uses butyl rubber as infill layer between the core and the restrainer pair. Each category of HyBRB consists of four specimens with different infill layer geometries. The experimental investigation is carried out with assembled HyBRB specimens connected diagonally to the test setup. The important mechanical characteristics of HyBRBs are evaluated from their hysteretic responses under a horizontal cyclic loading protocol with increasing displacement amplitudes.

The newly developed HyBRB exhibited stable hysteretic behavior with comparable tensile and compressive load carrying capacities under applied loading. All the mechanical parameters of the HyBRB fulfilled necessary design criteria. Formation of higher order restrained buckling modes of the steel core are observed visually at high axial core strains with no sign of damages in the bolted and welded connection. Further, no appreciable lateral deformation in the restrainer is observed. This establishes that the global buckling of the HyBRB is restrained effectively. Further, ease of assembling and disassembling of the restrainer pair facilitates inspection of the HyBRB core for any possible damage and replacement of the same, if needed after an event. The deformed shapes of the HyBRB cores at the end of the cyclic tests and the strain distributions in the restrainer wall and core establish that restrained buckling occurred first about the weak axis and subsequently about the strong axis, at 1.5-2% core strain level. This resulted in enhanced strength and stiffness of the HyBRB and hence increased energy dissipation in low to high level of strain. Further, the measured residual strain in the steel core is found to be in the range of 0.3-0.4% which is quite low as compared to the maximum applied core strain. Thus, HyBRBs with low residual displacement would ensure safety of the non-dissipative structural elements against high intensity seismic events.

Effective stiffness of the HyBRB with continuous butyl rubber infill layers is

found to be slightly higher than that of the HyBRB with continuous neoprene rubber layers. Further, effective stiffness values at low axial strains are found to be higher for specimens with discontinuous infill layers than those of specimens with continuous infill layers. Effective stiffnesses of all the specimens are observed to be in the similar range at higher axial strain levels. HyBRB specimens with continuous infill layers contributed to higher energy dissipation and therefore, have a higher damping factor as compared to those of HyBRBs with discontinuous infill layers. Further, the HyBRB specimens with neoprene infill layers exhibited higher energy dissipation capacities as compared to that of specimens with butyl rubber infill layer of same geometry. It is also observed that the energy dissipation in HyBRB specimens with longer discontinuous infill layers are higher than that in specimens with shorter discontinuous infill layers from each category. All variants of HyBRBs provided higher level (about 20%) of equivalent viscous damping in lower axial core strain levels. Further, equivalent viscous damping values observed for all variants in the higher strain levels is also reasonably high (about 18-22%) for effective seismic response control of structural system.

Phenomenological models like, Bouc-Wen hysteresis model, are often used for simulation of hysteretic behavior of various types of structural elements. An extended Bouc-Wen model, known as Bouc-Wen-Baber-Noori (BWBN) model, is used in this study to analytically simulate the force-displacement response of the tested HyBRB specimens. The model parameters are adjusted to match the output of the model by minimizing the error between the input and output data. Analytically simulated hysteretic behaviour of the HyBRBs are found to be in close agreement with that recorded during the experimental investigation. The effective stiffness and damping parameters calculated from simulated hysteresis loops are compared with these parameters obtained from experiments. The errors computed for the above mentioned parameters are found to be in between 0.6 to 8.9%.

Numerical investigation is carried out to evaluate the efficacy of HyBRB in reducing seismic vulnerability of a building with asymmetry in elevation. Nonlinear static and dynamic analyses of a sample soft-story building (G+3), located in zone V of the seismic hazard map of India, is carried out using SAP2000 v21.0.2 (2019). The same building is then considered for seismic retrofitting using HyBRBs, developed in the current study. The required core specifications for retrofitting the

sample building are computed using a displacement based design approach. Results of nonlinear static analysis showed that the retrofitted building exhibited higher capacity as compared to that of the original soft-story building, when subjected to monotonic lateral loading. Overall strength and stiffness of the building improved after retrofitting using HyBRBs. The hinge distributions in the structural elements of the original soft-story building were limited to the ground story level while hinges were widely distributed along the height in case of the retrofitted building. Thus, problem related to soft story mechanism is effectively mitigated.

Nonlinear time history analysis of the sample building is performed under eighty prescribed ground motions with varying characteristics. Performance levels or damage states are defined in terms of inter-story drift ratios. Probability of failure corresponding to these damage states for different PGA values of prescribed ground motions are computed and analytical fragility functions are plotted for both the original soft-story and the retrofitted buildings. Installation of HyBRBs reduced the inter-story drift ratios in the retrofitted building than that observed in the original building, which in turn reduced the probability of exceedance of the damage states of the sample building. Hence, the seismic vulnerability of the soft-story building is effectively mitigated by installing HyBRBs at suitable locations. Thus, it can be concluded that the newly developed HyBRB would provide a simple yet efficient energy dissipation device for seismic response control of structures.

Contents

List of Figures

List of Tables

Chapter 1

Introduction

Contents

1.1 General

Structural engineers are often tasked with the responsibility of designing structures ensuring the structural integrity and safety of the structures. Structures such as residential buildings, bridges and other civil engineering projects are particularly vulnerable to high intensity seismic excitations. Previous researchers have recorded the damaged and collapsed states of civil engineering structures as shown in Fig 1.1, which reflects severity of the earthquakes. Several types of structural control devices are being developed around the world to protect the structures and their components from the devastation caused by seismic activities. These techniques have been successfully used to keep internal forces, displacements, and residual deformations of the structures within allowable limits using response control devices. As a result, a new field of research on structural control systems has been proposed. One of the most commonly adopted approaches for ensuring the structural safety of buildings against seismic activity is to attenuate the input energy with the use of structural elements. Some of these techniques for ensuring safety against seismic events include isolating the building from the base or installing seismic energy dissipation devices at suitable locations throughout the building structure. These strategies ensure higher performance of structures during high intensity seismic events.

(a) (b)

Figure 1.1: Devastating effects on buildings due to (a) Bhuj Earthquake, 2001 and (b) Nepal Earthquake, 2015. *photo courtesy : Solomon and Haynes (2018); Jones (2015)*

1.2 Seismic Control Systems

Structural response control under seismic events is a rapidly expanding field in earthquake engineering. Seismic responses of a building can be controlled by modifying the mechanism of mobilizing restoring force when affected by seismic forces and damping of the building (Torunbalci, 2004). Responses of the structure subjected to seismic excitation can be controlled, by changing its mechanical characteristics like stiffness and damping. When stiffness of the building is decreased, the response acceleration also decreases and the displacement increases. On the other hand, response of acceleration and displacement can be decreased, by increasing the damping of the building.

There has been an increase in research and development activities in the field of structural control since 1980. It was discovered that one of the most effective ways of protecting structures against earthquake forces is to use structural control systems. Structural control systems have been used in many buildings, bridges and industrial plants in earthquake prone regions of the world. Various kinds of seismic control devices or dampers can be installed in the structures, individually or in combination. There are several devices that have been developed in order to retrofit the existing structures including historical buildings.

For the retrofitting purpose, different kinds of control systems are used in structures depending on their requirements. The family of control systems consists of active, passive and hybrid systems. Following sections briefly describe different types of commonly used seismic control systems and their working principles.

1.3 Classification of Seismic Control Systems

Seismic control systems are primarily classified as active, passive and hybrid control systems, as shown in Figure 1.2, based on their operation principles. Active control systems are typically activated by an external power source on receiving an analog signal. Passive systems control seismic responses by modifying the mechanical characteristics of structures using pre-installed devices. Hybrid control systems work combining both the active and passive systems. Working principles of different types of control systems are discussed in details in the following sub-sections.

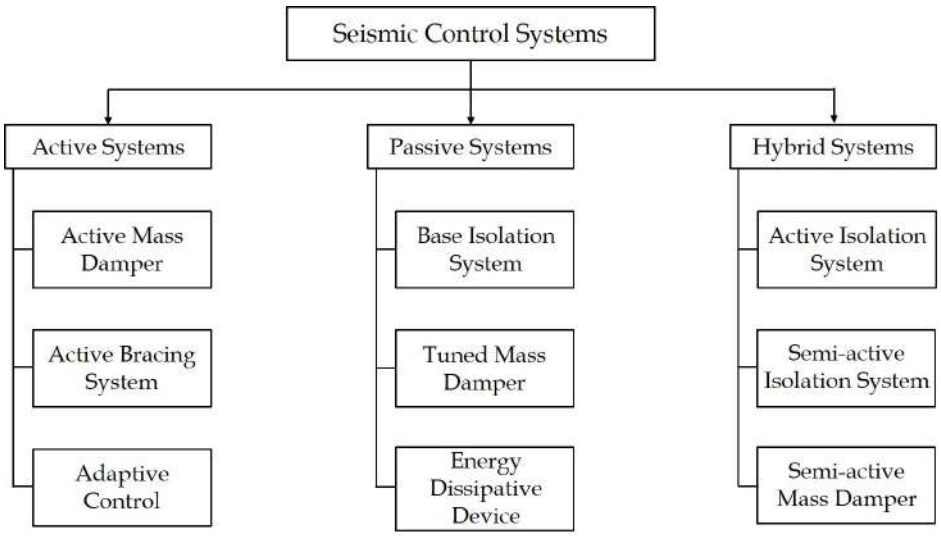

Figure 1.2: Classification of seismic control systems

1.3.1 Active Control Systems

Active control system use external energy sources to activate the control operation by providing analog signals to it. The system operates on a control algorithm which uses measured responses of structures (Datta, 2010). Active system can control the acceleration, displacement or velocity of structures. Based on the intensity of earthquake, active systems can adjust their rigidity and relative motion nearly in real time in order to control the seismic response, as shown in Fig 1.3. For the whole control operation, active systems depend on computer control, motion sensors, feedback mechanism and moving parts which again require routine maintenance. Also, active control systems need an emergency power source ensuring its uninterrupted operation during earthquakes and any immediate aftershocks. Hence, the installation and maintenance cost of these systems are high.

1.3.2 Passive Control Systems

Passive control systems are more simple and effective for practical implementations. These systems operate without any external energy source. Passive control devices are activated by ground motions of a certain threshold intensity measure and are capable of controlling the response of the structure under the external ground motion, as shown in Fig 1.4. These systems are proved to be cost effective as compared to the active systems.

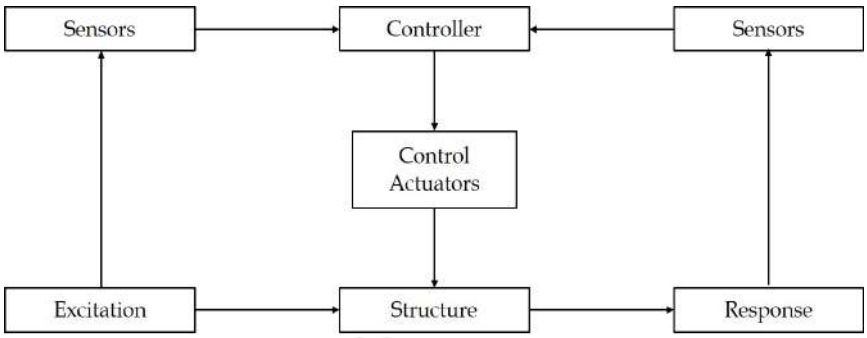

Figure 1.3: Schematic diagram of working principle of active control system (Soong and Spencer Jr, 2002)

Passive systems are designed in accordance to level of protection required up to earthquakes of certain intensity measures. These systems utilize a wide range of materials and devices for enhancing damping, stiffness and strength, and can be used for retrofitting of damaged structures (Constantinou et al., 1998, Soong and Dargush, 1999). These devices generally operate on principles such as frictional sliding, yielding of metals, phase transformation in metals, deformation of viscoelastic (VE) solids or fluids and fluid orificing (Soong and Spencer Jr, 2002).

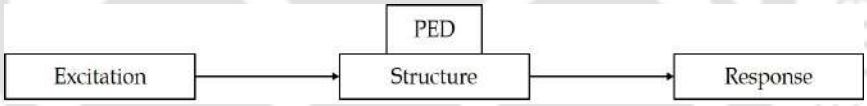

Figure 1.4: Schematic diagram of working principle of passive control systems (Soong and Spencer Jr, 2002)

1.3.3 Hybrid Control Systems

Hybrid seismic control system is a combined system, utilizing advantages of both the passive and active control systems, as shown in Fig 1.5. These systems have reduced power demands, improved reliability and reduced cost when compared to fully active systems. Passive systems absorbs a portion of energy of an earthquake resulting in lower demands in active control systems and thereby reducing the requirement of power resources. However, these devices are costlier than passive control devices.

Compared to passive systems, active control systems are advantageous because of its (a) enhanced effectiveness in response control, (b) relative insensitivity to

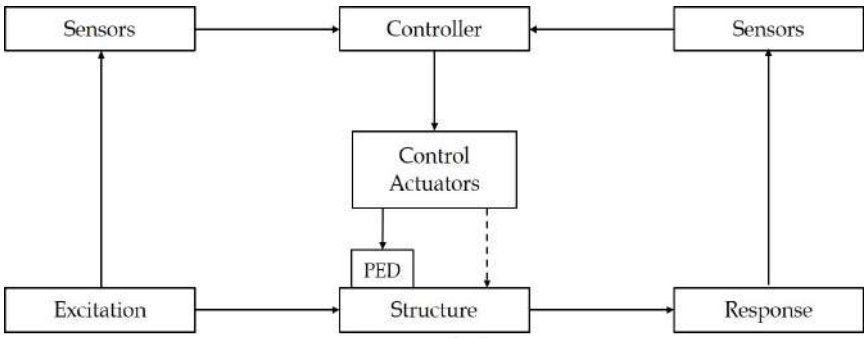

Figure 1.5: Schematic diagram of working principle of hybrid control systems (Soong and Spencer Jr, 2002)

site conditions and ground motions, (c) application in multi-hazard mitigation situations and (d) options in selection of control objectives. However, main drawback of active systems is its requirement of continuous power supply, which makes these systems costlier. Passive systems, on the other hand, are more effective in practical applications. These devices are easy to install, cost effective and prevent occurrence of damage in structures efficiently.

1.4 Braced Frames

Braced frames are structured frame systems which include an additional diagonal steel brace, generally connected through pins at both ends. The beams and columns are designed for vertical load only, assuming the brace carries all lateral loads acting on the frame during seismic activities. These braces are designed to carry the axial loads only, like a truss element. There are two main varieties of braced frames: (a) concentrically braced frame (CBF) and eccentrically braced frame (EBF).

CBFs generally consist of diagonal braces connected in the plane of the frame with both ends of the brace joined at the end points of other frame members (beams and columns). Thus, the center lines of each member at a joint intersects at a single point. Steel braces in CBFs can be arranged in several different configurations such as X, K, chevron or diagonal bracing, as shown in Fig 1.6. The brace members may be designed to act in tension or compression or both, based on requirements. CBFs have traditionally been viewed as high-strength, low-ductile systems. The braces in CBFs have more chances of failure due to buckling when

subjected to large compressive loads.

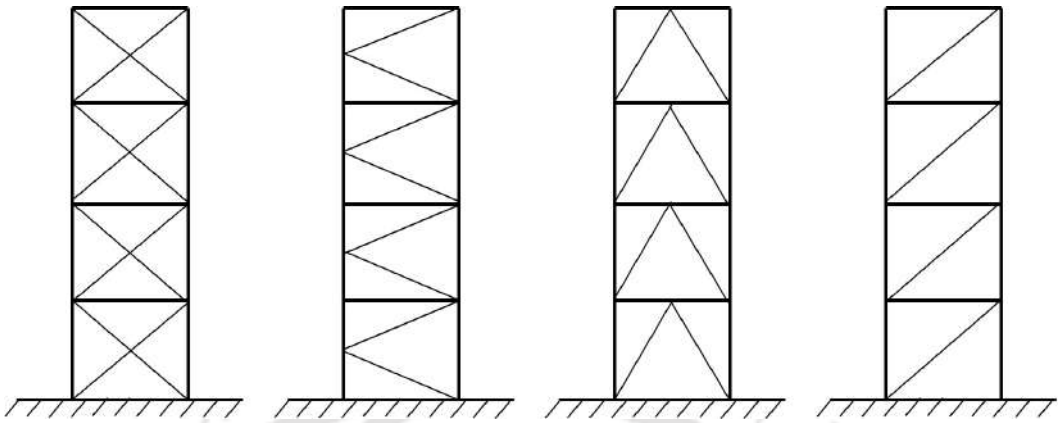

Figure 1.6: Schematic configuration of braces in CBFs

EBFs are lateral load-resisting systems which combine the advantages of conventional moment resisting frames (MRF) and CBFs, while minimizing their respective disadvantages. In EBFs, one end of each brace is connected to the end points of beams/columns or to the joints. Figure 1.7 illustrates several common EBF arrangements, where 'e' denotes eccentricity of the braces. The bracing members in EBFs provide high elastic stiffness, allowing the codal drift requirements. Further, properly designed and detailed EBFs provide enhanced ductility and energy dissipation capacity under severe earthquake loading. Thus, excellent performance EBFs is observed under severe seismic actions. However, significant vertical residual deformation and formation of plastic hinges in the beam link elements increase the chances of failure of EBFs.

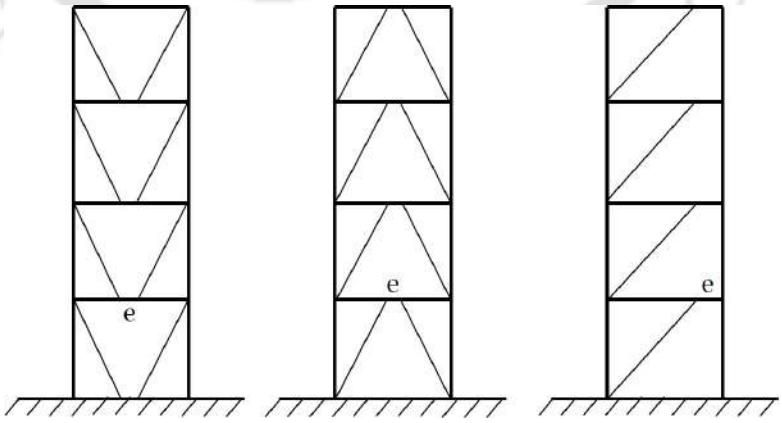

Figure 1.7: Schematic configuration of braces in EBFs

1.5 Buckling Restrained Braced Frame

Concentric and eccentric type of braces have been successfully used in frames over the years to minimize the effect of earthquake and wind forces. However, these braces experience buckling failure under large compressive forces, which induces unsymmetrical hysteretic behavior in tension and compression. Also, these braces exhibit substantial strength deterioration when subjected to compressive loading. To overcome the problems of these braces, buckling restrained braces (BRBs) were developed in 1980s. BRBFs are a special kind of CBFs in which buckling of brace core element is restrained by encasing it with concrete/cement mortar filled steel tube and thus, stable hysteretic behaviour under cyclic loading is achieved, as shown in Fig 1.8. By restraining the buckling of brace system, flexural strength and stiffness can be increased significantly, which, in turn helps the structural system to undergo large deformations (Xie, 2005).

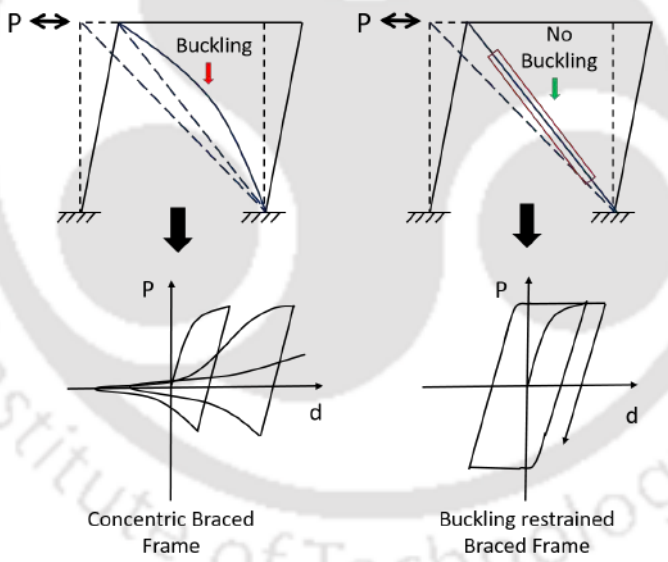

Figure 1.8: Hysteretic behaviour of concentric braced frame and buckling restrained braced frame

In the last few decades, BRBFs have become increasingly popular especially in Japan, Taiwan and the US for their remarkable performance in controlling the seismic response of structures. BRB was invented in the early 1980s and tested in the mid 1980s. It was first used in Japan in the 1990s.

1.6 Buckling Restrained Braces

Buckling restrained brace (BRB) is the type of passive energy dissipating device that combines the benefits of both ordinary braces and metal dampers in a single device. Unlike conventional steel braces, BRBs perform much better by preventing global buckling under compressive loading. This also enables them to attain stable hysteretic behaviour with comparable tension and compression capacities. In this process, BRBs inherently impart significant stiffness and strength to the structures. BRBs are composed of three basic components: (i) an axial load carrying steel core plate, (ii) a steel casing filled with mortar or concrete, together acting as a restrainer and (iii) a debonding agent or a gap between the core plate and restrainer, as shown in Fig 1.9. Desired attributes of an ideal BRB are:

- stable hysteretic behaviour and high energy absorption capacity,
- large deformation capacity,
- high ductility,
- high low-cycle fatigue property,
- simple and low cost of fabrication, construction and installation,
- ease of replacement or no need of replacement during service life.

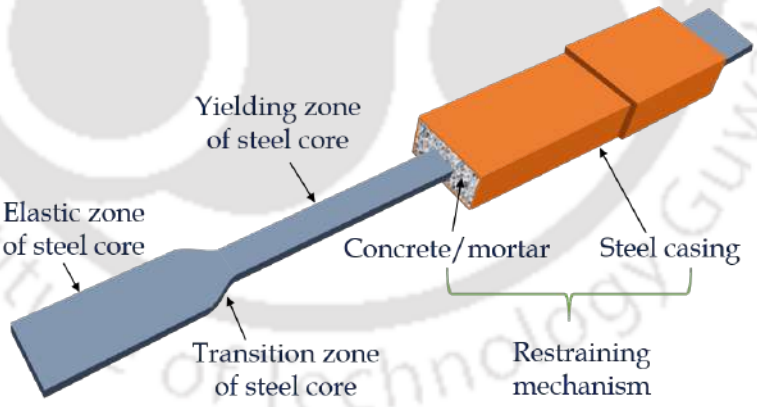

Figure 1.9: Typical view of a BRB device showing its main features

1.6.1 Classification of BRB

Conventional BRBs are categorized into two types based on the restraining mechanism, adopted for prevention of global buckling of steel core. These are: (a)

unbonded BRB, where global buckling of the core is restrained with concrete or mortar filled steel tube and (b) all-steel BRB, which consists of a steel core surrounded by built-up/stiffened steel sections acting as a buckling restraining mechanism. In each type of conventional BRBs, a debonding material layer or an air gap is provided to ensure that incoming axial load is carried by the core only and no part of it is transferred to the restraining mechanism. Debonding layers used in BRBs are usually thin sheets of resin, epoxy, vinyl tapes or similar material. The schematic diagrams of both types of conventional BRB cross-sections are shown in Fig 1.10.

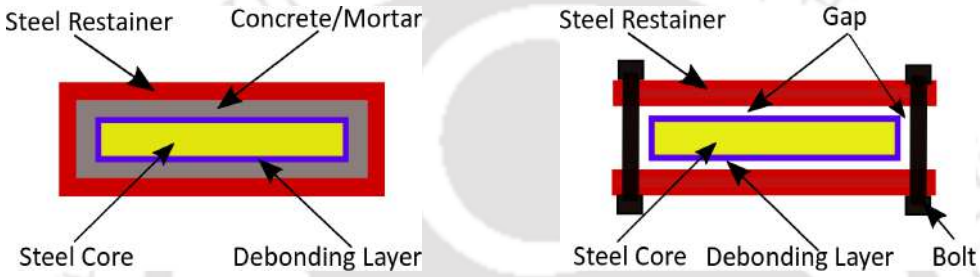

Figure 1.10: Schematic cross-sections of: (a) unbonded BRB, (b) all steel BRB

Due to the presence of concrete/mortar, unbonded BRBs are heavier and their fabrication time is longer. However, fabrication time is much shorter in all-steel BRBs, as no concreting is involved. Also, all-steel BRBs are lighter in weight which leads to convenient assembling, transportation and installation as compared to that of unbonded BRBs. In recent past, few studies investigated performance of hybrid BRBs with two different core materials made of high performance steel and low yield point steels. The following chapter briefly discusses various types of BRBs developed over the years.

In the present study, experimental evaluation of an inspectable hybrid BRB consisting of an all-steel BRB with rubber-like infill layers, placed between core and restrainer, would be carried out. This new BRB is designated as HyBRB. Generally, BRBs are efficient in energy dissipation in higher core strain levels. Addition of the infill material facilitates additional energy dissipation in lower strain levels. Therefore, HyBRB would be more effective for seismic response control because of its ability to dissipate energy in wide range of axial core strain levels.

1.6.2 BRB Connections

The connection of the braces to the beam-column joints is usually executed using gusset plates. Ends of a BRB can be connected to gusset plate in a beam-column joint through- (a) pinned connection, (b) welded connection and (c) bolted connection, as shown in Fig 1.11.

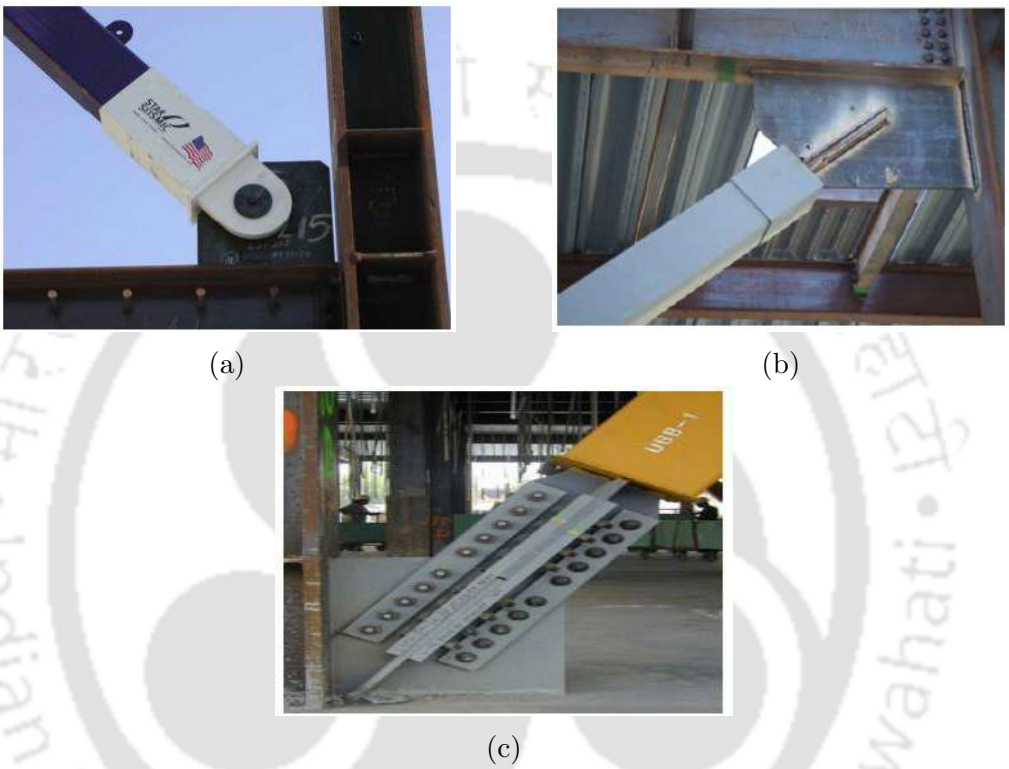

Figure 1.11: Different type of BRB connection; (a) pinned connection, (b) welded connection and (c) bolted connection

1.7 Objective of the Study

Based on the review of literature and gap area identified, following research objectives are finalized for the present study:

- To develop a new hybrid BRB (HyBRB) with stable hysteresis behaviour under cyclic loading and potential for residual displacement reduction.
- To propose a simplified design procedure for the newly developed HyBRB for enhanced energy dissipation in low to high range of axial strain levels.

- To design the restraining mechanism of the HyBRB for facilitating restrained buckling of the core about its both weak and strong axes, in succession.

- To evaluate the mechanical characteristics of HyBRB variants with different rubber-like infill materials through experimental investigation.

- To compare the performances of HyBRBs with continuous and discontinuous infill layers.

- To develop analytical model for simulation of axial force-displacement hysteretic behaviour of the HyBRBs.

- To carry out vulnerability assessment of a sample soft-story building before and after retrofitting with the newly developed HyBRBs.

1.8 Scope of the Study

The specific tasks undertaken to achieve the above mentioned objectives are as follows:

- A simplified step-by-step procedure for design of an inspectable HyBRB, modifying the existing design procedure for conventional BRBs, has been proposed.

- The lateral loads, corresponding to higher order buckling modes of the steel core, are analytically computed for appropriate design of restraining mechanism and connections.

- A reusable restrainer pair in the form of stiffened steel plates, connected by a series of bolts, is designed for effective restraint against global buckling. Different components of HyBRBs, which include restrainer pair, steel core and two rubber infill layers sandwiched between core and restrainers, are assembled together using connecting bolts. Provision of rubber infill layer allows limited deformation in both lateral and transverse directions to facilitate restrained buckling of the steel core about both weak and strong axes, in succession.

- HyBRB specimens with neoprene or butyl rubber infill layers of thickness 3 mm and different lengths are fabricated for evaluation of their mechanical characteristics. Different HyBRB variants with continuous infill layers of length 1000 mm (equal to yielding region length of BRB core) and discontinuous infill layers of length either 120 mm or 50 mm are considered.

- A new test-assembly is fabricated to conduct experimental investigation on force-displacement hysteretic behaviour of six HyBRB variants. The test specimen is diagonally connected to the test-assembly with its one end to a vertical element at top and other end to the strong floor at bottom. Thereafter, a horizontal displacement protocol is applied to the test-assembly using a servo-hydraulic actuator for performance evaluation of HyBRBs.

- Key performance parameters of tested HyBRB specimens are computed from the force-displacement hysteresis loops under applied displacement protocol. The evaluated performance parameters of the HyBRB specimens include compressive and tensile strength adjustment factors, effective axial stiffness and damping parameters. Further, strain values in the core and restrainer pair are measured for assessment of extent of damage and restrained local buckling formation of the core during applied displacement protocol.

- The hysteretic behaviour of the HyBRB specimens is analytically simulated using an extended Bouc-Wen model. A multi-objective optimization technique is used to identify the parameters of analytical model, which minimizes the difference between the output of the simulated model and the experimental force-displacement response.

- Effectiveness of newly developed HyBRB in reduction of seismic vulnerability of a sample soft-story building is evaluated by nonlinear static and dynamic analyses using SAP2000 v21. Seismic vulnerabilities of the sample building with and without HyBRB are compared using seismic fragility curves obtained considering eighty ground motion records with different characteristics.

1.9 Outline of the Thesis

In this thesis, a new HyBRB with different infill layer geometries is developed for enhanced load carrying and energy dissipation capacity. Detailed experimental investigation of model HyBRB is performed for evaluation of seismic performance. Analytical models for simulation of force-displacement hysteretic behaviour of tested HyBRBs are identified. Vulnerability assessment of a mid-rise soft-story building with and without retrofitting using HyBRBs is carried.

In Chapter 1, general description of several types of seismic control systems, different types of bracing systems and a brief introduction on buckling restrained braces are presented.

Chapter 2 provides a brief review on various types of BRBs developed over the years. Experimental and numerical investigations, stability issues as reported in different literature are also presented. Literature on vulnerability assessment of soft story buildings and application of BRB in various fields of civil engineering are also included in this chapter.

Chapter 3 reports the concept, working principle, design procedure and designations of proposed HyBRBs.

Chapter 4 presents a part of the experimental investigation carried out for performance evaluation of HyBRB specimens with continuous infill layers followed by critical analysis of the test results and behaviour of the test specimens under the applied loading protocol.

Chapter 5 presents a part of the experimental investigation on HyBRB specimens with different discontinuous infill geometries followed by critical analysis of the test results. Further, a comparative study on the performances of different variants of HyBRB is presented in this chapter.

Chapter 6 reports the identification of representative analytical models for simulation of the experimentally obtained force-displacement hysteretic behaviour of the tested HyBRB specimens.

Chapter 7 discusses the vulnerability reduction in a soft-story building retrofitted with a series of appropriately designed HyBRBs.

Chapter 8 reports a detailed summary on the development, design, experimental and numerical investigations on HyBRBs for their seismic performance evaluation. Major conclusions drawn based on the current research are reported. Finally, the future scopes to enhance the performance of the HyBRB device, developed in the present study, are outlined.

Chapter 2

Literature Review

Contents

2.1 General

The safety of structures against seismic events has always been a source of concern. The damages caused to the structures and their components by seismic energy are well documented in earthquake studies or reports. Different techniques, e.g., retrofitting of structural components, reduction of demand etc., are adopted by the researchers to reduce the vulnerability of such structures. Various structural control systems are designed to reduce the damages in structures caused by seismic events by controlling their responses. These systems are observed to be very effective and easy to implement as no special skill is required for installation. Among various control systems, use of passive energy dissipating devices are found to be advantageous due to non-requirement of power supply for initiation of the device. Initially, diagonal steel braces, similar to link elements, were used to provide additional strength and stiffness to the structures. By adding stiffness to the structure, these braces partially contributed in reducing the damages. They performed very well in tension, but collapsed due to buckling under compressive loading, resulting in a unstable structure. Researchers inserted steel braces within concrete/mortar panels in order to prevent the global buckling failure of the braces under compressive loading (Wakabayashi et al., 1973a; Watanabe et al., 1988; Mochizuki et al., 1979, 1980). In the early 80's, a group of Japanese researchers devised a new type of bracing where the steel brace was inserted into a mortar-filled steel tube to prevent buckling. This buckling restraining capability of the new brace enhanced its flexural stiffness capacity and thus, its performance under cyclic/seismic actions also improved. Further research revealed that the load carrying capacity in compression could be enhanced significantly by controlling the buckling of braces and the same would be nearly equal to that in tension. These properties made a buckling restrained brace (BRB) significantly superior as compared to other braces.

A detailed review on evolution of BRB and its recent advancements, various design aspects, experimental studies, parametric studies for performance enhancement of BRB and assessment of seismic vulnerability of structures equipped with BRBs are described in the following sections.

2.2 Early Developments

Yoshino and Karino (1971) were the first investigators to conduct researches on buckling prevention of steel braces. They conducted experimental study on two shear wall specimens with brace inside them, under a series of cyclical loading. The braces were made of flat steel plates which were then encased in reinforced concrete panels with debonding materials sandwiched in the spaces between the plates. One panel had a 15 mm clearance between its lateral sides and its surrounding panel, while the other did not have any clearance. It was reported that the panel with clearance on its sides had a greater deformation and energy dissipation capacity than the other one.

Wakabayashi et al. (1973a,b) made significant contributions in the development of BRB system similar to that of the shear wall with braces. Flat steel plates were encased in reinforced concrete panels with a debonding layer sandwiched between them, as shown in Fig 2.1. In order to ensure proper debonding effect in between the components of brace-panel system for axial load transfer to the brace, various debonding materials, such as epoxy resin, silicon resin, vinyl tapes, and other similar materials were investigated. Silicon resin layer on top of an epoxy resin layer was found to be most efficient debonding agent and was applied in the successive tests. It was observed that compared to bonded braces, the unbonded braces exhibited higher load carrying capacity.

Kimura et al. (1976) conducted tests on newly developed relatively compact buckling restrained brace, using steel braces encased in a mortar-filled square steel pipe with no debonding material or gap between the mortar and core braces. It was reported that mortar filled tube significantly improved the buckling restraining mechanism and hence the hysteretic behaviour of the BRB. However, a significant permanent void was developed during the compression cycle which allowed local buckling during successive compressive loading.

Subsequently, Takeda and Kimura (1979) developed four full-scale BRB specimens for their performance evaluation, out of which two had a small gap between the braces and the surrounding mortar. It was reported that all specimens exhibited good hysteretic behaviour. A guideline was also prescribed for designing the outer restraining tube to avoid global buckling.

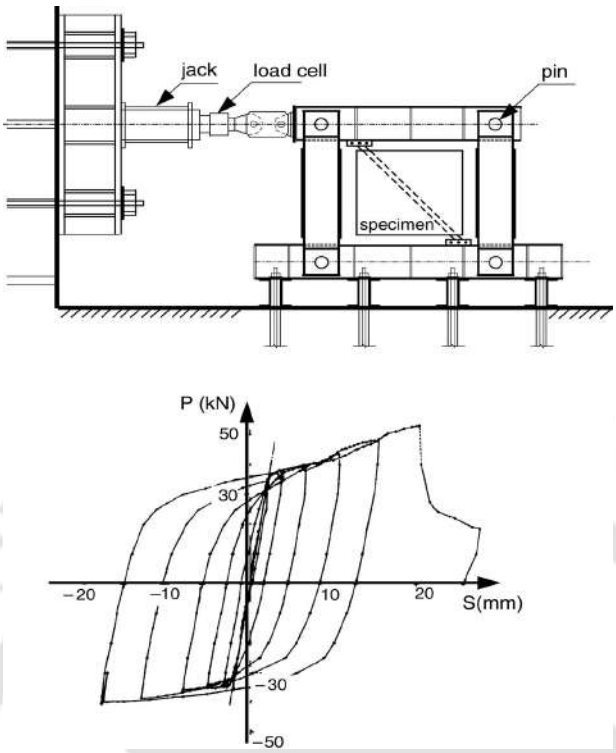

Figure 2.1: Test setup and its hysteretic behavior for brace-panel system (Wakabayashi et al., 1973a)

2.3 Unbonded BRB

In early 1980's, researchers in Japan refined the concept of encasing the steel core within a restraining member in order to improve the performance of the device, which eventually resulted in the development of what is now known as the unbonded BRB. In Japan, the unbonded BRB has been used extensively in buildings utilizing it as a structural fuse or damper.

Mochizuki et al. (1979, 1980) developed unbonded braces which included a shock absorbing material as a infill layer between the confined concrete and the steel core. It was reported that the surrounding concrete cracked as a result of repetitive loading and the buckling restraining effect of the concrete diminished. In order to address this problem, a coefficient factor was included that represented the stiffness degradation of a concrete panel after it had cracked.

Similar studies were conducted on BRBs by other researchers with variations in the restrainer, the steel core and debonding material arrangements. Fujimoto

et al. (1988) developed a new BRB suitable for practical implementation. In order to achieve stable and symmetric behaviour, they used rectangular steel tubes infilled with mortar as the restrainer. In their study, the optimal debonding material specifications to use were also finalized. Further, fundamental theory for designing the restrainer was proposed and thereafter, the first practical application of unbonded BRB in civil structures was carried out.

Watanabe et al. (1988) developed a brace with stable force deflection characteristics, with comparable compressive strength and tensile strength. The load carrying central core was a cross-shaped steel component which was exposed at its both ends and enclosed in a steel tube in the central zone. A layer of coating was used on the surface of core to prevent friction. Further, 3 mm thick layer of polystyrol was used on both sides of the core to fill the void between the core and the concrete in the thickness direction and 3 mm thick vinyl tape was used in the width direction of the steel core. It was reported that the braces exhibited stable hysteresis if the applied axial stress on the steel core was less than the Euler buckling load of the steel tube that surrounded it.

Lai and Tsai (2001) carried out similar study to investigate the unbonding efficiency of debonding materials in BRBs used between the core and the surrounding buckling restrainer. It was reported that the 2 mm thick silicon rubber sheets were most effective in minimizing the difference between peak compressive and tensile axial capacities of BRBs when subjected to cyclic displacement protocol.

Generally it is found that BRBs were connected through gusset connections. This type of connections were made either by welding or bolting the BRB to the gusset plate, which usually increases the connection length. Huang and Tsai (2002) developed double core BRB (DCBRB) to reduce the length and no. of bolts in brace-gusset connection in BRB connected frames. The importance of design parameters in DCBRB like cross-sectional area of core, connection region length, effective stiffness etc. were investigated.

Subsequently, Tsai et al. (2004) performed three full scale V-shapes BRBF testing with the DCBRBs having 2 mm thick unbonding layers of silicon rubber. The core strain demands were satisfactorily predicted from the story drift demand. It was reported that at large story drift, the tensile strain in the BRB was always higher than the compressive strain.

Nishimoto et al. (2004) successfully conducted sub-assembly testing of large

BRBs. Investigation on design parameters like yield strength and BRB length of the unbonded BRBs were carried out. Maximum compressive to tensile force ratio was found conforming with prescribed AISC recommendations. It was observed that the upper end of longer braces experienced much higher rotation than the lower end. Rotation was insignificant in case of shorter BRBs at both ends. Moreover, results of low cycle fatigue test showed that at higher story drift shorter BRB lost strength earlier than longer one.

The excellent hysteretic behaviour and ductility capacity of component BRBs was well defined from many researches. But their behaviour and ability to achieve full ductile capacity when connected to a frame was not verified. Earlier, large scale BRB frame (BRBF) tests demonstrated only the failure modes but did not fully exploit the ductility capacities of the BRBs. A comprehensive experimental study on unbonded BRBs were performed by Black et al. (2004) to investigate the inelastic capacity of BRBs under severe seismic activities. Five specimens with varied core geometries were adopted, out of which two had rectangular steel cores and other three had cruciform steel cores. It was reported that the plastic torsional buckling was the most critical failure mode, for the adopted configuration of BRBs.

A brief summary about the development of BRBs in Asia was reported by Xie (2005). Conventional braces show asymmetric hysteretic behaviour in tension and compression and buckles under high compressive loading. Restraining the buckling of brace ensures stables hysteretic behavior and nearly same strength both in compression and tension. A detailed discussion on the history of development of BRBs can be found in the summary presented by Xie (2005). Different BRB core configurations adopted in earlier researches and their restraining mechanism, as shown in Fig 2.2, for preventing the global buckling of BRBs were also discussed. A comparative study was presented on some key issues in a BRB design procedure. Further, criterion for overall buckling of BRB was also presented.

Fahnestock et al. (2007) conducted a comprehensive experimental study on BRBs to evaluate their elastic stiffness and ductility. Elastic axial stiffness values of BRBs were almost equal to the theoretical value. Further, maximum story drifts, residual deformations and BRB overstrength demand for design basis earthquake (DBE), maximum considered earthquake (MCE) and aftershock earthquake were evaluated. It was observed that all BRBs exhibited excellent ductility capac-

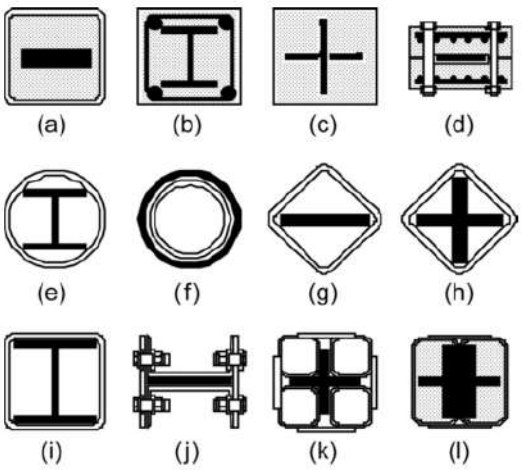

Figure 2.2: Different core configurations and restrainer arrangements adopted for unbonded and all-steel BRBs (Xie, 2005)

ities without losing significant amount of strength and stiffness.

Lin et al. (2012) developed two types of full scale BRBs which included thin BRBs and end-slotted BRBs with welded end connections. The thin BRBs can reduce the building partition wall thickness and increase usable floor space, while, the welded BRB end connection details result in a more compact joint than the bolted joint. Thus, the proposed thin BRB permitted use of longer yielding region of the BRB core and contributed in enhanced fatigue life. The provision of end-slots gave more ease of movement of end stiffeners at both ends of the BRB core.

Guo et al. (2015) developed a new light weight BRB and designated the same as core separated BRB (CSBRB). This BRB consisted of two separate conventional single core BRBs. The individual BRBs were combined together by one or several longitudinal web plates. The CSBRB had high load carrying capacity and also had the provision of using two individual BRBs separately, if required. Use of two core plates separated by longitudinal web plates ensured enhanced bending stiffness. Provision of adjusting the web plate height in CSBRB would further enhance its performance in a controlled manner.

Pandikkadavath and Sahoo (2016) conducted experimental investigation on reduced length BRB (RLBRB) to evaluate their hysteretic and overall performance under gradually increased cyclic loading. To inspect post-earthquake impact in yielding core, detachable encasing members were used providing a clearance between the core and restrained unit. Slow-cyclic loading test was conducted on

RLBRBs with varied core geometries. It was observed that RLBRBs exhibited excellent hysteretic response and energy dissipation with a maximum ductility of 30.

Lin et al. (2016) proposed a thin BRB to prevent local buckling failures. The thin configuration of the core reduced the width of the restraining member and thus reduced the overall size of BRB. Deformable debonding layers provided space for the steel core to form higher mode buckling waves. It was reported that the outward force was directly proportional to the debonding layer thickness and inversely proportional to higher mode buckling wavelength of the core plate. Also, the capacity of the restraining member in resisting the outward forces was estimated using upper bound theory of plastic analysis.

Bai and Ou (2016) used performance based plastic design method in earthquake resistant design of BRB-RC moment frames. Tri-linear force-displacement relationship of the dual system (RC-BRBF) was approximated as bilinear to obtain the yield displacement analytically. A design procedure of the RC-BRBF dual system was developed to account for the energy dissipation capacity and inelastic behavior under severe ground motion. RC frames with BRBs in chevron configuration were tested and effectiveness of the developed approach were validated through non-linear static pushover analysis and time history analysis.

Maurya et al. (2016) developed a miniature BRB (MBRB) which was similar to an ordinary BRB with a yield core plate and a restraining member filled with grout but had shorter length, smaller steel core dimensions and lower yielding capacity than an ordinary BRB. Field of application, design and detailing of MBRBs were presented in this study. Cyclic testing of the MBRB was carried out in this test program varying geometric parameters of the core plate. The stability criteria to prevent the failure of MBRB ends was also presented. Finally, a set of recommendations was presented for the design of proposed MBRB.

2.4 All-steel BRB

Problems in conventional BRBs, in form of higher self-weight, longer time for fabrication and quality control, transportation and installation issues, made many researchers to think about other types of BRBs like all-steel BRBs. All-steel BRBs were lighter than unbonded BRBs and their fabrication and assembling process

were much faster.

In case of all-steel BRBs, it was expected that the adhesion between the steel core and the restraining members would be negligible. The space required for the expansion of the core plate could be provided by controlling the gap between the core and the restraining members in all-steel BRBs. Iwata (2004) tested all-steel BRBs without the debonding materials. It was observed that the BRBs fractured as a result of the continuous progression the plastic deformation.

Later, Tremblay et al. (2006) compared the performance of the conventional BRBs to all-steel BRBs without the debonding materials and reported that debonding material was necessary to minimize the friction for developing uniform strain in the core plate.

Chou and Chen (2010) developed a detachable BRB, which could be easily disassembled by removing bolts and the damaged core sandwiched between restrainers can be replaced easily. The arrangement to disassemble the BRB and inspect it for possible damage provided the device an additional advantage over unbonded braces. Stable hysteresis behaviour was achieved for the proposed BRBs with peak compressive load of about 1.4 to 1.6 times the yield load. Cumulative plastic ductility (CPD) was observed to be much higher than that recommended in AISC seismic provisions.

Zhao et al. (2011) developed an angle steel BRB (ABRB) fabricated combining four steel angles to form a non-welded cruciform shaped core restrained in a steel tube made of two steel angles. Ends of the core were stiffened with the help of 8 welded stiffening plates to ensure elastic behaviour of the end regions. Choice of this kind of restrainer gave more design flexibility, less welding and higher moment of inertia. ABRBs developed in this study exhibited stable hysteretic behaviour with enhanced ductility capacity.

It was observed that the ductility and core strain level could not be attained the maximum limit in unbonded BRBs. To overcome these shortcomings of BRB, Tabatabaei et al. (2014) developed reduced length buckling restrained braces (RLBRB) which were lighter, economical and easily detachable. The RLBRB consisted of a shorter length core plate, encased in restrainer, with an elastic zone at both ends. It was designed to undergo axial yielding without any buckling while the RLBRB was working. Adopted core plate area of RLBRB was more than that of regular BRBs so that its yielding capacity and stiffness did not get affected

because of its short length.

One of the main disadvantage observed all-steel BRBs was longer connection region due to bolted/pinned joints. Tsai et al. (2014) experimentally investigated effect of welded connection and debonding mechanism on the performance of BRBs. It was reported that chloroprene rubber performed better than the other debonding materials. Further, experimental investigations were carried out on welded end-slot BRBs (WES-BRB) with chloroprene debonding material. The specimens sustained a cumulative plastic deformation of greater than 400 times the yield deformation.

In the subsequent research, Chuang et al. (2015) presented a procedure for design of WES-BRB and its connections to steel frames. 581 WES-BRB frame design cases were used to investigate the critical limit states for the proposed procedures. It was reported that a steel frame equipped with a WES-BRB could offer a cost effective solution for earthquake resistant design of steel buildings by controlling inter-story drift. A cloud service was also developed that enables anyone to design WES-BRBs and their connections.

Piedrafita et al. (2015) developed a new type of BRB called perforated core buckling restrained braces (PCBRB) for seismic design of buildings. PCBRB consisted of a perforated yielding steel core plate which was partially restrained by two U-shaped channels acting as restrainer. The core was fabricated with lateral bands along its length connected by equidistant transverse bridges. The lateral bands yield during axial loading while the transverse bridges were designed to remain elastic.

Chen et al. (2016) conducted a comparative study to estimate the effect of debonding materials on the low-cycle fatigue performance of the all-steel BRBs. Test results showed that all the BRBs exhibited excellent energy dissipation capacities with CPD value over 1000. However, significantly higher compression strength adjustment factor β was developed for the specimens without the unbonding materials. The gradually increasing friction force and the stick-slip mechanism between the core plate and restrainer induced significant non-uniform residual deformation in specimens without unbonding material.

During strong earthquake or subsequent repeated aftershocks, there is possibility of rupture of the BRB core. Jia et al. (2017) developed a new type of detachable high performance fish bone shaped BRB (FB-BRB) to maximize the

deformation capacity of the BRB by generating necking locations at regular intervals in the core plate. High seismic performance was achieved with the help of guided necking mechanism.

Ghowsi and Sahoo (2022) conducted sub-assembly testing on six all-steel BRBs (ABRBs) with bolted angle restrainers. The gap between core and restrainer, core geometry and position of stopper were varied in the experimental investigation. High cumulative ductility was observed in ABRBs with larger gap and stopper welded in elastic segments. It was reported that even for specimen with smaller gap, stable hysteresis behaviour was observed. Further, numerical models of the proposed ABRBs were developed which successfully predicted the hysteretic behaviour and fracture of core plate.

2.5 Self-centering BRB

Self-centering BRBs are comparatively new division of BRB. Undesirable residual deformation in structural elements after any seismic event could be effectively mitigated with the help of a recentering mechanism in conjunction with BRBs. This would lead to minimum or slight repair in structural elements to regain its functionality after an earthquake.

Eatherton et al. (2014) developed self-centering BRB (SC-BRB) using pretensioned shape memory alloy rods, in conjunction with a conventional BRB. The study examined the enhanced seismic performance of buildings when connected with SC-BRBs. A computational brace model was developed and calibrated with the data obtained from component testing. Parametric study was conducted to explore the design issues of SC-BRB. Finally, the effect of SC-BRBs in lateral resistance of a prototype building, subjected to a set of ground motions, was examined.

Zhou et al. (2015) experimentally tested a dual tube SC-BRB with pretensioned basalt fiber-reinforced polymer (BFRP) composite tendons. Cyclic tensile experiments were conducted first on two sets of BFRP tendons with different diameters. Further, quasi-static experiments were performed on two dual tube SC-BRBs with different core areas. It was reported that both specimens exhibited expected stable flag-shaped hysteresis response with a negligible residual deformation. The measured internal forces in the BFRP tendons and the gaps between the tubes and

end plates showed that both specimens met the expected performance criteria.

Wang et al. (2017) further refined the concept of SC-BRBs using two BRB cores welded to a central tube and restrained by the central tube and an outer tube. Further, a series of pre-stressed steel strands were coupled with two cover plates on the central and the outer tube to provide the self-centering mechanism. The cross-anchored technique was used to enhance the deformation capacity of the steel strands, which in turn enhanced overall deformability of the SC-BRB.

Xie et al. (2020) developed a new dual tube SC-BRB with friction fuses having self-centering and energy dissipation capacity. The SC-BRB was developed based on the elastic elongation capability of tendons present in the device. Additionally, a friction fuse was also introduced at the end of the BRB to increase the CPD capacity of the SC-BRB. The inclusion of friction fuse effectively prevented the snapping of tendons at large story-drifts. Nonlinear dynamic analysis of frames with SC-BRB mitigated soft-story problems and collapse probability of the structure.

Ghowsi and Sahoo (2020) investigated seismic performance of low to high-rise BRBFs equipped with SC-BRBs, conventional BRBs and hybrid system consisted of SC-BRB and conventional BRBs under near field ground motion. Nonlinear dynamic analyses were carried out on multiple BRBFs having 3-story, 9-story and 20-stories. It was reported that although SC-BRBs exhibited minimal residual deformation, they showed higher inter-story drifts as compared to that in BRBFs. Further, enhanced seismic performance was observed for 9-story and 20-story frames with hybrid systems.

SC-BRBs were successfully utilized by many researchers to reduce the residual deformation of structural elements. However, the pretension/recentering force should be optimized to satisfy optimal seismic performance with minimum repair cost of SC-BRB frames (SCBF) after an earthquake. Qing et al. (2021) examined the influence of pretension forces on the seismic response of SC-BRBs through nonlinear dynamic analyses of multiple mid to high-rise building. It was reported that with a modest reduction in pretension force, the SCBF satisfies both seismic performance demand and post-earthquake repairability of the structures. At a smaller pretension force, the SCBF exhibited effective energy dissipation capacity with reduced floor acceleration response.

2.6 Other Types of BRB

It was observed that conventional BRBs were very effective in seismic response control of structures. Excellent seismic performances of conventional BRBs and SC-BRBs were reported by various researchers. However, both conventional and self-centering BRBs had their own disadvantages. BRBs inherently provided large stiffness and strength, which in turn increased seismic acceleration and base shear in the structure. Moreover, they provided very low post-yield stiffness which resulted a rapid increase in brace deformation. The process of restoring mechanism in SC-BRB was very complex and needed skilled personnel for fabrication. To address the above mentioned issues, following researchers developed different types of BRBs, combining two or more material/energy dissipation technique, for effective seismic response control of structures.

Marshall and Charney (2010a,b) developed an innovative hybrid passive control devise (HPCD) for reduction of structural response. HPCD was designed as a two stage damping device which consisted of a high damping rubber in series with a conventional BRB. In the initial phase, damping for a wide range of loading was achieved with the help of high damping rubber. The BRB component of the device was activated using a locking mechanism. Once activated, the BRB could provide sufficient damping through axial yielding of its core.

Atlayan and Charney (2014) introduced a steel BRB, termed as hybrid BRB, which was designed to optimize structural performance in both low as well high seismic hazards. The core of the hybrid BRB system composed of different types of steel, including carbon steel, high performance steel (HPS) and low yield point steel (LYP). It was reported that the hybrid BRB performed better than conventional BRBs because of its significant residual displacement reduction capability.

Pandikkadavatha and Sahoo (2014) developed a hybrid brace combining an elastic buckling type brace and short length BRB (SLBRB) in series. Aim of the study was to increase of the lateral stiffness of BRBFs, which can reduce the drift response by maintaining the symmetric hysteresis and enhance ductility in SLBRB. The length of yielding region was adopted as 30% of total length of BRB. Hybrid braces were arranged in chevron configuration in a 3-story braced frame for their seismic evaluation. Nonlinear static and dynamic analyses were conducted on hybrid braced frame (HBF) to assess the ductility demand requirements and

compared the same with that obtained for BRBF.

Hsiao et al. (2016) developed a new type of steel brace called naturally buckling brace (NBB). NBB was composed of two different type of steels, namely, low-yield (LY) steel and high-strength (HS) steel, connected by transverse steel battens. LY steel plate played role of energy dissipater by early yielding. The large stiffness requirement post-yielding of LY segment was ensured by HS steel, which remained elastic and undamaged even after very large deformation. Thus, NBB combined the advantages of HS steel with large elastic deformation capacity and LY steel with sufficient ductility to undergo large strain limits, providing an improved seismic performance of the steel braced frames.

Qu et al. (2018) successfully investigated seismic performance of an innovative and reusable BRB with replaceable steel angle fuses. Seven BRBs with varied fuse details and debonding material are tested under different loading protocols. The proposed BRBs achieved stable hysteretic behaviour under fairly high fuse strain levels. Proper design of fuses channeled the failure modes of the BRB through ruptures of the angle fuses only. Authors reported that the repaired BRBs, by replacing only fuses, demonstrated satisfactory results in the following tests.

Sun et al. (2018) developed an assembled double-stage yield steel BRB (DYB) to provide the required rigidity satisfying structural drift limits and sufficient energy dissipation capacity. The core component of DYB comprised of a small core plate and a large core plate connected in series. The axial deformation was allowed to concentrate first at the small core plate of DYB and then it was shifted to the large core plate through a activation mechanism.

Li et al. (2019) proposed a two-level yielding BRB (TYBRB) to avoid low-cycle fatigue observed in conventional BRBs. TYBRB combined a metal tube damper with conventional unbonded BRB. It was designed to yield under frequent earthquakes of small to medium magnitudes, while the core of TYBRB was designed to yield under larger magnitudes earthquakes. Two specimens were tested under cyclic loading tests. It was reported that the tube dampers satisfactorily met the criteria of low-cycle fatigue resistance. Also, the performance of conventional BRB in TYBRB was not harmed due to its combination with tube dampers.

Similar studies based on the concept of double stage yielding of core were carried out by Wang and Liu (2021) and Huang et al. (2021). Wang and Liu (2021) developed a novel miniature dual stiffness damper (MDSD) with the advantages

of ease of assembling and low cost. It was reported that the proposed MDSD, with different stiffness ratios of the large yield segment to the small yield segment, showed stable hysteretic behaviour and the dual stiffness could be successfully achieved through successive yielding in small and large yield segments.

Huang et al. (2021) proposed an all-steel assembled double-cores BRB (DCBRB), with Q195 low yield steel and Q235 high yield steel acting as two cores. The restraining mechanism, consisted of two channel sections, effectively resisted the global instability of the DCBRB. Hysteretic performance of DC-BRBs were investigated through quasi-static cyclic loading. It was reported that stable hysteresis behaviour were achieved till 1.5% of applied axial core strain. Further, cumulative plastic deformation capacities were reported to be higher than 300 for all specimens.

2.7 Stability Issues

Although stable hysteretic behaviour under cyclic axial loading are observed in existing BRBs, one of the key limit states is global flexural buckling, which can produce an undesirable response. Other major limitations of conventional BRBs include failure of steel core in torsional and local buckling, premature rupture of steel core due to stress concentration near rupture plane etc. The parameters which make significant influence on BRB performance are: axial force on core plate, restrainer strength and stiffness, gap between core and restrainer, connection strength and effective bucking length.

Black et al. (2004) carried out an extensive study on structural stability of core to verify the theoretical analysis with experimental analysis. Stable hysteresis behavior of the tested BRBs were reported with no local and global buckling. However, it was reported that the torsional buckling of the inner core was more critical among the three major buckling failures. Further, it was recommended that the width to thickness ratio of the flanges of cruciform shaped core should always be less than 5 to prevent torsional buckling.

Koetaka and Kinoshita (2009) studied stability conditions for a BRB frame with the Chevron configuration, where the lower gusset plate end was assumed as rotationally rigid. The upper beam-BRB connection region at mid span was modelled as a rotational and a horizontal sway spring. Also, the restrainer ends

were modelled as pin joint assuming the bending moment transfer capacity at ends to be zero. Based on the above boundary conditions stability limits were presented and criteria for design of BRB was outlined for prevention of out-of-plane buckling.

Stability and strength of a BRB can be affected if the restrainer wall thickness is very small compared to cross-section of the core plate, resulting in local buckling failure. Takeuchi et al. (2010) carried out cyclic testing of BRBs to investigate the influence of local buckling of the restrainer on BRB strength and ductility. A significant increase in transverse strain on the restrainer wall was observed during cyclic loading. However, the bending at the end connections did not have much influence on the occurrence of local buckling failures. It was also reported that, the effect of length of core was insignificant if the local buckling wavelengths were in a range of 3.5-4 times the core plate width.

In the subsequent research, Takeuchi et al. (2012) proposed a strategy to prevent the in-plane local buckling failure of the BRB. Cyclic tests on unbonded BRBs were conducted to investigate the effect of mortar strengths and sectional geometries of the restrainer on local buckling failure of BRBs

Hikino et al. (2013) further investigated stability of a BRB with boundary conditions similar to that of the study carried out by Koetaka and Kinoshita (2009), but modelled the BRB connection and restrainer components as rigid. Stability limits were proposed estimating the limiting buckling force which was simplified by considering a perpendicular member offering significant horizontal stiffness.

Takeuchi et al. (2014) presented concepts on BRB out-of-plane stability, including bending moment transfer capacity at restrainer ends for various connection stiffness values with initial out-of-plane drifts. A unified set of equations for controlling BRB stability was proposed. Moreover, a series of cyclic loading tests with initial out of-plane drifts were conducted and the results were compared with those of the proposed equations. It was reported that the restrainer moment transfer capacity significantly influenced the BRB out-of-plane stability.

In the subsequent research, Takeuchi et al. (2016) extended the proposed set of equations for asymmetrical boundary conditions observed in chevron configurations in BRBF systems. Cyclic loading tests of chevron configuration with initial out-of-plane drifts were performed to verify the proposed analytical model of BRB behaviour.

Wu et al. (2014) conducted cyclic loading tests on all-steel BRBs using different loading patterns to investigate the higher order buckling modes of steel core. Design of an inspectable BRB was proposed, which could be conveniently disassembled and the damaged core plate could be replaced easily. Experimental and analytical results confirmed that the higher order local buckling wavelength was related to the core plate thickness and the applied loading protocol. The larger the axial compressive strain was applied, the shorter the higher order buckling wavelength developed.

Wu and Mei (2015) conducted similar study on the buckling mechanism of steel core of BRBs. The development of buckling modes was observed to be related to increasing axial load. Further, formula for estimating the maximum contact force was proposed for different end conditions. The corresponding maximum bending moments of the restraining member during compression cycle of loading protocol were also obtained. The analytical results were further validated using finite element analysis.

Guo et al. (2015) investigated elastic buckling behavior of CSBRBs. An analytical study to determine the critical loads for pin-ended and fix-ended CSBRBs was presented. The analytical results were further verified by finite element analysis. A unidirectional elastic buckling analysis of CSBRBs was carried out. Monotonic axial compression loading was applied on BRBs with different the restraining ratio, which governs the global buckling behavior. The restraining ratio was found to be a reliable indicator of axial compression behavior of BRBs.

2.8 Numerical and Analytical Investigations

Usami et al. (2003) analytically predicted cyclic behaviour of BRBs with a proposed finite element (FE) model. Elasto-plastic behaviour of BRBs under monotonic and cyclic loading was investigated using FE analysis. The core plate was modelled using beam element and debonding material by lateral spring distributed along the length. Constitutive behaviour of the core plate was considered as a modified two-surface model. The proposed model successfully reproduced the fundamental deformation of core, which, gradually shifted to higher order with increasing applied load.

Similar study was carried out by Takeuchi et al. (2010) to investigate the local

buckling behaviour of the restrainer. The core plates were modelled considering their direct contact with the restrainer walls. The deformation and rotation of the core about the weak axis were restrained and initial irregularities were introduced to the core plate. Shell element was used for modelling the core plate and restrainer walls. It was observed that the increase of strain in the restrainer wall became more significant for a thinner restrainer wall and larger gaps in between the edge of core and restrainer.

Wigle and Fahnestock (2010) studied performance of BRB connections using nonlinear FE models of BRB incorporated in a prototype building and compared the numerical results with experimental results. Important factors influencing seismic performance were defined considering varied connection configuration. It was observed that BRB end configuration had little influence on story drift, stress and strain demand in connection region. However, significant change in these parameters was observed for different beam end conditions, e.g. continuous and splice.

Hoveidae and Rafezy (2012) conducted a parametric study to investigate the effects of restrainer, gap and initial imperfections in core of a BRB on global buckling behavior of the core. It was reported that flexural stiffness of the retraining mechanism could significantly affect the global buckling response of the BRB, regardless of the interface/gap details. A minimum ratio of Euler buckling load of the restrainer to the yield load of the BRB core was also recommended for designing BRBs. Further, application of unbonding material with a proper thickness was recommended.

To study higher order buckling modes about weak axis of an all-steel BRB core, FE simulations were carried out by Wu et al. (2014). The core plate was modelled using the eight-node solid elements with the material model considering isotropic and kinematic hardening properties. To simplify the FE model, the pair of restraining members was represented by a pair of rigid plates in the weak axis. To prevent the core plate from flexural buckling in the strong axis, a couple of rigid plates were used. The simulated hysteresis responses obtained using the proposed FE material model were found in good agreement with the experimental responses of all specimens.

Jiang et al. (2015) investigated the influences of strength and stiffness of restrainer, core length, and other parameters on the performance of BRB using

a simplified model. It was seen that the lateral restraining capacity depended on strength and stiffness of restrainer. The contact force generated during higher order buckling was observed to be significantly affected by gap-to-core plate thickness ratio. It was recommended that core plate width-to-thickness ratio should be below 10 and the maximum gap should not be larger than 2 mm.

To investigate the outward force induced during higher order buckling about weak axis of core a thin BRB, FE analysis was conducted by Lin et al. (2016) considering two simplified BRB models. The steel core, mortar, and steel tube were represented by 3-D solid elements. The material model adopted for the core plate and the restrainer was same as that considered by Wu et al. (2014). The effective flexural stiffness of the restrainer was computed from the double modulus theory and the FE analysis results. Further, estimation of maximum outward force using the peak axial force and higher order buckling wavelength was also presented.

Hosseinzadeh and Mohebi (2016) compared performances of all-steel BRBs with varying geometries using FE analysis. Main aim of the study was to minimize instability of the core section and maximize energy dissipation capacity. FE modelling was done considering combined isotropic-kinematic hardening nonlinearity. Maximum Euler buckling load to yield strength of the core ratio was found to be greater than 1.5, indicating safety against global buckling. However, it was reported that the gap of more than 10 mm could lead to decreasing strength of the BRB resulting in local buckling failure.

Over the years, Bouc-Wen model had been extended to describe various characteristics of hysteretic responses, e.g., stiffness degradation, pinching effect, asymmetry in peak restoring forces etc. For this, Bouc-Wen type hysteresis model had been used in a wide range of applications such as steel structures, concrete structures, base isolation devices and other different dampers.

A macroscopic hysteretic model was proposed by Black et al. (2004) using the research work of Bouc (1967) and Wen (1976). The main aim was to replicate the hysteretic responses of the tested BRBs using an analytical model. The test results were calibrated first and the Bouc-Wen model parameters were estimated. A single set of calibrated model parameters were further used to predict the cyclic and transient behavior of the unbonded BRBs under a variety of loading cases satisfactorily.

Sireteanu et al. (2010) proposed an extended Bouc-Wen model for improv-

ing the capability to represent the experimental hysteretic behaviour. A genetic algorithm approach was adopted to identify the parameters of Bouc-Wen model from the experimental responses under cyclic loading. Performance of the adopted approach was further validated for two types of passive seismic control systems: elastomeric base isolator and buckling restrained brace.

Similar studies were conducted by Wu et al. (2021) to accurately evaluate the additional damping ratio provided by the BRB. Explicit analysis using Bouc-Wen model was carried out and an analytical solution of energy dissipation of the model was proposed. The formula for calculating the additional damping ratio of BRB was proposed and the solution obtained from the same was further validated using numerical examples.

The component level performance and key design aspects of both types of conventional BRBs were studied by different researchers. Review of these studies are presented in the preceding sections. However, performances of structures retrofitted with the BRBs, under earthquake loading, were yet to be evaluated.

Dizaj et al. (2018) compared the seismic performances of reduced length BRB with conventional BRB using probabilistic approach. The performances of BRBs were quantitatively evaluated in terms of two limit states: immediate occupancy and collapse prevention. The fragility curves were plotted using the probabilistic demand analysis. It was observed that, the reduced length BRB performed better up to immediate occupancy limit state. However, for collapse prevention limit states, in some cases, reduced length BRB exhibit improved performance while in some other cases, conventional BRB performed better.

Li et al. (2020) carried out multi-hazard fragility assessment of two steel-concrete composite structure with and without BRBs. The effectiveness of BRBs in reducing the structural responses and reducing vulnerability under the combined action of earthquake and wind loads was evaluated. Opensees platform was used to calculate the responses of both structures under simultaneous action of earthquake and wind. Finally, a polynomial function was employed to generate the multi-hazard fragility surfaces corresponding to different predefined damage states.

Seismic behaviour and vulnerability assessment of a soft first story building rehabilitated with BRBs was carried out by Ruiz et al. (2019). The sample building had regular RC moment resisting frame in the soft ground story and masonry infill

walls in the upper stories. Multiple earthquake records were used for evaluating the response of the building. The damage states were defined based on the maximum story drift profiles of the building under prescribed ground motions. Finally, the fragility curves corresponding to predefined values of maximum inter-story drift were generated.

2.9 Applications

Passive control systems are becoming more popular for retrofitting existing RC or steel buildings that were not designed for earthquake-resistance in pre-code era or that were designed using older structural codes. Use of BRBs was found to be a promising technique for improving structural stability as well as dissipation of seismic energy efficiently.

Kim and Seo (2004) proposed a direct displacement-based procedure for designing steel frames with BRBs. The proposed structure was designed in such a way that only the BRBs resisted all lateral loads. Time history analyses of the numerically modelled frame were used to validate the applicability of the proposed design procedure. The seismic performance of the structure was found to be in good agreement with the design objectives.

Kasai and Ito (2004) proposed a procedure for seismic design of an elasto-plastically damped building. The design approach was based on the single degree-of-freedom idealization of multistory building, which considers the effects of stiffness and ductility demand on the seismic performance of the building. The accuracy of the proposed design approach was further validated by time history analyses of different types/classes of multistory buildings.

Usami et al. (2005) studied application of BRBs as energy dissipation dampers for better seismic performance of steel arch bridges. BRB components were first tested to study their hysteretic behaviour under displacement controlled pseudo static loading. BRBs were then used in real bridges replacing some inefficient diagonal braces for improving seismic performance of the bridge. These BRBs were found to dissipate energy during severe seismic events efficiently as compared to ordinary steel braces.

Park et al. (2012) validated the applicability of BRBs in low rise steel frames by conducting a performance based design procedure for its seismic retrofitting. It

was observed that the maximum displacements obtained from numerical analysis matches well with the target displacements.

Della Corte et al. (2015) successfully retrofitted an existing RC building with full scale all-steel dismountable BRBs. Design of BRBs for the seismic upgrading of the damaged RC building was carried out in two phases. In first phase, BRB strength and stiffness necessary to achieve the design objectives were evaluated. In the next phase, mechanical characteristics and geometrical details of various components of prototype BRBs were finalized.

Wang et al. (2016) investigated the effectiveness of BRBs in retrofitting the existing straight RC bridges. The use of BRB reduced the column bent drift and prevented deck unseating caused by shear key failure. Further addition of BRBs to the bridge bents redistributed the stiffness in the transverse direction between bridge bents and abutments and thus reduced the original shear demand through BRB's hysteretic behavior. It was reported that the addition of BRBs also prevented/delayed the formation of column plastic hinges near pier-cap joints.

Performance of a deficient reinforced concrete bridge bent retrofitted with BRBs was experimentally evaluated under quasi-static cyclic loading by Bazaez and Dusicka (2016). Two BRBs were designed for large-scale experimental investigation to assess their effectiveness in improving overall performance of the retrofitted bent. A third test was carried out to check the behaviour of bent in built-in non retrofitted condition. Cyclic behaviour and damage progression study was carried out for each specimen both globally and locally. Results established effectiveness of the BRBs in achieving high displacement ductility of the retrofitted structure.

Castaldo et al. (2021) numerically investigated the efficacy of BRBs for seismic retrofit of an existing RC building with masonry infills. A 3D model of the sample building was developed in OpenSees, with masonry walls modelled as equivalent struts. Seismic performance of the building, before and after retrofit with BRBs, was evaluated using nonlinear static and incremental dynamic analyses. The effect of BRB on seismic performance was investigated using seismic fragility curves developed for prescribed ground motions.

2.10 Gap Area

Various types of BRBs were developed for passive seismic response control of structures. Analytical and experimental studies were carried out by different investigators for evaluation of performances of these devices. Parametric studies on BRB core and restrainer configuration, connection type, gap/debonding material and buckling mode assessment were also conducted to investigate the efficiency of BRBs. Finite element analyses were carried out by many researchers and results of numerical analyses were validated by comparing with experimental results. Existing literature on development of different types of BRBs and recent advancements, key design issues and performances are critically reviewed in this chapter and several limitations of the existing BRBs are identified. Following are some of the gap areas in the existing literature those are yet to be investigated:

- Most of the researchers carried out R&D works to develop different varieties of either conventional all steel BRBs or BRBs with concrete filled tubes as restrainer. Both types of conventional BRBs have their own limitations. Thus, development of a new type of BRB, which could overcome the limitations of the conventional BRBs and facilitate replacement of damaged core, would be useful.

- Conventional BRBs provide very insignificant hysteretic damping to the structure at low storey drift level. Thus, development of a BRB with more than one core plate or BRB which is capable of providing hysteretic damping at very low as well as high story drift can be an exciting area of research.

- Inspectable all-steel BRBs enable to check extent of damage in the BRB core, through visual inspection and core axial strain measurement, during/after seismic events and to replace the damaged core before occurrence of next earthquake. However, very limited studies were carried out on inspectable BRB, which offers ease of rapid replacement of the steel core, if necessary.

- Energy dissipation of BRBs in low to high level of axial core strains could be improved with the addition of rubber pads, in series with the steel core, through shear deformation. However, there is limited literature on hybrid BRBs that utilizes highly deformable rubber pads, sandwiched between the

steel core and restrainer, to improve energy dissipation capacity and overall performance of BRBs.

- In conventional BRBs, restrained buckling of the steel core is generally allowed either about weak axis or strong axis. However, no literature is available on the utilization of restrained buckling of the BRB core about the weak axis first and subsequently about the strong axis at higher axial steel core strain for enhanced energy dissipation. Development of a hybrid BRB with aforementioned attributes would reduce residual displacement of structures due to enhanced stiffness at higher axial strain, which was previously achieved through complex self-centering devices.
- There is a scope for analytical simulation of force-displacement hysteretic behaviour of BRBs using Bouc-Wen hysteresis model. This simulated analytical model could be used for nonlinear dynamic analysis of structures retrofitted with BRBs.
- There are very limited literature available on seismic retrofitting of structures with vertical irregularities using hybrid BRBs. Thus, assessment of reduction in seismic vulnerability of a structure with vertical irregularities such as soft-story building retrofitted with hybrid BRB can be an interesting area of research.

2.11 Concluding Remarks

The distinct advantages of BRBs over other types of passive seismic response control devices are discussed. Experimental and numerical studies, carried out by various researchers, showed excellent seismic performance of BRBs in enhancing strength, energy dissipation capacity and ductility in different types of structures. These attributes promoted use of BRBs as a structural fuse around the world. Large volume of research works on BRBs are reported in the literature. All important papers, related to experimental, analytical and numerical studies on development and evaluation of performances of BRBs, are collected. These are classified into different categories and critically reviewed for identification of gap areas in the existing research works. Based on these, objectives of the present study are finalized.

Chapter 3

Design of HyBRB

Contents

3.1 General

Structural stiffness and damping are greatly enhanced by the use of BRBs. As a result, BRBs are well-suited for a wide range of applications, including rehabilitation of damaged structures, retrofitting of structures vulnerable to severe seismic actions. Understanding the performances of new hybrid types of BRBs, their components and connections, and their overall effect on the performance as a system is limited. In the preceding chapter, extensive literature review has been presented for identification of gap areas and scopes of the study for development of hybrid BRB. More researches are required to address the performance enhancement of conventional BRBs and development of a design methodology, ensuring ease of assembling and mountable facilities in realistic structural frames. This chapter describes the concept and a step-by-step procedure for designing a new hybrid BRB (HyBRB). The design procedure is then used to fabricate a set of HyBRB specimens which are further assessed under cyclic loading for their performance evaluation.

3.2 Concept of HyBRB

Flat steel core in combination with stiffened steel restrainers and connection arrangements result in an efficient and attractive all-steel BRB (Chou and Chen, 2010). A thin profile of BRB core and stiffened steel restrainers enable all-steel BRB to achieve stable hysteretic behaviour with generation of higher order local buckling modes about weak axis inside the restrainer (Wu et al., 2014). Another group of researchers successfully carried out studies on guided higher order local buckling of core about its strong axis by completely restricting the weak axis movement of the steel core (Takeuchi et al., 2010, 2012). Debonding layer thicknesses of 1 to 2 mm are utilized by various researchers for achieving guided local buckling of the core either about its weak or strong axes. Detailed experimental studies by several researchers report that the use of a debonding material is effective in case of both unbonded and all-steel BRBs. The presence of a thin debonding material layer between the BRB core and the restrainer pair reduces friction, resulting in less stress concentration and therefore greater safety against fracture. Conventional BRBs contain mortar or concrete as infill with a layer of debonding agent

on surfaces of the steel core. All-steel BRBs employ one or more pin like features to maintain the gap between restrainer mechanism and BRB core. Provision of a rubber-like infill layer would eliminate the uncertainty of maintaining uniform gap between the core and the restrainer of conventional BRBs.

It is observed that available BRBs exhibit insignificant damping at low level of axial strain in the steel core. Very few literature discusses about the role of a rubber-like infill layer in enhancing the performance of BRB by dissipating additional energy through shear deformation. An infill layer would allow lateral deformation and formation of restrained buckling modes of the core inside restrainer pair. Thus, it would help BRBs to achieve higher energy dissipation capacity in low to high levels of axial strain loading. Presence of the infill layer and their mechanical properties/geometries could play an important role on the restrained local buckling mode formations of the steel core. Existing research works report restrained buckling of the core either about its weak axis or about strong axis only. Proper arrangement of infill layer and appropriate connection of restrainer pair could facilitate restrained local buckling of the core about both weak and strong axes, in succession, and thus, enhance overall performance of a BRB. However, there are very limited studies that utilizes infill layer as a tool to achieve desired buckling modes and enhanced seismic performance of BRBs. Objective of the current study is to combine the advantages of highly compressible material as an infill layer and the hysteretic behaviour of prismatic steel core of a BRB.

In the present study, the combination of a conventional all-steel BRB with neoprene and butyl rubber of thickness 3 mm in form of infill layers is designated as hybrid buckling restrained brace (HyBRB). The infill layer is sandwiched between the steel core and the restrainer pair. Fig 3.1 shows different directions/designations of axes for definition of buckling about both the lateral axes of the HyBRB core. Lateral view of the proposed HyBRB, as shown by Fig 3.2(a), displays the layers of infill material pads and possible restrained buckling modes of the proposed HyBRB specimens. Addition of high damping rubber materials, as infill layers, would enhance energy dissipation capacity in lower axial strain levels. A gap of 10 mm is provided along the lateral directions of the steel core, between the core and the connecting bolts, as shown in Fig 3.2(b). Provision of two infill layers on transverse directions (+ve/-ve) of the flat core facilitates higher order restrained buckling of core about both its weak and strong axes, in succes-

sion, as shown in Fig 3.2(a-b). This would increase energy dissipation capacity of the HyBRB in both low as well as high axial strain levels. Moreover, formation of restrained buckling modes about the strong axis of core would enhance effective stiffness of HyBRB at higher axial strain loading. The infill material layers are provided in HyBRB to achieve the following goals: (i) to prevent friction between the core and the restrainer, (ii) to accommodate lateral deformation allowing restrained buckling of steel core about weak axis, (iii) to contribute in energy dissipation during initial loading through shear deformation and (iv) to allow side-wise movement of the core facilitating restrained buckling about strong axis. During initial loading phase, infill layers are expected to contribute in energy dissipation through shear deformation. Moreover, the brace core is also expected to dissipate energy first by buckling locally about its weaker axis. Thereafter, local buckling of core about its stronger axis is facilitated at higher levels of axial strain. Thus, the proposed HyBRB would be more effective for seismic response control because of its ability to dissipate energy in a wide range of axial core strain levels.

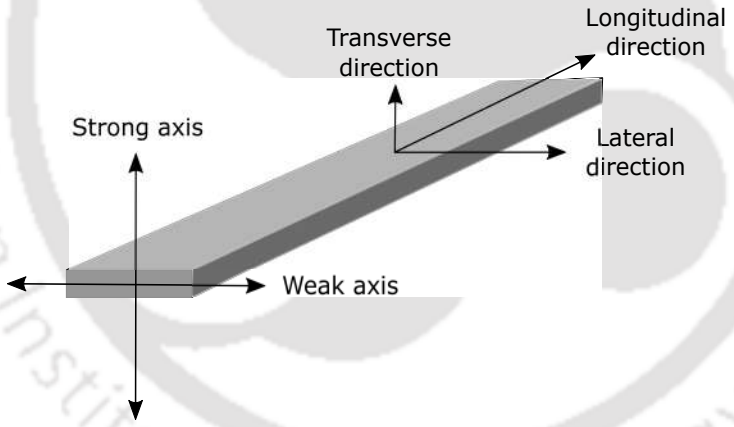

Figure 3.1: Designations of axes of the HyBRB core

3.3 Evaluation of Critical Buckling Load

The load carrying capacity of a HyBRB is largely governed by restrained buckling modes of the steel core. Formation of higher restrained buckling modes inside the restrainer pair would ensure a higher buckling load. The development of buckling mode formations about the lateral and transverse axes of the steel core inside the restrainer pair and corresponding responses of the restrainer pair can be analyzed

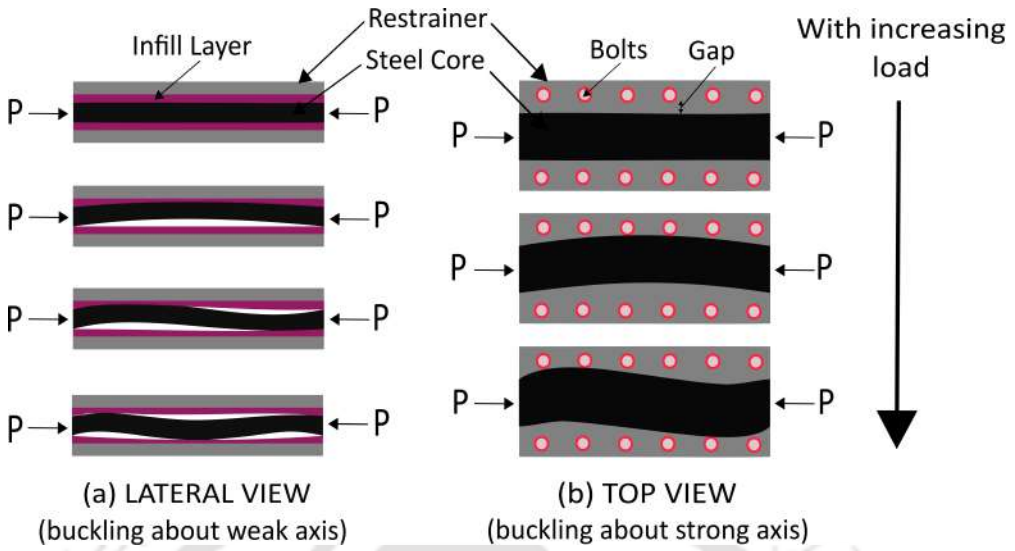

Figure 3.2: Working principle of HyBRB subjected to axial loading

by using the assumed HyBRB core-restrainer schematic diagrams, as shown in Fig 3.3. Only the yielding zone of the core inside the restrainer is considered for the analysis. Both ends of the yielding zone are considered as pinned as shown in Fig 3.3(a). The length of the steel core is l, axial force acting on the steel core is P, contact force from restrainer is N, clear gap between the core and the restrainer on either transverse direction is $y_0/2$, E and I are Youngs modulus and area moment of inertia respectively.

3.3.1 Buckling About Weak Axis

At the lowest critical load, the yielding zone of the core undergoes buckling about its weaker axis and tends to touch the inner surface of the restrainer pair and a contact force N generates, as shown in Fig 3.3(b). The moment equilibrium equations for yielding zone of the core, considering no axial yielding in compression of the steel core and the rigid restrainer pair and neglecting friction between the core and the restrainer, can be written as (Wu and Mei, 2015):

$$\begin{aligned} EIy_1'' + Py_1 &= \frac{N}{2}x; \quad 0 \le x \le \frac{l}{2} \\ EIy_2'' + Py_2 &= -\frac{N}{2}x + \frac{N}{2}l; \quad \frac{l}{2} \le x \le l \end{aligned} \tag{3.1}$$

Applying initial boundary conditions ($y = 0$ at $x = 0$ and $y = y_0$ at $x = l/2$),

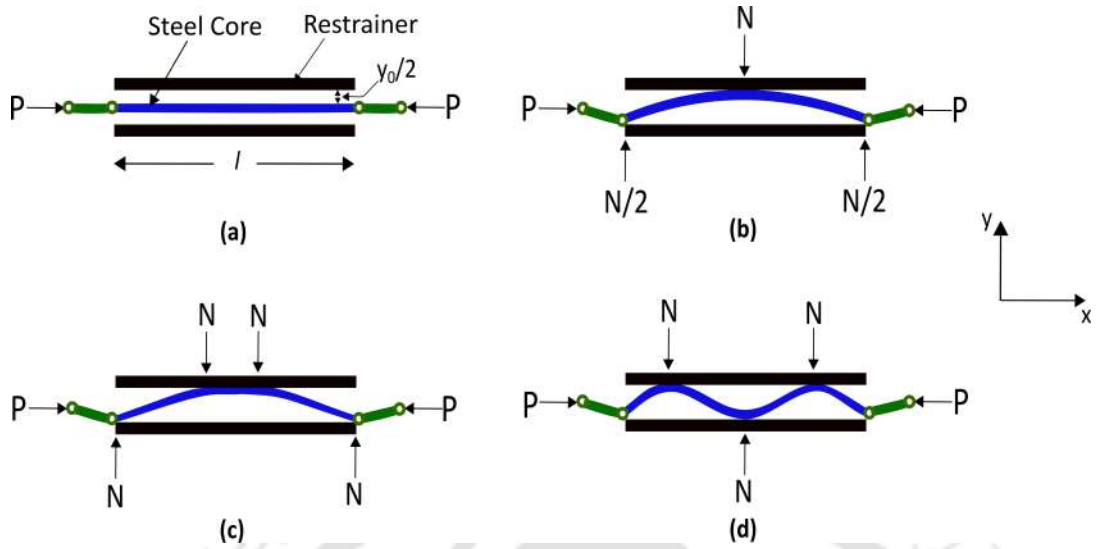

Figure 3.3: Buckling mechanism of flat steel core about its weaker axis inside restrainer pair

deflection at a distance x from either end of the BRB core can be computed as:

$$y = \frac{y_0 - \dfrac{Nl}{4P}}{\sin\left(\dfrac{kl}{2}\right)} \sin kx + \frac{N}{2P}x; \quad 0 \leq x \leq l \tag{3.2}$$

And the lateral contact force due to resistance from the restraining members is expressed as:

$$N = \frac{4Pky_0}{kl - 2\tan\left(\frac{kl}{2}\right)} \tag{3.3}$$

where, $k = \sqrt{P/EI}$

The slope of deflected core equals to zero where it tends to touch the restrainer wall. With increase in loading, a segment of the core tends to push the inner side of the restrainer wall as shown in Fig 3.3(c). On further loading, initiation of the next buckling mode formation starts. A third order buckling mode forms after completion of the first order buckling mode as it is highly unlikely to observe the second order buckling mode about weaker axis of the steel core for the restrained buckling scenario (Wu and Mei, 2015). The third order buckling mode formation reduces the chances of eccentric loading on the restrainer pair. The critical buckling load required for transforming the buckling mode from first order to higher

order can be computed by equating the curvature to zero at the center of the restrainer ($y''|_{x=l/2} = 0$) and it is expressed as:

$$P_{wn} = \frac{4n^2\pi^2 EI_w}{l^2}; \quad n = 1, 3, 5.. \tag{3.4}$$

3.3.2 Buckling About Strong Axis

Initial buckling of the steel core about strong axis is similar to a column buckling, with its both ends pinned, under compressive load. Steel core undergoes higher mode restrained buckling due to presence of series of closely spaced stainless steel bolts along the lateral directions of restrainer pair, acting nearly as a resisting wall. The critical load for buckling about strong axis of steel core can be computed as:

$$P_{sn} = \frac{4n^2\pi^2 EI_s}{l^2}; \quad n = 1, 2, 3... \tag{3.5}$$

Equations 3.4 and Eq. 3.5, are valid only for the axially incompressible steel core. Flexural stiffness of the steel core about both weak and strong axes reduces significantly due to yielding of steel core during higher mode of buckling formations. The effective flexural stiffnesses, $(EI_w)_{\text{eff}}$ and $(EI_s)_{\text{eff}}$, during higher mode buckling about the weak and the strong axes considered in this study are 6% and 2% of the corresponding flexural stiffnesses (EI_w and EI_s) respectively (Takeuchi et al., 2010; Wu et al., 2014). Therefore equations, Eq. 3.4 and Eq. 3.5 can be modified as:

$$\begin{aligned} P_{wn} &= \frac{4n^2\pi^2 (EI_w)_{\text{eff}}}{l^2}; \quad n = 1, 3, 5.. \\ P_{sn} &= \frac{4n^2\pi^2 (EI_s)_{\text{eff}}}{l^2}; \quad n = 1, 2, 3.. \end{aligned} \tag{3.6}$$

Also, for a HyBRB with a flat core (width $b = md$; d being the thickness of the plate and m an integer), the area moment of inertia about strong axis of plate cross-section is m^2 times the same about its weak axis. Therefore, Eq. 3.6 expresses the critical loads for higher order buckling modes for a particular HyBRB core configuration. The critical loads then can be arranged in ascending order for different values of m. From basic understanding of geometry, a core configuration can be termed as a flat one if the width of the core is much higher than the thickness of the core plate. So, HyBRB specimens with flat core ($b =$

$md; m \geq 3$) configuration are expected to undergo higher order restrained buckling inside restrainer pair as per following order of critical buckling loads for first few values of m:

$$\begin{aligned} &P_{w1} \leq P_{s1} \leq P_{w3} \simeq P_{s2} \leq P_{s3} \leq P_{w5}; \quad m = 3 \\ &P_{w1} \leq P_{s1} \leq P_{w3} \leq P_{s2} \leq P_{s3} \leq P_{w5}; \quad m = 4 \\ &P_{w1} \leq P_{s1} \leq P_{w3} \leq P_{w5} \simeq P_{s2} \leq P_{s3}; \quad m = 5 \end{aligned} \tag{3.7}$$

3.4 Design of HyBRB Components

As discussed in the earlier section, objective of the current study is to take advantages of both high damping of infill material layer and axial yielding of steel core through successive restrained buckling. All components of a steel BRB are designed first and then the same is assembled with layers of high damping rubber materials, such as neoprene or butyl rubber, as the infill layers. Design of a geometrically scaled HyBRB is carried out following the AISC guidelines and other available literature (AISC 341-10, 2010; Takeuchi et al., 2010; Wu et al., 2014; Chuang et al., 2015). Shear stiffness of the infill rubber layer is insignificant as compared to the axial stiffness of the steel core used. Therefore, the stiffness contribution of infill material can be ignored during HyBRB design. The proposed HyBRB is designed to ensure following characteristics/behaviour:

- Steel core to withstand the axial load from applied cyclic displacement,
- Adequate flexural capacity of the restrainer pair to prevent global buckling,
- Restrained buckling of the steel core inside the restrainers,
- Suitable end connections to make sure that only the HyBRB core yields due to imposed loading.

Following sub-sections briefly present a step-by-step procedure for design of the components of the HyBRB specimen.

3.4.1 HyBRB Core

The core is designed as an axial load carrying member to withstand the entire load transmitted to the HyBRB. Therefore, load is transferred to restrainers at no point. The maximum design strength of steel core is calculated considering the strain hardening factor, compressive strength adjustment factor and material

overstrength factor. The cross-sectional area of the yielding zone of the core is calculated as:

$$A_c = \frac{P_{ysc}}{\sigma_y} \tag{3.8}$$

where, A_c is the area of the core yield zone, P_{ysc} is the nominal BRB strength in kN, and σ_y is the material yield strength in MPa.

The maximum BRB compressive and tensile axial force capacities are expressed as (AISC 341-10, 2010):

$$P_{\max\_c} = P_y \times R_y \times \Omega_h \times \beta \tag{3.9}$$

$$P_{\max\_t} = \frac{P_{\max\_c}}{\beta} \tag{3.10}$$

where, $P_{\max\_c}$ and $P_{\max\_t}$ are the maximum force demands under compressive and tensile loading respectively, R_y is the material over-strength factor, Ω_h is the strain hardening factor and β is the compression strength adjustment factor.

3.4.2 Restraining Member

Design strength of the restrainers is determined considering the maximum load carrying capacity of the proposed HyBRB. Under compression, the steel core undergoes transverse deformations and a normal outward force acts on the contact points of the inner side of restrainer wall. The pair of restrainers restricts tendency of the core to buckle globally and facilitate restrained buckling of the same inside the pair of restrainers. To prevent global buckling of the HyBRB, the critical buckling load of the restrainer must be greater than the maximum axial compressive force, which is satisfied by the following condition (Wu et al., 2014).

$$I_{sc} \geq \frac{P_{\max} L_{sc}^2}{\pi^2 E} \tag{3.11}$$

where, I_{sc} is the combined moment of inertia of restrainer pair, L_{sc} is the length of the restrainer, $P_{\max}$ is the maximum design compressive force.

3.4.3 Core End Details

Design of proposed HyBRB ensures that the specimen dissipates energy solely through axial yielding of the central plastic zone of its steel core. Two perpendic-

ular stiffeners are used to stiffen both ends of the steel core, which includes the transition zone, to ensure that the ends stay in elastic condition during all phases of the testing. Afterwards, the stiffened core ends are joined to a square steel plate in order to make provisions for connection of the HyBRB with the test assembly. A couple of pin joints are designed at both ends of the stiffened core for connecting the HyBRB with the test assembly. The pins are expected to withstand the maximum tensile load that is likely to be experienced by the HyBRB specimen during the testing process through double shear.

3.4.4 Connection Details

The maximum load carrying capacities of the HyBRB specimen are taken into consideration for designing the welds joining its various components. The welds for stiffening both ends of the HyBRB core, as well as the proposed pin joints, are designed to carry the maximum tensile force experienced by the HyBRB specimens. The design specifications of the welds and the connecting bolts in the restraining member of the HyBRB core are estimated by taking into account the maximum transverse thrust encountered by the restraining members while preventing the global buckling of the HyBRB core. The specifications of bolts required for HyBRB-test assembly connections are decided based on the maximum design shear force to be encountered by the pin strips.

A simplified procedure describing the steps for designing the various components of the HyBRB specimen are shown in Fig 3.4. The design calculations for each components of the HyBRB specimens are presented in Annexure-A.

3.5 HyBRB Variants

As described in Section 3.2, a combination of an all-steel BRB and highly deformable infill material layers, to achieve enhanced damping characteristics, is designated as HyBRB as shown in Fig 3.5. The present research involves investigation of HyBRBs with two different infill materials. Based on the infill material used, HyBRBs are classified in two groups: (a) HyBRB-A, and (b) HyBRB-B. Neoprene and butyl rubber of different geometries are used in HyBRB-A and HyBRB-B, respectively. Each category of HyBRB is again comprised of four types of specimens depending on the size and arrangement of infill layer used

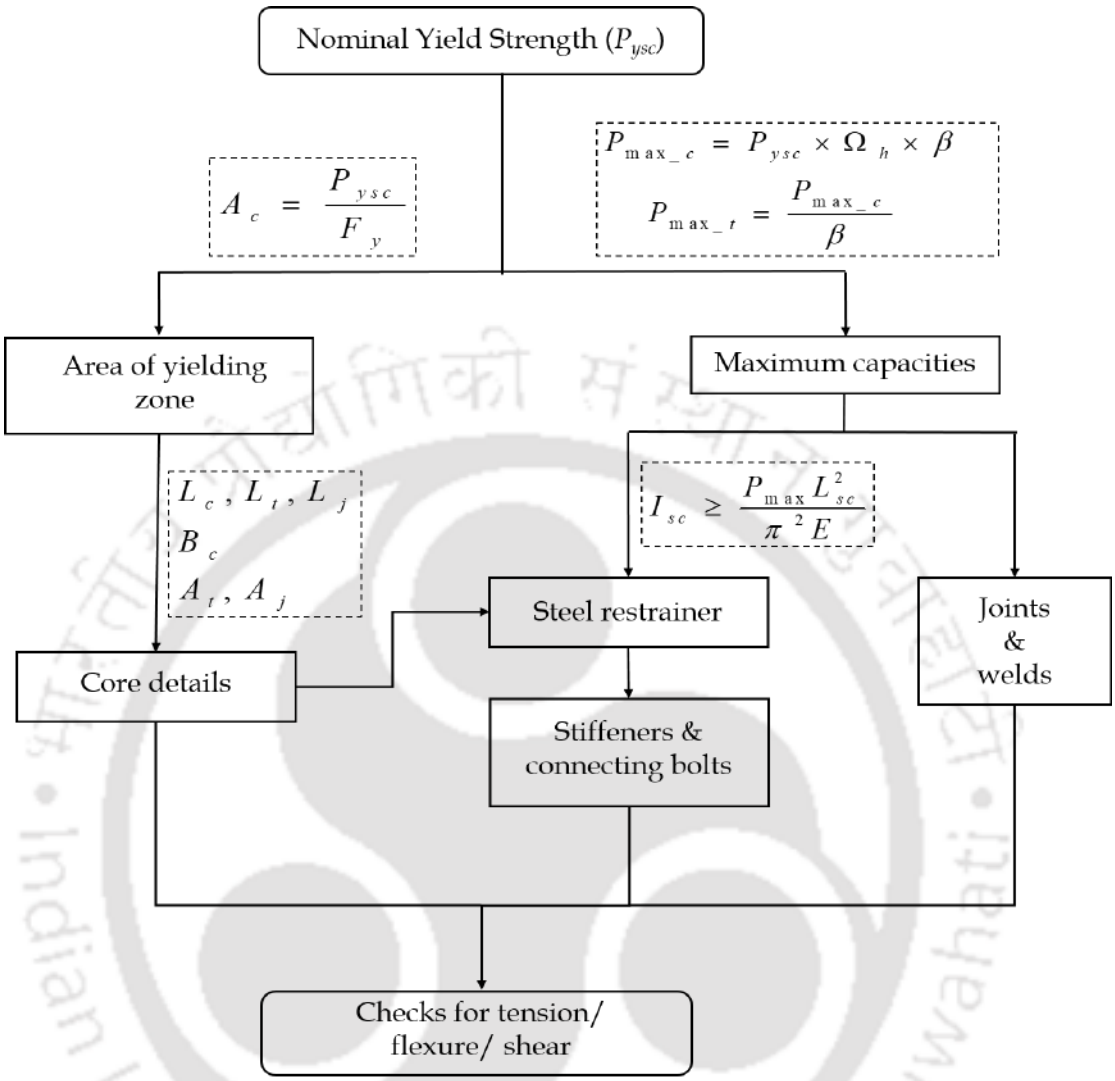

Figure 3.4: Steps for designing the components of HyBRB specimens

inside the restrainer pair. Two specimens in each category use continuous infill layers of length 1000 mm, while other two use discontinuous infill layers of two different lengths, 120 mm and 50 mm. Therefore, a total of six variants of HyBRB specimens are fabricated and assembled for experimental evaluation. Fig 3.5(a-b) show details of two different varieties of HyBRB specimens in disassembled condition while Fig 3.5(c) shows configuration of HyBRB specimens after assembling all the components. Table 3.1 describes designation of different specimens from each category of HyBRB.

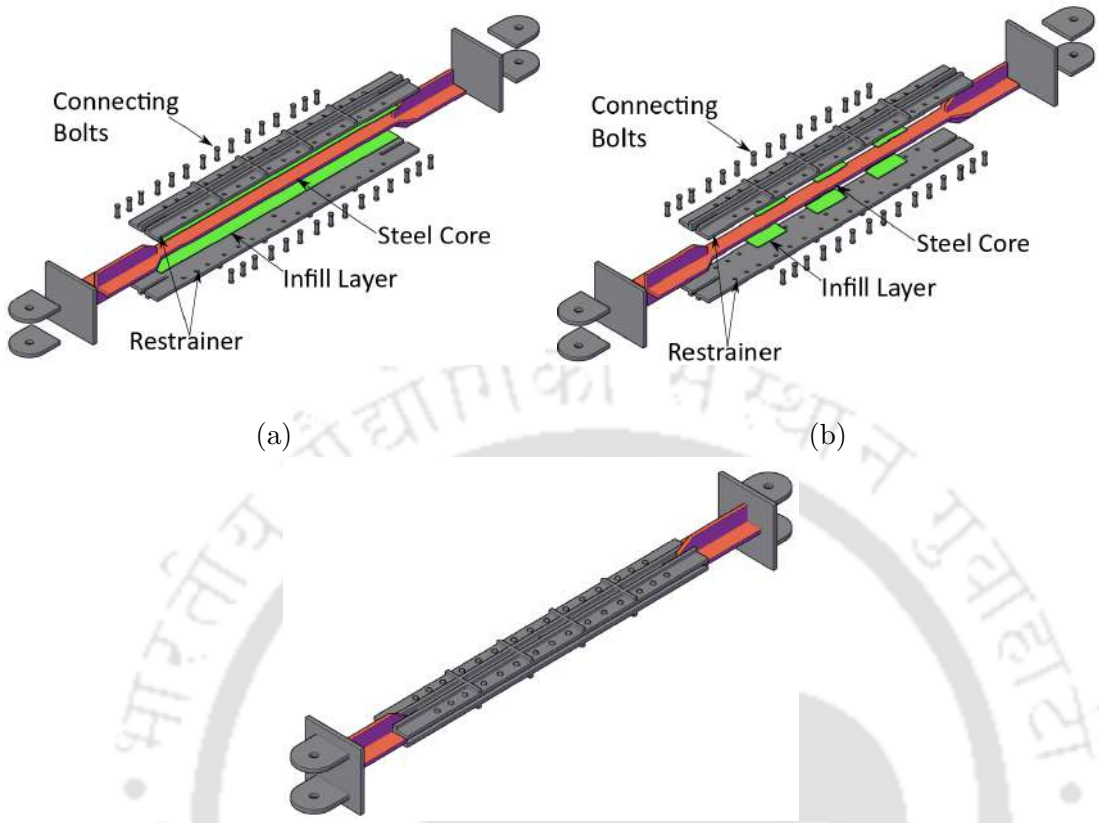

Figure 3.5: Proposed HyBRB configurations in: (a) disassembled condition with continuous infill layer, (b) disassembled condition with discontinuous infill layer and (c) assembled condition

Table 3.1: Designation of proposed HyBRB specimens

Category	**Infill material**	**Dimensions**	**No.of pads in each layer**	**HyBRB designation**
HyBRB-A	Neoprene	1000 × 50 × 3	1; full length	A1; A2
		120 × 50 × 3	3; @250 mm c/c	A3
		50 × 50 × 3	3; @250 mm c/c	A4
HyBRB-B	Butyl	1000 × 50 × 3	1; full length	B1; B2
		120 × 50 × 3	3; @250 mm c/c	B3
		50 × 50 × 3	3; @250 mm c/c	B4

3.6 Concluding Remark

This chapter highlights a detailed discussion on the advantages of the proposed hybrid BRB (HyBRB) over conventional BRBs. The concept and working principle of the proposed HyBRB are discussed. Analysis of restrained buckling mechanism of steel core is presented and a simplified design methodology of HyBRB is also outlined. Different components of the geometrically scaled HyBRB specimen are finalized for fabrication based on the modified design procedure proposed in this study.

Chapter 4

Experimental Investigations on HyBRBs with Continuous Infill Layers

Contents

4.1 General

A detailed discussion on evolution and various performance related aspects of conventional BRBs is carried out in Chapters 1 and 2. Chapter 3 thoroughly discusses the motivation and concept behind the development of the proposed hybrid BRB. Various literature report that multiple cores with varied yield strengths can be used to increase energy dissipation capacity of BRBs (Tsai et al., 2004; Atlayan and Charney, 2014). In conventional BRBs, the use of flat core geometries has also been proven to be favourable (Takeuchi et al., 2010; Wu et al., 2014; Lin et al., 2016). An infill layer would allow lateral deformation and formation of restrained buckling modes of the core inside the restrainer. Thus, it would help BRBs to achieve higher energy dissipation capacity in low to high levels of axial strain loading. Presence of the infill layer and their mechanical properties/geometries could play an important role on the restrained buckling mode formations of the steel core. In view of above, a new hybrid BRB, designated as HyBRB, is developed in this study, where, the infill layer is sandwiched between the steel core and the restrainer pair according to specific arrangements. This chapter presents the details of the experimental study conducted for the evaluation of seismic performance of the newly developed HyBRB specimens. Total six HyBRB specimen variants are examined and the obtained results are then compared. The overall behaviour and force-displacement hysteretic behaviour of the HyBRB specimens is studied using a 1000 kN servo-hydraulic MTS actuator in the Structural Engineering Laboratory of the Civil Engineering Department, Indian Institute of Technology Guwahati (IITG).

4.2 Tensile Test of the Core Steel

All components of the HyBRB specimens are made from Fe250 grade mild steel plate of thickness 10 mm. Five test coupons are made from the mild steel plate, used for fabrication of the core of HyBRB, as per the specifications outlined in the Indian Standard code, IS 1608 (2005). Tensile testing of the coupons is performed prior to the start of the experimental study for mechanical characterization. The coupon specimens are tested under uniaxial tensile load, as shown in Fig 4.1(a), using the 250 kN servo hydraulic universal testing machine available at the Central Instrumentation Facility (CIF) at IIT Guwahati. Gauge lengths of the coupon

specimens are 50 mm. The applied rate of tensile loading in the testing of coupons is kept constant at 0.08 mm/sec. Fig 4.1(b) shows a sample stress *vs.* strain plot as obtained from the tensile testing of the coupons. It is observed that the average yield stress value of the steel material is 255 MPa, whereas the average ultimate stress value is observed to be 430 MPa. Youngs Modulus of the steel is found to be 2.12 x 10^5 MPa. The shear modulus of the neoprene and butyl rubber material are around 0.9 and 0.8, respectively, while, the hardness of both rubber materials are in the range of 60±5 and 55±5 (IRHD), respectively.

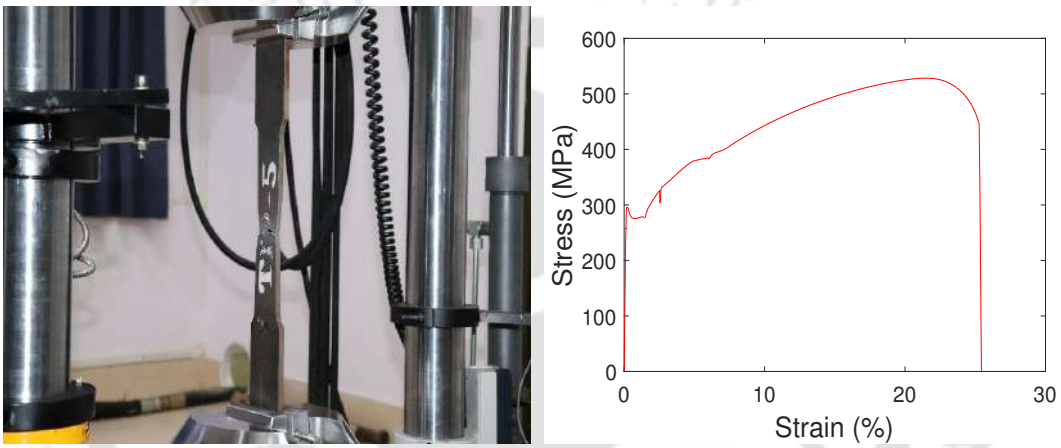

(a) (b)

Figure 4.1: (a) Tensile testing of coupon specimen, (b) Sample stress *vs.* strain curve

4.3 Specimen Details

Total eight HyBRB specimens are fabricated for experimental evaluation under uniaxial cyclic loading. These specimens are primarily divided in two categories based on the type of infill material. Each category of HyBRBs consists of four specimens, two with discontinuous infill layers of different geometries and other two with continuous infill layers of the same material type. Mild steel of grade Fe250 and thicknesses of 10 and 12 mm are used for fabrication of the components of the HyBRB and joint regions, respectively. The dimensions of the brace core, end stiffeners, weld specifications and joint details are decided based on the maximum design axial load (in compression and tension) on the HyBRB. The details of the restrainer pair are decided considering the maximum expected lateral thrust on the inner walls of the restrainer pair. Following sub-sections provide details of all

the components of the HyBRB along with relevant information on its different variants.

4.3.1 Core Details

The central steel core is cut in the shape of a double headed spoon as shown in Fig 4.2. The length of the steel core is divided into three zones: (a) central rectangular yielding zone of cross-sectional area 50 mm × 10 mm and length (L_c) 1000 mm, (b) outer most rectangular zone of cross-section 110 mm × 10 mm and length (L_j) 200 mm and (c) trapezoid shaped transition zone of a diverging cross-section of length (L_t) 50 mm, as shown in Fig 4.2(a). HyBRB is primarily designed to dissipate energy through axial yielding of the central rectangular region of the core. End regions of the steel core are stiffened by two stiffeners, inserted perpendicularly at its both ends as shown in Fig 4.2(b), to ensure elastic behaviour. The central flat region, designed for restrained buckling, is designated as plastic zone. The trapezoidal region between elastic and plastic zones is defined as transition zone. Two square steel plates of size 200 mm × 200 mm and thickness 12 mm are welded at both ends of the stiffened end zone of the HyBRB. Arrangement for double pin connection is made at both ends of the HyBRB as shown in Fig 4.2. Two semi-circular steel strips of length (L_{con}) 130 mm and width (B_{con}) 120 mm are welded to the square steel plates at both ends, as shown in Fig 4.2(b,d). Geometric details of the stiffened steel core of the proposed HyBRB are furnished in Table 4.1.

Table 4.1: Geometric details of core segment of the proposed HyBRB

Specimen	L_{HyBRB}	L_c	B_c	L_t	B_t	L_j	B_j	L_{con}	B_{con}
HyBRB core	1785	1000	50	50	110	200	110	130	120

NOTE: L_{HyBRB} = total length of HyBRB, B_c, B_t, B_j are width of core at plastic, transition and elastic zones, respectively.

4.3.2 Restrainer Details

The restraining member of HyBRB specimens consists of stiffened steel sections made from the mild steel plate of thickness 10 mm. Two plates of cross-section 120 mm × 10 mm and length 1100 mm are cut and stiffened with steel strips on the outer surface of both the flat plates as shown in Fig 4.3. Two longitudinal

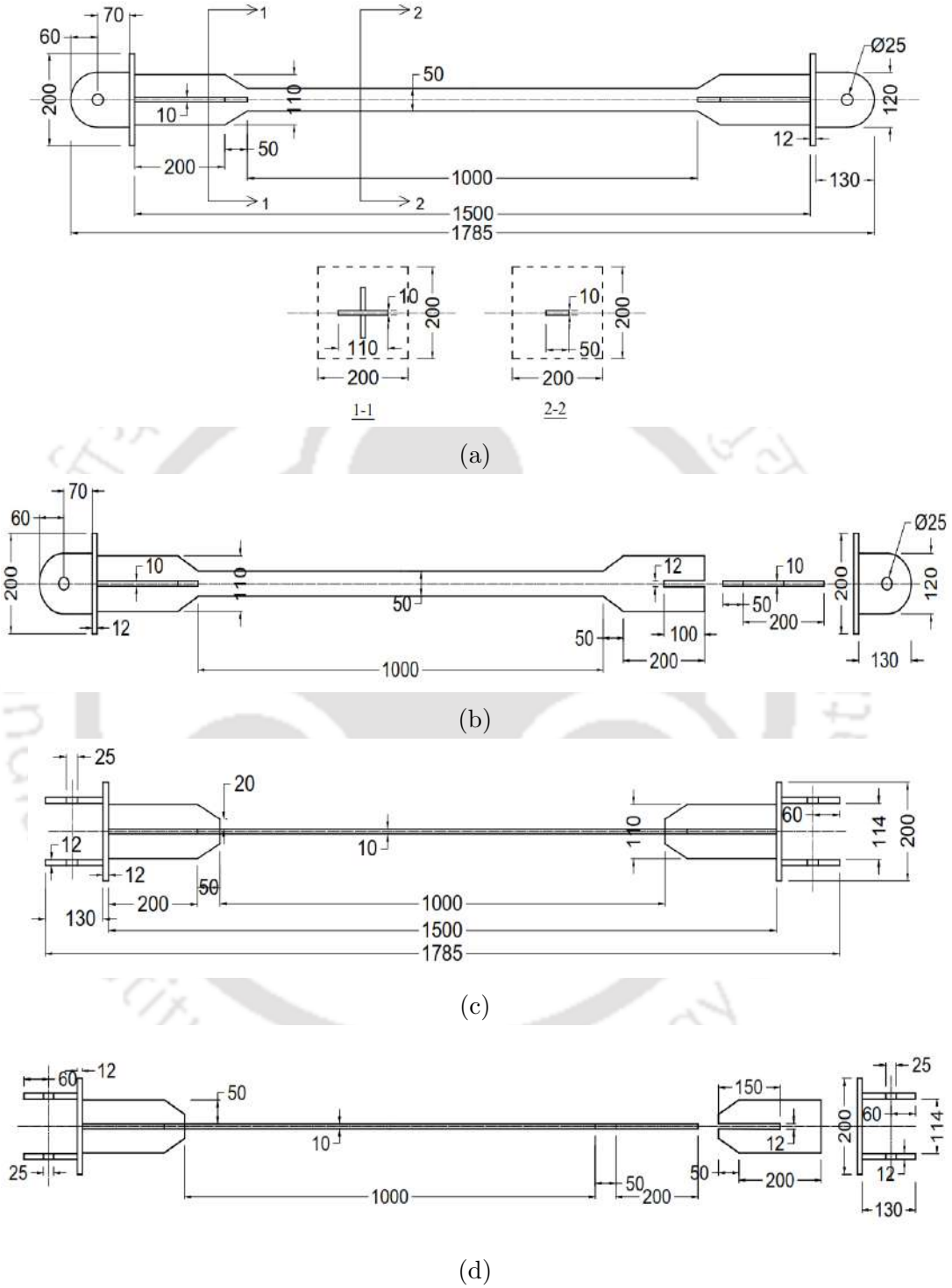

Figure 4.2: Details of (a) assembled core (top view); (b) disassembled core (top view), (c) assembled core (side view); (d) disassembled core (side view)

stiffeners of cross-section 20 mm × 10 mm and length 1100 mm are placed at a c/c distance of 30 mm and four numbers of transverse stiffeners are then placed at a c/c distance of 190 mm. Both longitudinal and transverse stiffeners are welded properly with both the plates for their flexural strengthening to prevent global buckling of the HyBRB core. The pair of stiffened restrainer plates are then connected using 30 numbers of stainless steel bolts of diameter 10 mm as shown in Fig 4.3. Longitudinal slots of length 100 mm and width 12 mm are cut on both ends of the restrainer pair for allowing movement of the end stiffeners of the steel core. Design of the restrainer pair and their connection arrangement ensures that negligible axial load is transferred to the restrainer pair during an experimental program or any seismic event.

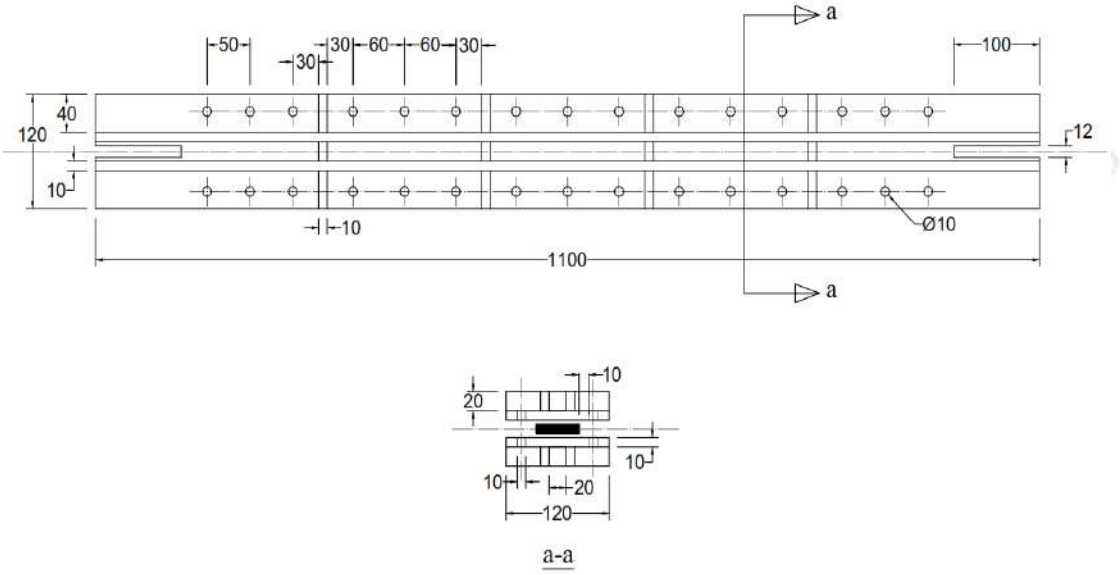

Figure 4.3: Details of restraining mechanism

4.3.3 Details of HyBRB Variants

Phase-I of experimental investigation considers a total of four number of specimens for evaluation of their mechanical characteristics. Two specimens from each category with continuous infill layers, designated as, HyBRB-A1/A2 and HyBRB-B1/B2, are considered for experimental investigation. All the specimens have similar steel core and joint specifications. The HyBRB is designed in such a way that the restrainer pair remains undamaged and only the deformed/buckled steel core (local restrained buckling) needs to be replaced after completion of an ex-

periment or any other event. Table 4.2 presents the geometric details of different components of the HyBRB specimens considered in the Phase-I of experimental study. The HyBRB components are painted with a two-coat anti-corrosion/anti-friction paint before assembling.

Table 4.2: Details of the HyBRB specimens considered in Phase-I

Core Zones (mm)	**Restrainer Details** (mm)	**Infill Material**		**HyBRB**
		Type	**Size**	
Plastic zone 1000×50×10; ***Transition zone***	Two plates (1000×120×10) stiffened	Neoprene	1000×50×3	A1
				A2
50×10 to 110×10; ***Elastic zone*** 200×110×10	longitudinally and connected with 10ϕ bolts	Butyl	1000×50×3	B1
				B2

4.4 Experimental Setup

A detailed experimental program is planned to evaluate the parameters which influence the seismic performance of HyBRB specimens. Both the variants of test specimens are subjected to cyclic loading using a servo hydraulic actuator available in the Structural Engineering Laboratory of Civil Engineering Department, IIT Guwahati. Fig 4.4(a) shows the schematic diagram of test assembly with a diagonally connected HyBRB specimen. Accordingly, a test facility is fabricated for performance evaluation of the HyBRB specimens as shown in Fig 4.4(b). One end of the HyBRB is connected to the vertical element of the test assembly, which is hinged at bottom and connected to the swivel head of the actuator at top, while the other end of HyBRB is connected to the strong floor as shown in Fig 4.4. One end of the actuator is connected to the strong wall while its other end is connected to the vertical element of the test assembly, as shown in Fig 4.4. Both ends of the HyBRB specimen are pin jointed with the help of high strength friction grip bolts of grade 8.8 and diameter 25 mm, acting as pins. The center lines of the HyBRB, the vertical element of the test assembly and the actuator are aligned in the same vertical plane to prevent eccentric loading to the test specimen. Loading arrangement, shown in the Fig 4.4, ensured application of cyclic axial load in the test specimens. Two lateral roller supports are employed to avoid any out-of-plane

displacement of the test specimen and the test assembly.

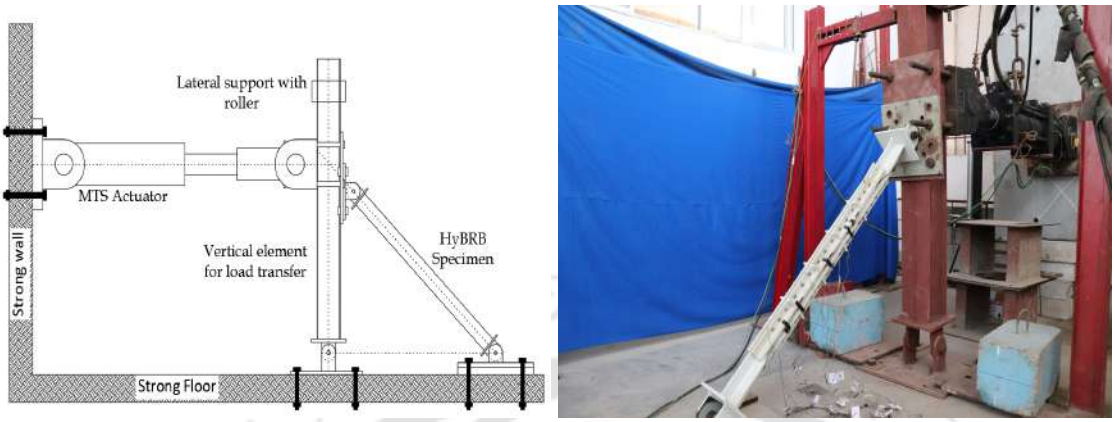

(a) (b)

Figure 4.4: Experimental set-up of HyBRB: (a) schematic diagram, (b) photograph of test set-up

4.5 Loading Protocol

A horizontal displacement protocol, as shown in Fig. 4.5, is applied through a 1000 kN capacity servo-hydraulic actuator (make: MTS Inc., USA) having a stroke length of ±250 mm. Applied displacement protocol is a sequence of triangular cyclic displacements corresponding to ±0.5%, ±0.75%, ±1%, ±1.5%, ±2%, ±2.5% and ±3% axial strain of the steel core yielding zone, with three repetitions of each displacement cycles. The frequency of the applied displacement protocol is kept at a constant rate of 0.025 Hz. Application of command protocol to the servo-hydraulic actuator and acquisition of feedback signal are carried out by the built-in data acquisition system (DAQ) of the controller (make: MTS Inc., USA, Model: FlexTest-GT).

4.6 Instrumentation

Sides of the plastic zone of the flat steel core and the outer surfaces of the restrainer are instrumented with strain gauges to record the strain values during experiments. A total of ten electrical strain gauges (make: TML, Japan, Model: Type FLA-6-350-11-1L) having resistance of 350 Ω and gauge length of 6 mm are employed. Four strain gauges are attached to the steel core to measure the axial strains of the steel core. These are placed at the center of both the open sides of the steel

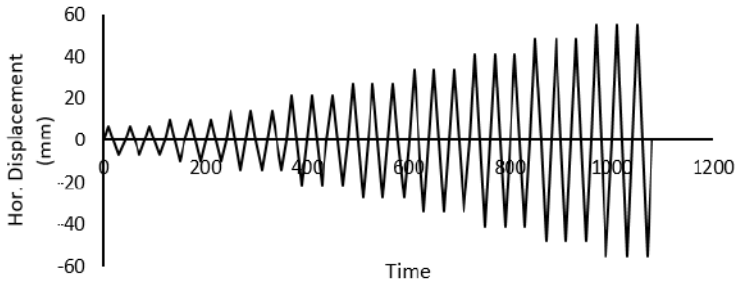

Figure 4.5: Applied displacement history for all HyBRB specimens

core and at two quarter points of the opposite open sides of the core as shown in Fig. 4.6(a). Three strain gauges, at center and both quarter points, on each component of the restrainer pair are attached to measure the longitudinal strain as shown in Fig. 4.6(b). Acquisition of the strain values is carried out using a DAQ (make: HBM, Germany, Model: MGC plus) having 20-bit resolution. A sampling frequency of 50 Hz is considered for all the four experiments. Axial force-displacement responses of the test specimens are measured using the built-in load cell and the tempo-sonic displacement sensor of the servo-hydraulic actuator.

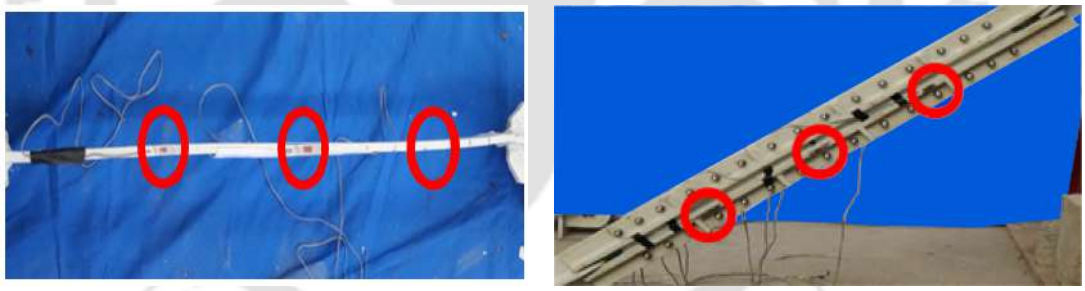

(a) (b)

Figure 4.6: Strain gauge locations on (a) steel core, (b) restraining component

4.7 Experimental Results and Discussions

In this section, discussion on the results obtained from the experimental study on two types of HyBRBs is presented. HyBRB specimens A1 and A2 have continuous neoprene rubber pads of length 1000 mm as infill layers, while, HyBRB specimens B1 and B2 have continuous butyl rubber pads of the same length as infill layers.

The test specimens are subjected to a cyclic displacement protocol of increasing amplitudes corresponding to different levels of axial strains in the steel core. HyBRB specimens developed in this study have excellent potential for practical implementation as structural dampers because of their comparable compressive and tensile strengths, with no sign of global buckling. The key issues/parameters evaluated in this experimental investigation are: (i) restrained buckling mode formations in HyBRB core, (ii) hysteretic behaviour, (iii) compression and tension strength adjustment factors, (iv) effective stiffness, (v) energy dissipation capacity and (vi) equivalent viscous damping.

4.7.1 Restrained Buckling of HyBRB Core

It is observed that the tensile and compressive strengths of the HyBRB specimens are comparable under cyclic loading. Also, higher order restrained buckling modes of the steel core are observed visually at higher displacement amplitudes with no sign of damages in connection bolts and welds. Further, no appreciable lateral deformation in the restrainer is observed. This establishes that the global buckling of the HyBRB could be restrained effectively. The local deformation patterns of the core at the end of the testing under applied loading protocol are shown in Fig. 4.7. A sample distribution of strain developed in the restrainer pair corresponding to different axial strains is shown in Fig. 4.8. Longitudinal strains at the end of the restrainer pair are considered to be zero. Although the physical development of the restrained buckling modes can be observed through side openings, it is helpful to use the recorded data to assess the effectiveness of the restrainer for prevention of global buckling but allowing restrained buckling of the core. In small displacement amplitudes, restrainer and infill layer facilitate formation of higher modes of restrained buckling of the steel core about the weak axis until the axial load exceeds the critical buckling strength of the same about the strong axis. The presence of highly deformable rubber material enables accommodation of lower order weak axis buckling modes through axial compression of the thick infill material layers.

The strain distribution in the restrainer wall of HyBRB-B1 specimen due to restrained buckling about the weak axis of the steel core is shown in Fig. 4.8(a). Flexural deformation of the outer surface of restrainers is not appreciable as the corresponding strain values are very small. During the initial three cycles, first

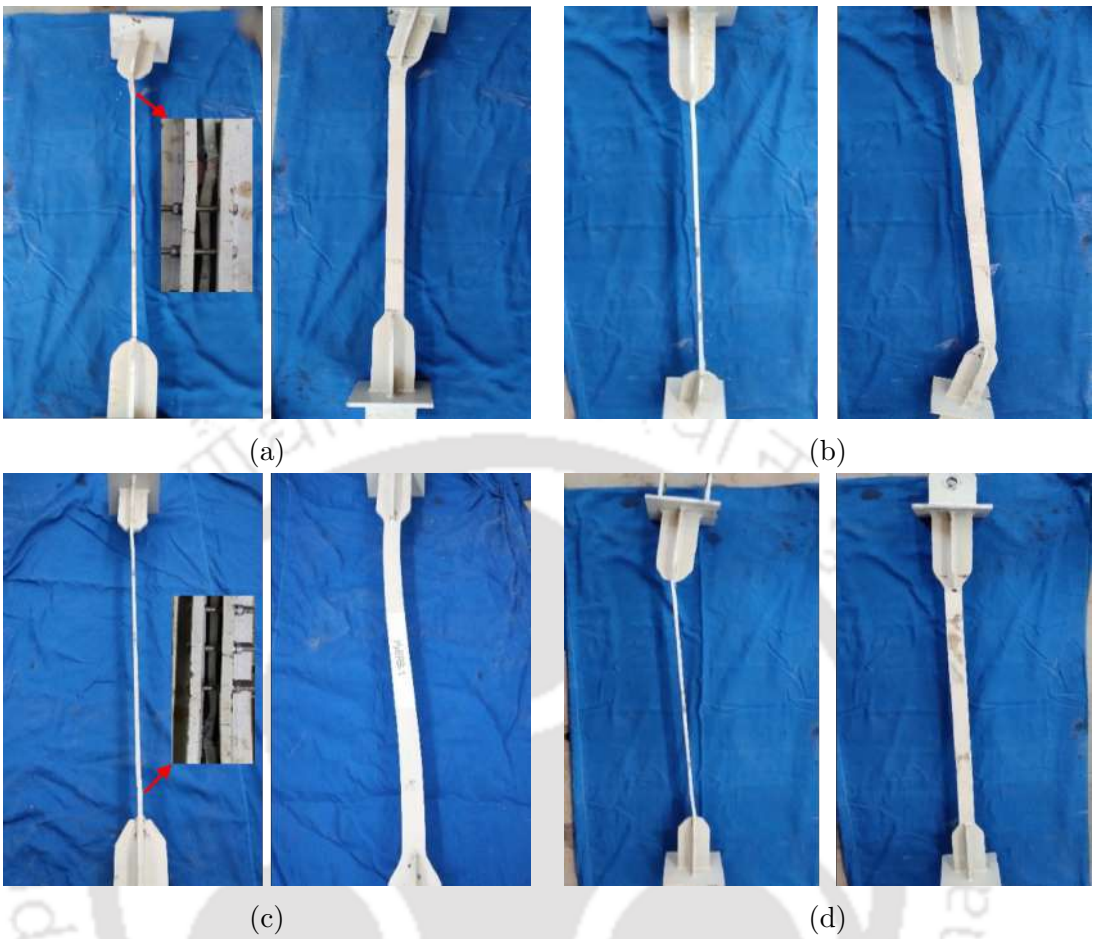

Figure 4.7: Deformed shapes of steel cores on disassembling specimens (a) HyBRB-A1, (b) HyBRB-A2, (c)HyBRB-B1 and (b) HyBRB-B2

order restrained buckling modes of HyBRB core are observed which is followed by initiation of third order buckling mode at 1.5% axial strain of core plate. At 2% axial strain, 3rd order buckling about the weak axis can be seen. Beyond this, initiation of buckling mode about the strong axis of the HyBRB core is observed. At the end of 3% axial strain, high tensile strain values are recorded on strain gauges placed at both quarter points of steel core with negligible strain experienced at the center of the core as shown in Fig. 4.8(b). This validates the formation of restrained buckling modes about the strong axis of the HyBRB core at higher axial displacement, which is evident during experiment. Moreover, on disassembling the restrainer pair, a permanent 2nd order strong axis buckling is observed along with visible weak axis buckling as shown in Fig. 4.7(c). It may also be mentioned that the observed residual strain in the steel core is in the range

of 0.3-0.4% which is quite low as compared to the maximum applied strain of 3%. This attribute of HyBRBs will ensure sufficient safety of the non-dissipative structural elements against severe seismic activities.

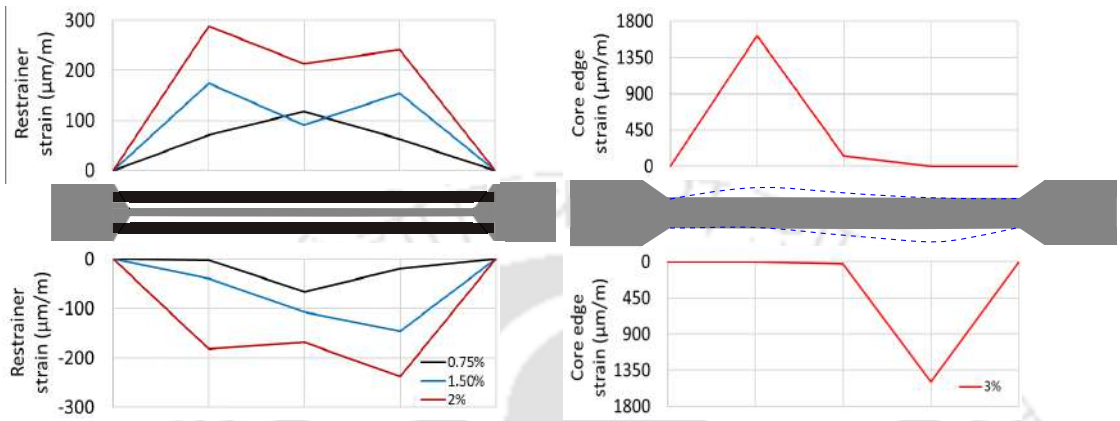

(a) (b)

Figure 4.8: Strain variation along the length of (a) restrainer walls and (b) core edges of a sample HyBRB specimen (B1) at different axial strain amplitudes

Strain time history of the restrainer wall at the center and corresponding axial strain of steel core plate of the HyBRB-B1 specimen is displayed in Fig 4.9. Peak value of strain at the center of the restrainer wall is observed to be much smaller than the yield strain of the material used. These data show that restrainers in the form of stiffened steel plates are found to be highly effective in controlling the global buckling of specimens. It may also be mentioned that the same restrainer pair is used in multiple experiments by replacing the HyBRB core only.

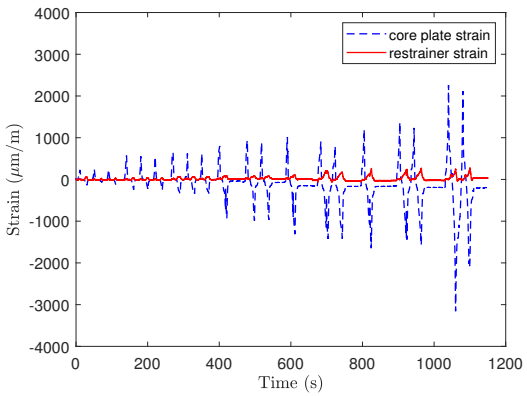

Figure 4.9: Strain time history at the center of restrainer of HyBRB-B1

4.7.2 Hysteretic Behaviour

The HyBRB specimens under investigation exhibited stable hysteretic behaviour with significant strength and stiffness at higher displacement amplitudes due to formation of buckling mode about the strong axis. Development of restrained buckling about the strong axis of the core is initiated at about 1.5%-2% of axial strain following initial restrained local buckling about the weak axis. This results in increased stiffness at a higher axial strain, which in turn helps in achieving this unique shape of hysteresis loops of the HyBRBs. This unique characteristic of the HyBRB specimens is likely to reduce residual displacement of structural systems. The infill layer arrangements adopted in this study play a vital role in determining the shapes of hysteresis loops and their energy dissipating characteristics. During the initial applied loading, energy dissipation in the HyBRBs takes place mainly due to shear deformation in the neoprene/butyl rubber infill layer until an axial strain of about 1%. Thereafter, energy is dissipated predominantly through axial yielding of the steel core during higher order restrained buckling about the weak strong axes of the core, in succession. Fig. 4.10 displays force-displacement responses of HyBRB specimens corresponding to each displacement amplitude. HyBRB A1, A2 and B1 showed comparable capacities in both tension and compression phases of the applied loading protocol. However, specimen B2 exhibited a slightly lesser capacity in compression during the final loading cycles because of rotation of the transition zone of the specimen, which may be due to imperfection in fabrication.

4.7.3 Compression Strength Adjustment Factor (β)

The compression strength adjustment factor represents the increase in compressive strength with respect to corresponding tensile strength at the same strain level. It is defined as the ratio of maximum compressive force ($P_{\max\_c}$) to the maximum tensile force ($P_{\max\_t}$) of the specimen.

$$\beta = \frac{P_{\max\_c}}{P_{\max\_t}} \tag{4.1}$$

The values of β at the end of applied displacement protocol for different variants of HyBRB are presented in Table 4.3. This factor is found to be in the range of 0.85

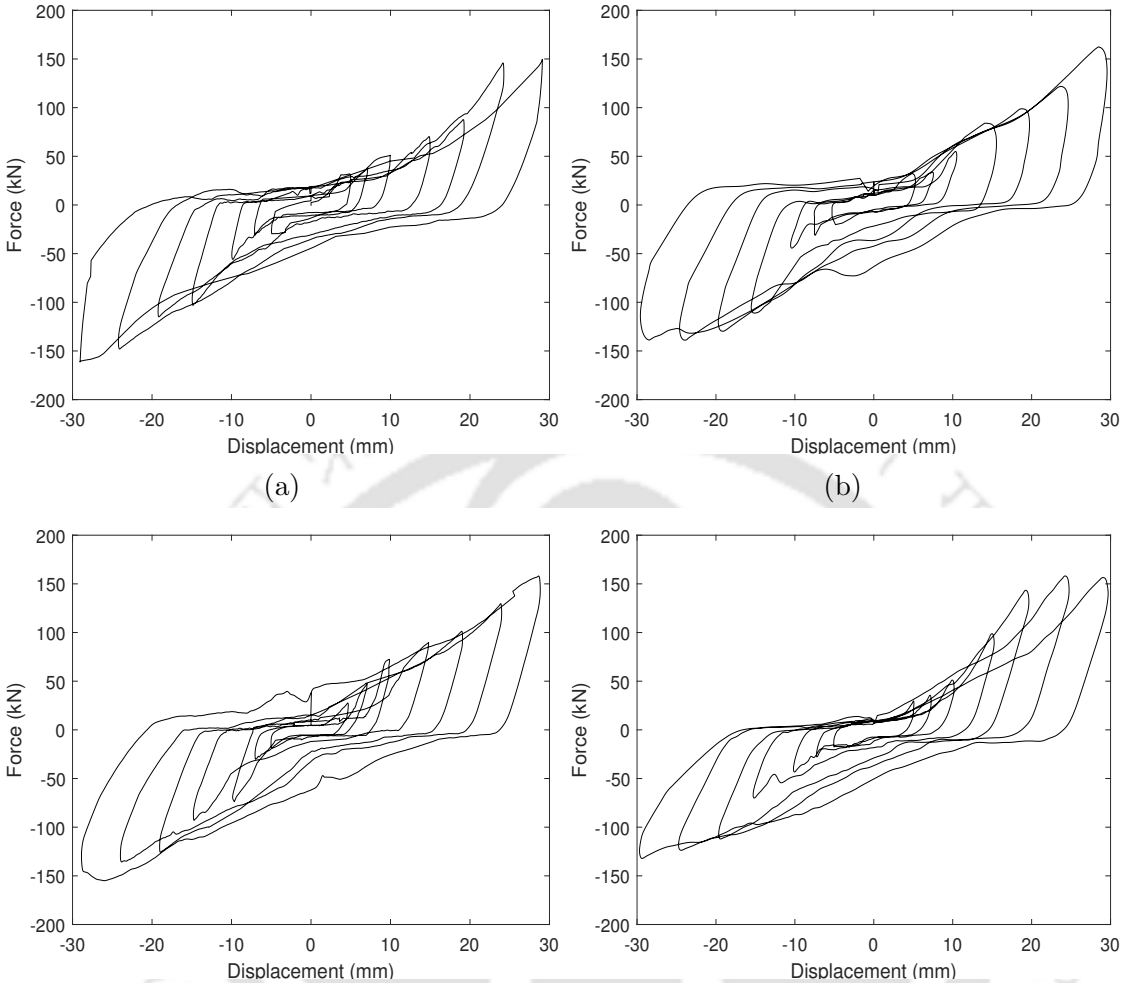

Figure 4.10: Experimental force-displacement hysteretic behaviour of specimens: (a) HyBRB-A1, (b) HyBRB-A2, (c) HyBRB-B1 and (d) HyBRB-B2

to 1.1. Past studies suggested the value of β should be less than 1.3 (AISC 341-10, 2010; Wu et al., 2014; Chen et al., 2011). Infill layers allow restrained buckling of the steel core about its weak axis until the critical buckling load about the stronger axis of core is smaller than the applied axial load, at a particular strain level. Beyond this strain loading, restrained buckling of the steel core about the strong axis initiates due to provision of movement along both the open sides of the steel core. The cores of both HyBRB-A and B specimens are observed to buckle significantly about their strong axes after 2% axial strain, as shown in Fig 4.7 and thus contributes to achieve higher compressive strengths.

4.7.4 Strain Hardening Factor (Ω_h)

The tension-strength adjustment factor represents the strain-hardening property of a HyBRB, i.e., the tensile response of the specimen compared to its yield strength measured from coupon testing. This factor is defined as the ratio of maximum tension capacity to design tensile yield strength, computed as the product of core area (A_c) and core yield stress, (σ_y).

$$\Omega_h = \frac{P_{\max\_t}}{R_y P_{ysc}} \tag{4.2}$$

where, R_y is the material overstrength factor. This factor is considered as unity if the yield strength of core (P_{ysc}) is computed using the yield stress determined from coupon test results.

A prior information on the maximum load carrying capacity of the HyBRBs beyond yielding is very important for the design of non-dissipative structural elements, from the capacity design perspective. The observed tensile strength adjustment factor (Ω_h) values refer to the strain hardening capability of the tested HyBRB specimens. Value of Ω_h typically varies depending on the manufacturing process, plastic zone length of the steel core and other features of the HyBRB. Generally, this value should always be less than 1.5. The values of Ω_h for the tested HyBRB specimens corresponding to the final displacement amplitude are presented in Table 4.3. It is observed that the value of this factor for all specimens lies in the range of 1.16 to 1.27.

4.7.5 Effective Axial Stiffness (K_{eff})

Effective axial stiffness, K_{eff} of the HyBRB specimens at each axial loading cycle is computed using the following expression:

$$K_{\text{eff}} = \frac{|P_{\max\_t} - P_{\max\_c}|}{|u_{\max\_t} - u_{\max\_c}|} \tag{4.3}$$

where, $u_{\max\_t}$ and $u_{\max\_c}$ are the maximum displacements in tension and compression phases of the loading protocol, respectively.

Stiffness of HyBRB specimen depends on the details of the steel core as well as the restraining mechanism (including infill material layers). Present study includes

evaluation of HyBRB specimens having steel core and restrainer pair of constant geometries. So, the infill layer arrangement is the only parameter, which affects the effective stiffnesses of HyBRB specimens. The values of K_{eff} of the HyBRB specimen at the end of the applied displacement protocol are presented in Table 4.3. The present study reveals that the type A specimens have lower axial stiffness values as compared to that of the type B specimens as shown in Fig 4.11(a). Infill material used in the case of type B specimens is less compressible as compared to that of type A specimen, which leads to marginally higher values of K_{eff} observed in type B specimen.

4.7.6 Energy Dissipation (W_d)

The amount of hysteretic energy dissipated for any kind of damper is an important measure of its seismic performance. It can be computed by evaluating the area under the force-displacement curve corresponding to a particular displacement amplitude. Energy dissipation capacities per hysteresis loops of HyBRB specimens corresponding to final displacement amplitude are reported in Table 4.3. The energy dissipation potentials of the HyBRB specimens are displayed in Fig. 4.11(b). It is evident that the energy dissipation rate of the tested HyBRBs increases with the increase in axial strain level as compared to the nearly linear relationship observed in conventional BRBs. Dissipation of energy is similar for both the variants of HyBRB at lower displacement protocols, while, type A specimens exhibited slightly higher energy dissipation capacities than that of type B with increased displacement amplitudes. The higher energy dissipation per cycle in case of type A specimens is due to the high damping of neoprene rubber layers used as infill material. The rate of energy dissipation per cycle is observed to be higher in type A specimens than that of type B specimens for large displacement amplitudes.

4.7.7 Equivalent Viscous Damping Factor (ζ_{eq})

Equivalent viscous damping factors of HyBRB specimens are computed from their axial hysteretic force-displacement behaviour. The enclosed area under the hysteretic loop represents the energy dissipated by the specimen. Equivalent viscous damping factor ζ_{eq} of HyBRB specimens is computed from the energy dissipated

in each loop using the equation as given below:

$$\zeta_{\text{eq}} = \frac{W_d}{2\pi K_{\text{eff}} u^2} \tag{4.4}$$

where, u is the absolute value of displacement amplitude of the loading cycle ($\simeq |u_{\max\_t}| \simeq |u_{\max\_c}|$).

ζ_{eq} values of the newly designed HyBRBs are on the higher side due to combined energy dissipation from axial deformation of the steel core as well as shear deformation of the infill layers. Fig 4.11(c) shows damping profiles of all the specimens with ζ_{eq} values ranging from 16% to 22% corresponding to the final displacement amplitude. The layers of neoprene/butyl rubber infill materials on both sides of the steel core contributes substantially in total energy dissipation through shear deformation at lower applied displacement levels resulting in enhanced equivalent viscous damping. HyBRB-A specimens showed slightly higher ζ_{eq} values than that of the type B specimens due to higher damping of neoprene rubber used in the type A specimens.

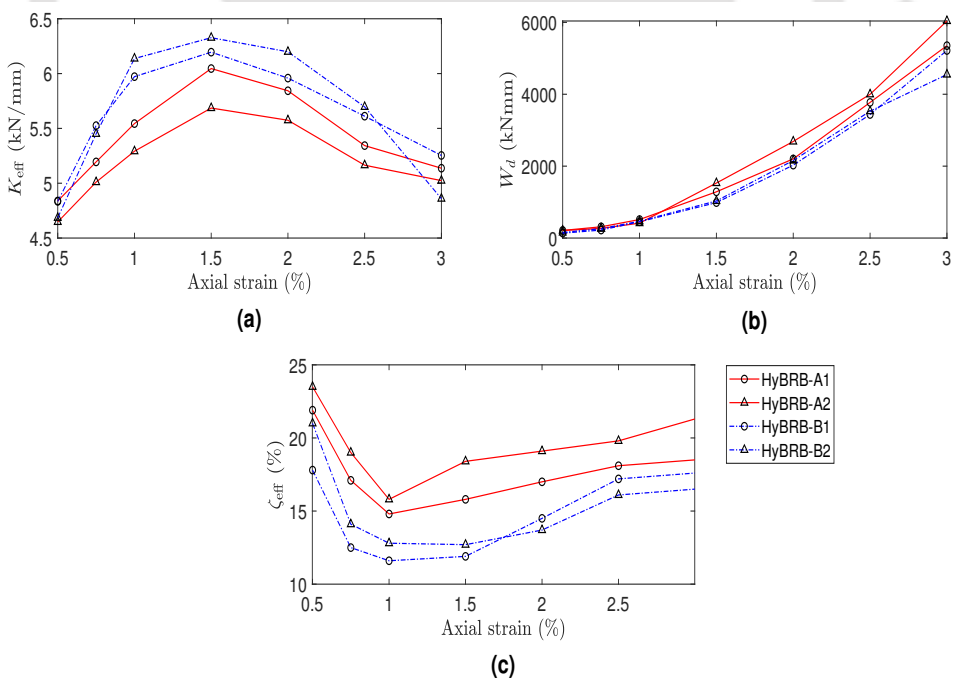

Figure 4.11: Variation of mechanical parameters: (a) effective axial stiffness, (b) energy dissipation, (c) equivalent viscous damping factor of the HyBRB specimens with axial strain level

Table 4.3: Mechanical parameters of tested HyBRB specimens with continuous infill layers at the final displacement amplitude (3% strain level)

Specimen	P_{max_t} (kN)	P_{max_c} (kN)	K_{eff} (kN/mm)	ζ_{eq} (%)	β	Ω_h	W_d (kNmm)
HyBRB-A1	148	160	5.13	18.5	1.08	1.16	5352
HyBRB-A2	162	139	5.02	21.3	0.86	1.27	6038
HyBRB-B1	160	155	5.25	17.6	0.97	1.25	5218
HyBRB-B2	158	134	4.86	16.5	0.85	1.23	4549

4.8 Concluding Remarks

This chapter presents a detailed report on experimental evaluation of the newly developed HyBRB specimens of categories- A and B, with continuous (1000 mm long) neoprene and butyl rubber material as infill layers, respectively. Technical specifications regarding the test specimens and the test setup arrangements are presented in detail. Loading arrangements and instrumentations specified for acquisition of test results are described. Experimental force-displacement hysteresis results of the tested HyBRB specimens are reported and the mechanical characteristics are computed. Finally, the behaviour of tested specimens and other key parameters which influence the performance of HyBRBs are critically discussed and compared for both the variants of HyBRB under consideration. The major conclusions that are drawn from the results of Phase-I of experimental study are summarized as follows:

1. The newly developed HyBRB exhibited stable hysteretic behavior with comparable tensile and compressive load carrying capacity. All the mechanical parameters of the HyBRB fulfilled necessary design criteria.

2. Inspectable and detachable HyBRBs would allow visual monitoring and measurement of strains in the core and the restrainers for assessment of the damage state of the steel core. The damaged steel core can be replaced quickly after a seismic event, if needed.

3. The deformed shape of the HyBRB core at the end of the cyclic tests, strain distributions in the restrainer wall and core established that restrained buckling about weak axis occurred first and subsequently restrained buckling

about strong axis got initiated at about 2% core strain level. This resulted in enhanced strength of the HyBRB and hence increased energy dissipation at a higher strain level, which is likely to reduce residual displacement level in the structural systems after a high intensity seismic event.

4. Effective stiffness of the HyBRB with continuous butyl rubber infill layers is slightly higher than that of the HyBRB with neoprene infill layers. However, energy dissipation capacity of the HyBRB with neoprene infill layers is marginally higher than that of the HyBRB with butyl rubber infill layers.

5. Both variants of the HyBRB provide higher level (about 20%) of equivalent viscous damping in lower axial core strain levels. Further, equivalent viscous damping factor (about 22%) in the higher strain level is also reasonably high for effective seismic response control of structural system.

Chapter 5

Experimental Investigations on HyBRBs with Discontinuous Infill Layers

Contents

5.1 General

Phase-I of the experimental investigation on the HyBRB specimens, with continuous infill layers, is discussed in Chapter 4. Specifications of the test specimens and experimental set-up are described in detail in the previous chapter. Further, application of loading protocol and acquisition of the responses of the HyBRB specimens under applied loading are also specified. This chapter discusses the Phase-II of the experimental investigation on four variants of the HyBRB specimens with different discontinuous infill types and geometries. Important seismic performance related parameters like, overall behaviour and deformed shapes, force-displacement hysteretic behaviour, effective axial stiffness and damping parameters are examined for the considered HyBRB specimens. Finally, a comparative study on the seismic performances of the HyBRB specimens, tested in Phase-II, is carried out.

5.2 Details of HyBRB Variants

Four specimens with continuous infill material layers have already been tested during Phase-I for their seismic performance evaluation. Four more specimens, with different infill material types and geometries, are considered for performance evaluation in Phase-II of the experimental program. As discussed earlier, neoprene and butyl rubber materials are utilized as infill layers, between the core and restrainer pair. Two different lengths, e.g., 120 mm and 50 mm, of rubber materials of each type are adopted. The infill layers on each flat side of the steel core consists of three pads of either 120 mm or 50 mm length, placed at a c/c distance of 250 mm. The details of different variants of HyBRB specimens considered for Phase-II of experimental study are presented in Table 5.1. All the considered HyBRB specimens have steel core and end specifications of constant geometries, similar to those of the specimens used in Phase-I study. The components of the HyBRBs are painted with a two-coat anti-friction paint before assembling. The restrainer pair and connecting bolts are checked for damages after Phase-I testing and the same are considered for reuse in Phase-II experimental study as no damage has been observed.

Table 5.1: Details of the HyBRB specimens considered in Phase-II

Core Zones (mm)	Restrainer Details (mm)	Infill Material		HyBRB
		Type	Size	
Plastic zone 1000×50×10; ***Transition zone***	Two plates (120×1000×10) stiffened	Neoprene	120×50×3	A3
			50×50×3	A4
50×10 to 110×10; ***Elastic zone*** 200×110×10	longitudinally and connected with 10Φ bolts	Butyl	120×50×3	B3
			50×50×3	B4

5.3 Experimental Investigation

Phase-II of the experimental study includes investigation on total four numbers of specimens, two each from both categories. The components of the HyBRB specimens are fabricated and assembled as discussed in the preceding chapter. The test specimens are then connected to the test assembly for evaluation of their mechanical characteristics under the applied cyclic loading protocol. The test setup, loading arrangement and data acquisition process are same as that of the Phase-I experimental program.

5.4 Experimental Results and Discussions

This section discusses the seismic performance evaluation of the HyBRB specimens tested during Phase-II of the experimental program. The key parameters, related to seismic performance of the newly developed HyBRB specimens, under consideration in this experimental investigation are: (i) overall response and buckling formations of HyBRB core, (ii) hysteretic behaviour, (iii) compression and tension strength adjustment factors, (iv) effective stiffness, (v) energy dissipation capacity and (vi) effective viscous damping.

5.4.1 Restrained Buckling of HyBRB Core

The HyBRB specimens developed in this study have sufficient energy dissipation capacity for seismic response control of structures. All the specimens considered

in Phase-II investigation exhibit good hysteretic behaviour with comparable load carrying capacities in both tension and compression. No global buckling is observed in any of the HyBRB specimens. The presence of discontinuous infill layer helps in enhancing the energy dissipation capacities at low axial strains through shear deformation. Restrained buckling of the steel cores about the weak and strong axes, in succession, is observed for all specimens. This helps to achieve enhanced load carrying capacities and increased stiffnesses at higher displacement amplitudes in all specimens. The final deformation patterns of the steel cores of the HyBRB specimens are shown in Fig 5.1. The deformed shapes and figures in inset gives a visual confirmation of the higher order restrained buckling mode formations inside the restrainer pair. All the specimens, except specimen HyBRB-B3, underwent buckling about the strong axis at higher axial core strain levels, as shown in Fig 5.1(c). The transition zone of the core of HyBRB-B3 specimen is observed to buckle in the out-of-plane direction, marginally reducing its load carrying capacity at higher strain levels.

Strain distribution profile along the length of the restrainer pair of specimen HyBRB-A3 at displacement amplitudes corresponding to axial strains of the plastic zone of core is shown in Fig 5.2. The steel core of specimen HyBRB-A3 exhibited a gradual shift from first mode to higher mode of buckling about its weak axis with increase in the axial core strain levels, as shown in Fig 5.2(a). Further, the core experienced restrained buckling about its strong axis at thigher displacement amplitudes (at around 2.5%-3% axial strain), which is evident from the strain distribution profile of the core, as shown in Fig 5.2(b). The same can also be verified by the deformed shapes of the specimen as shown in Fig 5.1(a), which in turn contributed in achieving enhanced effective stiffness as well as energy dissipation capacity.

Strain distribution profile along the length of the restrainer pair of specimen HyBRB-A4 at different axial strains is shown in Fig 5.3. The steel core experienced first order restrained buckling inside the restrainer pair about its weak axis at the initial applied displacement amplitudes (corresponding to 0.5% - 1.5% axial strain), as shown in Fig 5.3(a). At displacement amplitude corresponding to around 2% axial strain, the restrained buckling mode formation about the weak axis gradually started shifting from first order to higher order. The local buckling formation of the steel core is observed to be concentrated at one end of the steel

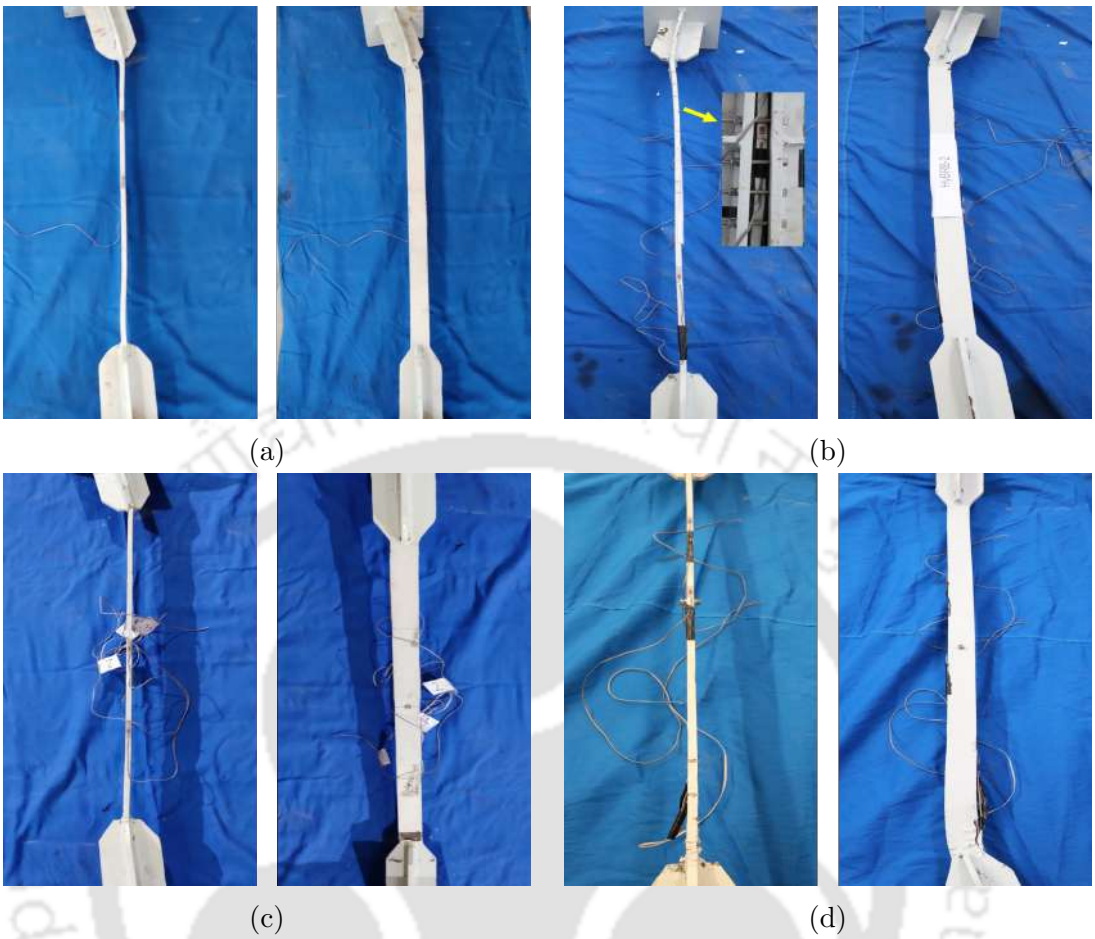

Figure 5.1: Deformed shapes of steel cores on disassembling specimens (a) HyBRB-A3, (b) HyBRB-A4, (c)HyBRB-B3 and (b) HyBRB-B4

core of the HyBRB specimen as observed from the strain distribution profile of the restrainer in Fig 5.3(a) and the same is evident from the deformed shapes of the steel core as displayed in Fig 5.1(b). This asymmetric deformation might be due to the eccentricity in loading, mobilized during the application of higher displacement amplitudes. At final displacement cycle, the steel core is observed to reach the peak restrained buckling mode about both the weak and strong axes simultaneously as shown in Fig 5.3(a-b). The strain variation profiles for the specimens HyBRB-B3 and B4 also confirmed the formation of multiple higher order buckling modes about both weak and strong axes, in succession, similar to those observed for the specimens HyBRB-A3 and A4.

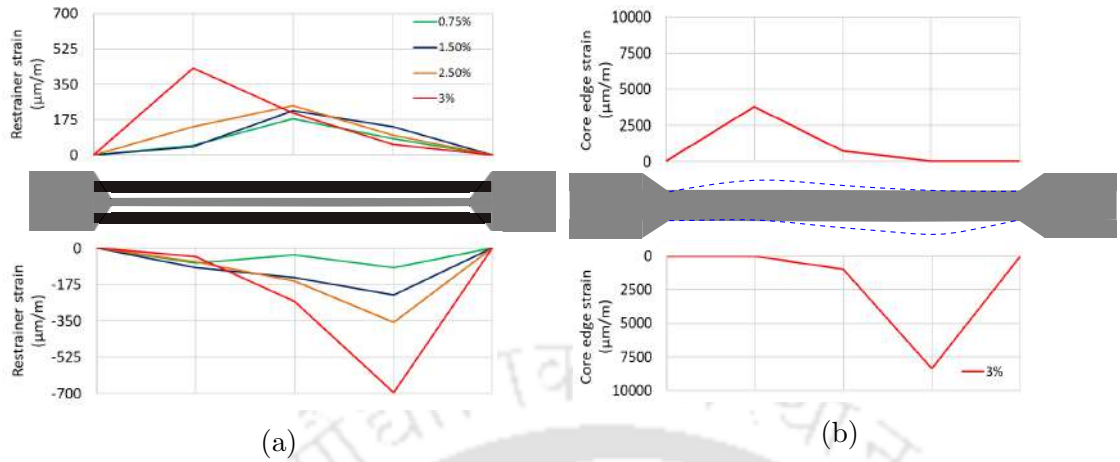

(a) (b)

Figure 5.2: Strain distribution profile along the length of restrainer pair of specimen HyBRB-A3

5.4.2 Hysteretic Behaviour

Both categories of the HyBRB specimens, subjected to applied loading protocol, exhibited stable axial force-displacement hysteretic behaviour with significant increase in strength at higher displacement amplitudes, as shown in Fig 5.4. Narrow central zone and wide end zones of the force-displacement hysteresis loops of the HyBRB specimens is due to the increase in their stiffnesses at higher displacement amplitudes. Increase in stiffness is attributed to switching of restrained buckling modes formation about weak axis to that about strong axis of the steel core, at about 1.5%-2% of axial core strain level. All variants, except HyBRB-B3, exhibited stable force-displacement hysteretic behaviour with comparable compressive and tensile strengths. In the case of specimen HyBRB-B3, compression load carrying capacity is observed to be marginally lesser due to out-of-plane deformation of the transition zone as discussed in the preceding section. Further, peak load carrying capacities in both tension and compression is found marginally higher in case of HyBRB specimens with discontinuous neoprene infill layers.

5.4.3 Compression Strength Adjustment Factor (β)

All HyBRB specimens with discontinuous infill layers, subjected to same axial displacement loading protocol, have β values of similar order. Past studies suggested that the value of this parameter should be below 1.3. β values for the tested HyBRB specimens are found to be in the range of 0.83 to 0.89 at the end of the

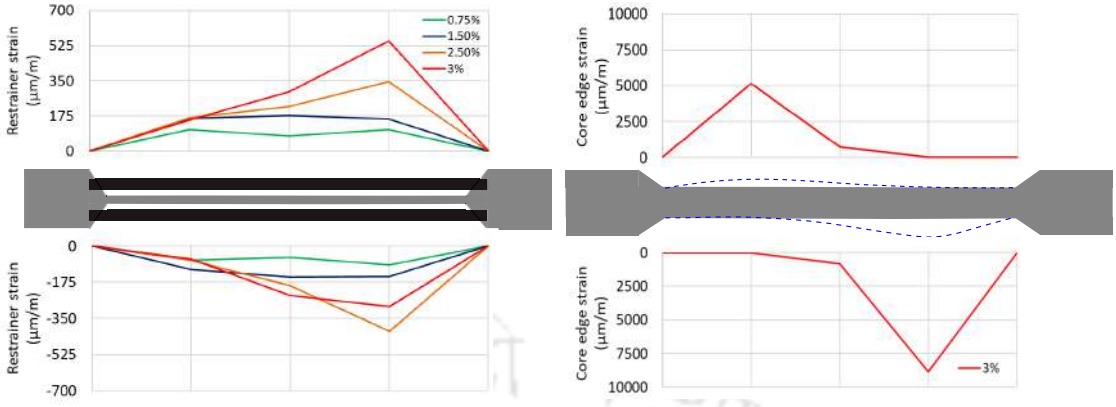

Figure 5.3: Strain distribution profile along the length of restrainer pair of specimen HyBRB-A4

cyclic loading protocol, as shown in Table 5.2, which indicates that the compressive strengths of HyBRB specimens are almost equal to their tensile strengths. This establishes the efficacy of the specimens to act as passive energy dissipating devices without any global buckling failure.

5.4.4 Strain Hardening Factor (Ω_h)

The values of Ω_h for all the HyBRB specimens corresponding to the final displacement amplitude of applied loading protocol are found to be in the range of 1.22 to 1.29 and are presented in Table 5.2. Ω_h values are observed to be slightly lower for the HyBRB specimens with 50 mm long infill layers than those of the specimens with 120 mm long infill layers, in each category. Use of longer discontinuous infill pads minimizes hard contact area between the core and restrainer and hence, carries higher tensile loads during loading and unloading cycles. On the other hand, provision of a relatively large hard contact area between the core and the restrainer, as seen in specimens with 50 mm long infill pads, results in lower Ω_h values of the respective specimens.

5.4.5 Effective Axial Stiffness (K_{eff})

Effective axial stiffnesses of the tested HyBRB specimens are calculated from their force-displacement hysteresis loops using Eq. 4.3. Fig 5.5 displays the profile of K_{eff} values of the HyBRB specimens of both categories corresponding to each axial strain level. Initial stiffnesses of the HyBRB specimens with butyl rubber as infill

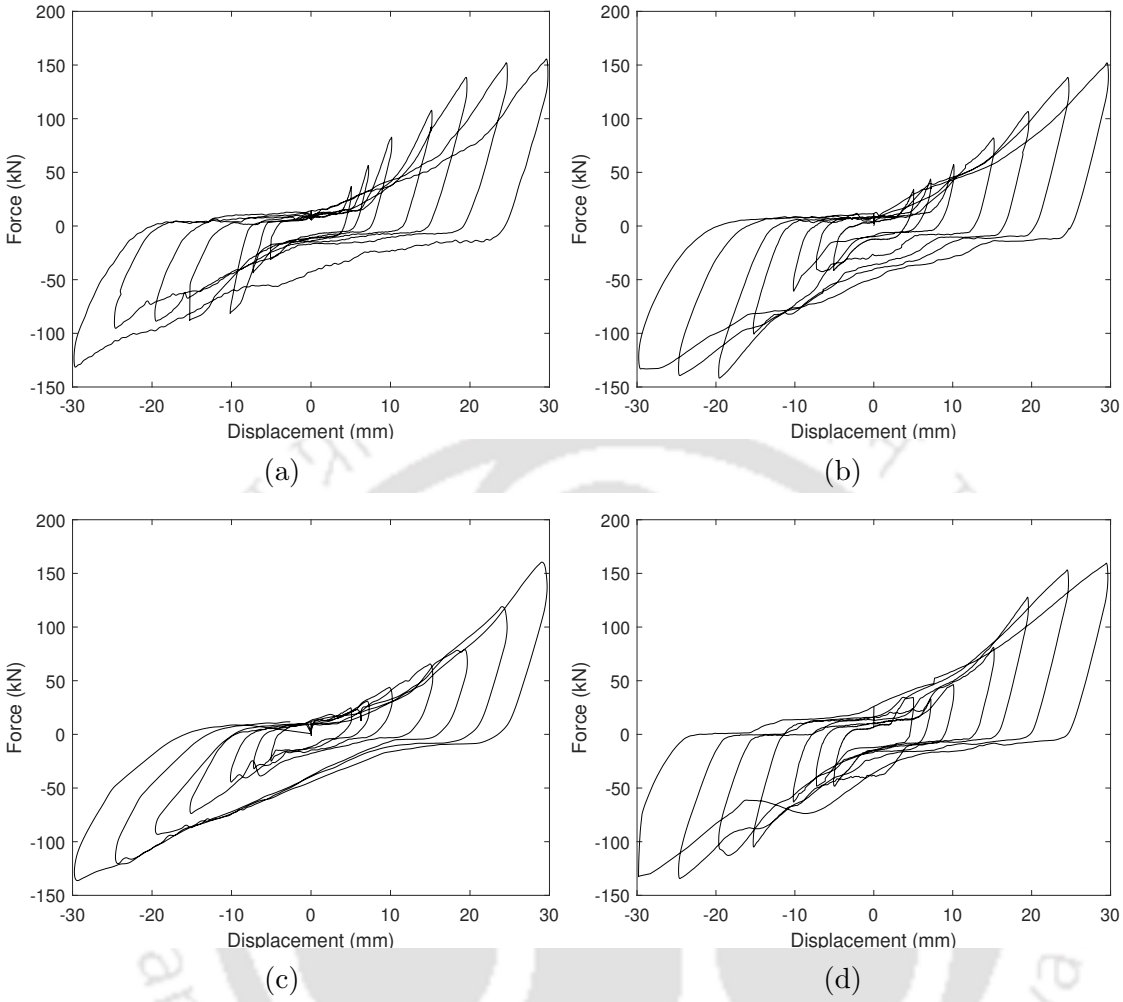

Figure 5.4: Experimental force-displacement hysteretic behaviour of specimens: (a) HyBRB-A3, (b) HyBRB-A4, (c) HyBRB-B3 and (d) HyBRB-B4

layer are observed to be on a slightly higher side than those of the specimens with neoprene rubber. Moreover, the HyBRBs with 50 mm long infill material pads in each category are observed to possess higher axial stiffness values under cyclic loading due to larger hard contact area between the core and the restrainer. Final stiffnesses of all the variants of the HyBRBs are found to be in the similar range with HyBRB-B specimens showing marginally higher effective stiffness values than those of HyBRB-A specimens, as displayed in Table 5.2.

Compared to the test results of Phase-I experimental study, the effective stiffnesses are found to be higher for all HyBRB variants which utilize butyl rubber as infill material irrespective of their geometries. Moreover, the rate of stiffness

degradation at larger displacement amplitudes is also higher for the specimens with butyl rubber than that of the specimens with neoprene rubber. This is mainly due to the nonuniform formation of restrained buckling modes about strong axis of the steel core of specimens with butyl rubber, as compared to that of the specimens with neoprene rubber, at higher axial core strain levels.

5.4.6 Energy Dissipation (W_d)

The quantification of the hysteretic energy dissipation potential (W_d) of a HyBRB is an important parameter for seismic design. The energy dissipation capacities per hysteresis loop of HyBRB specimens corresponding to different axial strain levels of plastic zone of steel core are displayed in Fig 5.5. Energy dissipation capacities are nearly similar up to strain level of 1% for all specimens. However, energy dissipation per cycle is observed to be higher for HyBRB specimens with 120 mm long infill layers of both material types. Further, HyBRB-A specimens showed marginally higher energy dissipation potential than that of HyBRB-B specimens at larger displacement amplitudes for respective infill pad lengths, as shown in Table 5.2.

When compared to the test results of Phase-I experimental study, it is observed that the energy dissipation per cycle of applied displacement amplitude is higher for specimens with continuous neoprene infill layers. Moreover, the rate of increase of energy dissipation at large axial strains is found to be higher for specimens with neoprene infill layers.

5.4.7 Equivalent Viscous Damping Factor (ζ_{eq})

Excellent equivalent viscous damping (ζ_{eq}) of around 20% is observed for all the variants of HyBRB specimens at initial axial strain levels. Higher ζ_{eq} values of the HyBRB specimens at lower displacement amplitude is observed mainly due to the presence of infill material layers in between the steel core and restrainer pairs. With further loading, ζ_{eq} values decrease initially, until higher order restrained buckling of steel cores about their weak and strong axes are initiated, at displacement amplitudes corresponding to axial strain of around 1.5%. Once the restrained buckling about strong axis is started, the rate of increase of equivalent viscous damping increases significantly for the all variants of HyBRB specimens. Overall viscous damping is observed to be higher for the HyBRB specimens with

neoprene infill layer. Also, the specimens with 120 mm long infill pads in each category exhibit higher damping potential than those of the specimens with 50 mm long infill pads of respective categories.

When compared with the test results of Phase-I experimental study, equivalent viscous damping is observed to be higher for the specimens with neoprene rubber than that of the specimens with butyl rubber for respective infill layer geometry. Also, equivalent damping is observed to be higher for the specimens with neoprene rubber at higher axial strain as compared to that of the specimens with butyl rubber.

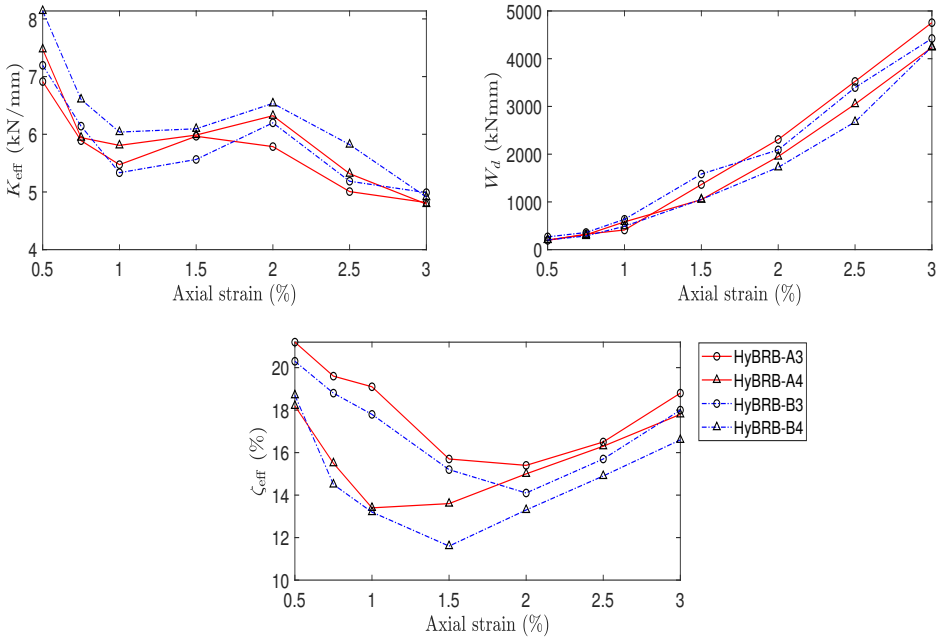

Figure 5.5: Variation of mechanical parameters: (a) effective axial stiffness, (b) energy dissipation, (c) equivalent viscous damping of the HyBRB specimens with discontinuous infill layers subjected to the applied displacement protocol

5.5 Concluding Remarks

This chapter presents a detailed report on the findings of the experimental evaluation of HyBRB specimens of two categories- A and B, each with two different discontinuous geometries. Experimental force-displacement hysteretic behaviour of these HyBRB specimens are reported along with their mechanical characteris-

Table 5.2: Mechanical parameters of HyBRB specimens with discontinuous infill layers at the final displacement amplitude (3% strain level)

HyBRB	$P_{\max\_t}$ (kN)	$P_{\max\_c}$ (kN)	K_{eff} (kN/mm)	ζ_{eq} (%)	β	Ω_h	W_d (kNmm)
A3	155.6	131.5	4.82	18.8	0.85	1.25	4755
A4	151.9	133.2	4.79	17.8	0.89	1.22	4248
B3	160.4	136.3	4.99	15.3	0.85	1.29	4423
B4	159.5	132.6	4.91	18	0.83	1.28	4236

tics. Deformed shapes, strain distributions in both the core as well as the restrainer of the HyBRB specimens are examined. All the variants of HyBRB provide reasonably high energy dissipation capacities in the low to high levels of axial core strain. Finally, comparison of mechanical characteristics of the tested HyBRB specimens, with both neoprene and butyl rubber having different geometries, is also presented.

The following conclusions are drawn on the basis of experimental study reported in this chapter:

1. Stable hysteretic behaviour with comparable tensile and compressive load carrying capacities were observed in the newly developed HyBRB specimens with different discontinuous infill layer geometries. Overall behavior of the tested HyBRB specimens established that the global buckling of the device core could be prevented effectively.

2. The deformed shape of the HyBRB core and the strain distribution profile at critical points of the core and restrainer pair confirm that restrained buckling about the weak axis occurred first, and later restrained buckling about the strong axis commenced at about 2% axial core strain level. This resulted in enhanced stiffness of the HyBRB and hence increased energy dissipation at higher strain levels which in turn would reduce the residual displacement in structures subjected to high intensity seismic events.

3. The core and restrainer pair of the specimens with shorter discontinuous infill layers experience larger hard contact area and hence provide higher axial stiffness. Whereas, specimens with longer discontinuous butyl layers experience smaller hard contact area between core and restrainer pair resulting in

lower axial stiffness.

4. Energy dissipation capacities of the HyBRB specimens with longer discontinuous infill layers is observed to be higher than those of the specimens with shorter discontinuous infill layers from each category. Further, the specimens with continuous infill layers possess higher energy dissipation and damping capacities than those of the HyBRBs with discontinuous infill layers. Each variant of the HyBRB provides high level of equivalent viscous damping in the range 18-20% in low to high axial strain level, which is reasonably high for effective seismic response control of structural systems.

Chapter 6

Simulation of Hysteresis Behaviour of HyBRBs

Contents

6.1 General

The Bouc-Wen model is widely used in the field of structural engineering for analytical simulation of hysteretic behavior of various types of structural elements. Bouc-Wen model parameters are adjusted to match the output of the model for simulation of corresponding experimental force-displacement hysteretic behaviour. The updated force-displacement loop is considered as a good approximation of the target hysteresis loop when the computed error obtained from the difference in experimental force-displacement response and output of the simulated model is negligibly small. This updated model can then be used to study the dynamic behavior of different systems with the tested structural elements or devices under different dynamic loadings.

6.2 Extended Bouc-Wen Model of Hysteresis

A dynamic system described by the following equation considers a hysteretic model $F[x(t), z(t); t]$, which was proposed by Bouc 1967 and later modified by Wen 1976 for better performance.

$$m\ddot{x}\left(t\right) + c\dot{x}\left(t\right) + F\left[x\left(t\right), z\left(t\right); t\right] = f\left(t\right) \tag{6.1}$$

where, m is the mass of the system, c is the viscous damping coefficient, $x(t)$ is the displacement and $f(t)$ is the external excitation.

The restoring force, $F[x(t), z(t); t]$ is expressed as:

$$F\left[x\left(t\right), z\left(t\right); t\right] = \alpha k x\left(t\right) + \left(1-\alpha\right) k z\left(t\right) \tag{6.2}$$

where, $\alpha k x(t)$ represents the pre-yielding component (instantaneous) and $(1 - \alpha)kz(t)$ is the post-yielding component, k is the stiffness of the system, α is the ratio of the post yield to initial stiffness, and $z(t)$ is a virtual displacement which controls the hysteresis shape.

Later, Baber and Noori (1985) modified the Bouc-Wen model of hysteresis by introducing degradation and pinching parameters, which enhanced the capacity of the model to simulate hysteresis loops. This modified model is known as the Bouc-Wen-Baber-Noori (BWBN) hysteresis model. Although the restoring force

as expressed in Eq. 6.2 remains same, the relation between $z(t)$ and $x(t)$ is modified as follows:

$$\dot{z}(t) = h(z(t)) \frac{A(\varepsilon)\dot{x}(t) - \upsilon(\varepsilon)\left(\beta|\dot{x}(t)||z(t)|^{n-1}z(t) + \gamma\dot{x}(t)|z(t)|^{n}\right)}{\eta(\varepsilon)} \tag{6.3}$$

where, functions $A(\varepsilon)$, $\upsilon(\varepsilon)$, $\eta(\varepsilon)$ and $h(z(t))$ represents hysteresis amplitude, strength degradation, stiffness degradation and pinching in the system, respectively.

The degradation functions are expressed in terms of the dissipated hysteretic energy $\varepsilon(t)$, which is given by:

$$\varepsilon(t) = (1-\alpha)\omega^2 \int_0^t z(\tau)\dot{x}(\tau)\, d\tau \tag{6.4}$$

Computing the values for $\varepsilon(t)$, the parameters $A(\varepsilon)$, $\eta(\varepsilon)$ and $\upsilon(\varepsilon)$ are determined as:

$$\begin{aligned} \upsilon(\varepsilon) &= \upsilon_0 + \delta_\upsilon \varepsilon(t) \\ A(\varepsilon) &= A_0 - \delta_A \varepsilon(t) \\ \eta(\varepsilon) &= \eta_0 + \delta_\eta \varepsilon(t) \end{aligned} \tag{6.5}$$

where, the values of δ_υ, δ_A and δ_η are constants which specify the amount of stiffness and strength degradation.

The pinching function $h(z(t))$ is expressed as:

$$h(z(t)) = 1 - \zeta_1(\varepsilon)\exp\left(-|z(t).sign(\dot{x}(t)) - qz_u|^2/\zeta_2^2(\varepsilon)\right) \tag{6.6}$$

where, $sign(\dot{x}(t))$ is the signum function of $\dot{x}(t)$, z_u is the last value of $z(t)$ which can be computed by;

$$z_u = \left[\frac{1}{\upsilon(\varepsilon)(\beta+\gamma)}\right]^{1/n} \tag{6.7}$$

and, the values of ζ_1 and ζ_2 are given by:

$$\begin{aligned} \zeta_1(\varepsilon) &= \zeta_0\left(1 - e^{-p\varepsilon(t)}\right), \\ \zeta_2(\varepsilon) &= (\psi + \delta_\psi\varepsilon(t))(\lambda + \zeta_1(\varepsilon)) \end{aligned} \tag{6.8}$$

where, p is a constant which controls the initial change in the slope, ζ_0 is a measure of the total slip, ψ is a factor to simulate the pinching behavior, δ_ψ is a constant

which measures the dispersion rate of the pinching phenomenon, and λ controls the variation of the parameters $\zeta_1(\varepsilon)$ and $\zeta_2(\varepsilon)$.

6.3 BWBN Models Corresponding to HyBRBs

A set of parameters, given by $X = \{\xi, \alpha, \beta, \gamma, n, \upsilon, \delta_\upsilon, A_0, \delta_A, \eta, \delta_\eta, p, \zeta_0, \psi, \delta_\psi, \lambda, q\}$, as mentioned in the preceding section defines the extended BWBN hysteresis model. This numerical study aims to identify these parameters from the experimentally obtained force-displacement response of the HyBRB specimens. To achieve this, a multi-objective optimization technique is adopted which was developed by Ortiz et al. (2013). The optimization technique uses a Non-dominated Sorting Genetic Algorithm (NSGA-II), developed by Deb et al. (2002), to minimize the values of the assumed objective functions by adjusting the model parameters. The objective functions used in the present study are as follows:

1. The absolute error computed from the experimentally measured displacement $x_n(t)$ and corresponding displacement $\hat{x}_n(t|X)$ computed from the BWBN model for a given set of above mentioned parameters X:

$$f_1(X) = \sum_{i=1}^{n} |x(t_i) - \hat{x}(t_i|X)|$$

2. The maximum error calculated from the displacement obtained from experiment $x_n(t)$ and the same obtained numerically using the BWBN model as:

$$f_2(X) = \max_{1 \le i \le n} \{x(t_i) - \hat{x}(t_i|X)\}$$

3. The error obtained from the total dissipated energy computed from experimental response ε_{total} and corresponding energy $\hat{\varepsilon}_{total|X}$ obtained from the BWBN model for the given set of parameters X:

$$f_3(X) = \left|\varepsilon_{total} - \hat{\varepsilon}_{total|X}\right|$$

4. The maximum error computed from the dissipated energy obtained from experimental record $\varepsilon_{total}(t_i)$ and the same obtained numerically using the BWBN

model as:

$$f_4(X) = \max_{1 \leq i \leq n} \{\varepsilon_{total}(t_i) - \hat{\varepsilon}_{total}(t_i|X)\}$$

The adjusted parameters corresponding to the best fit of the BWBN model are identified by optimizing the above mentioned objective functions. The list of the parameters for best fit of the experimental responses of the HyBRB specimens using the mentioned multi-objective optimization technique is shown Table 6.1.

Table 6.1: Best identified parameters of BWBN hysteresis model of the tested HyBRB specimens

Parameters	**HyBRB**							
	A1	**A2**	**A3**	**A4**	**B1**	**B2**	**B3**	**B4**
α	0.29	-0.1	0.29	0.3	0.28	0.29	0.08	0.22
β	1.98	1.72	1.08	2.67	0.14	2.78	1.38	1.77
γ	-1.92	-1.7	-1.05	-1.94	-0.1	-2.7	-1.35	-1.75
n	1.07	1.03	1	1.25	1.68	1	1.15	1.01
ν_0	0.71	0.17	0.15	1.24	0.13	0.95	1.4	0.39
δ_ν	0.59	0.3	0.37	0.04	2.81	0.84	0.03	0.28
A_0	2.51	3.82	2.81	2.8	4.54	2.44	2.3	2.89
δ_A	-8.07	-2	-0.33	-2.77	-5.5	-8.4	-4.31	-1.87
η_0	0.62	3.02	2.21	2.95	3.8	0.51	2.03	2.02
δ_η	8.37	2.82	1.31	1.72	6.93	3.99	4.57	2.95
p	9.06	9.75	7.09	1.69	9.57	5.31	1.34	9.32
ζ_0	-4.64	0.8	-3.43	-2.13	-5.8	0.67	0.57	-0.1
ψ	1.52	2.94	-1.78	1.99	1.05	1.68	2.77	3.59
δ_ψ	-1.29	-0.1	-0.02	0.87	-0.3	0.86	1.01	-0.17
λ	3.35	-1.7	1.58	1.72	5.27	3.99	-3.55	1.56
q	-0.2	0.02	0.65	-2.55	0.18	0.46	-0.56	1.11

Fig 6.1 shows a reasonably close match of the analytically simulated force - displacement response of the HyBRB specimens using the BWBN model with that recorded during the experimental investigation. The effective stiffness and damping parameters calculated from the simulated hysteresis loops are compared with that obtained from the experiments and these parameters are presented in Table 6.2. The errors computed for all three parameters of HyBRB specimens are found to be varying between 0.6 to 8.9%. The updated numerical model can further be used for computation of reasonably accurate seismic response of the structures retrofitted with HyBRBs for seismic response control.

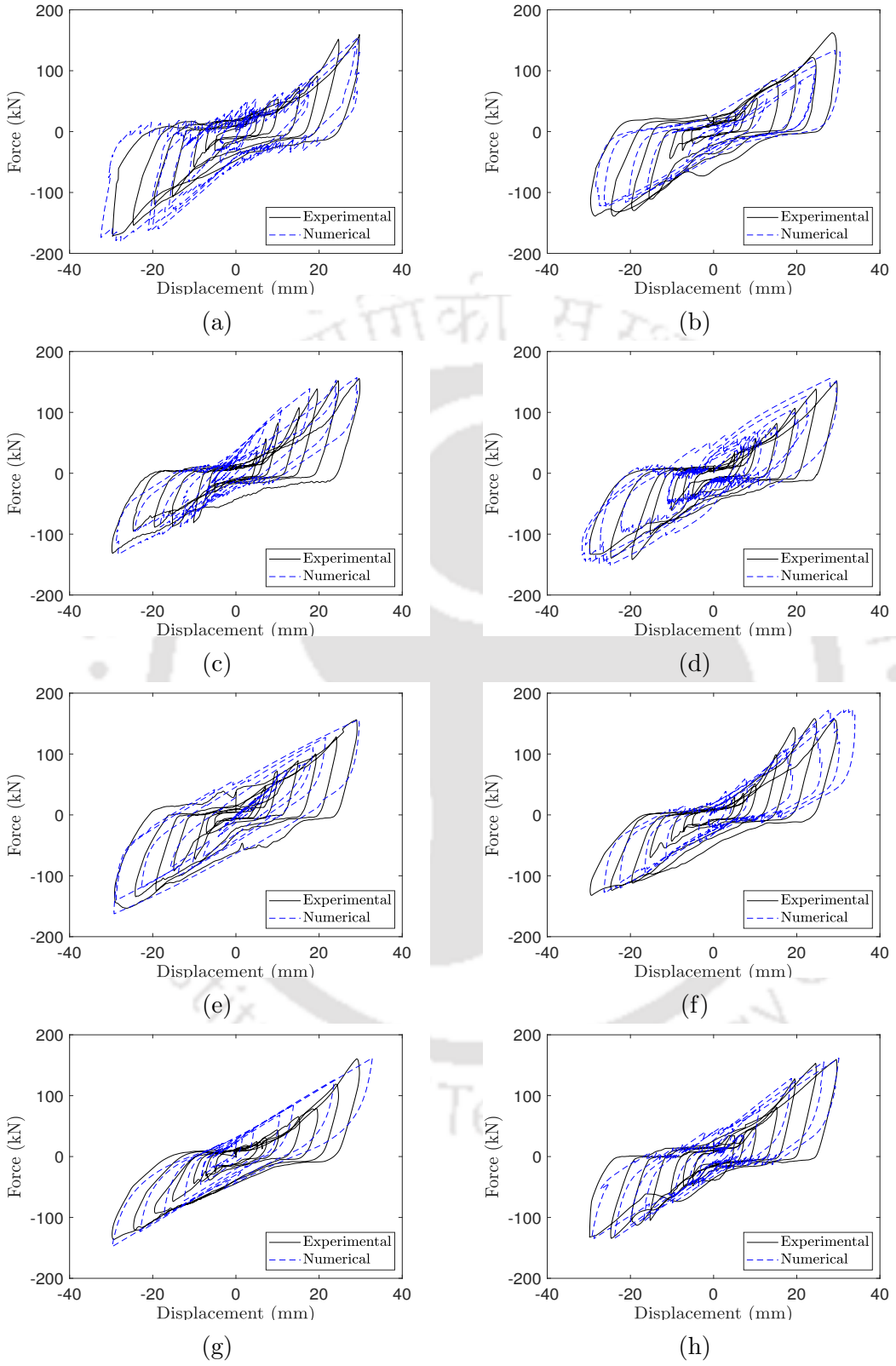

Figure 6.1: Comparison of simulated and experimental hysteretic behaviour of HyBRBs: (a) A1, (b) A2, (c) A3, (d) A4, (e) B1, (f) B2, (g) B3 and (h) B4

Table 6.2: Comparison of experimental and numerically simulated results at 3% axial core strain

Specimen	K_{eff} (kN/mm)			W_d (kNmm)			ζ_{eq} (%)		
	Exp	Num	Err	Exp	Num	Err	Exp	Num	Err
HyBRB-A1	5.13	5.28	2.9	13652	12871	5.7	18.5	20.0	8.1
HyBRB-A2	4.77	4.67	2.1	15145	14589	3.7	21.3	22.0	3.3
HyBRB-A3	4.81	5.00	3.9	10681	11084	3.8	15.8	16.9	6.9
HyBRB-A4	4.79	5.03	5.1	12883	13407	4.1	17.8	19.4	8.9
HyBRB-B1	5.43	5.35	1.5	12480	12670	1.5	17.6	18.7	6.3
HyBRB-B2	4.86	5.02	3.3	12152	12051	0.8	16.5	16.8	1.8
HyBRB-B3	4.98	4.95	0.6	11377	11205	1.5	15.3	15.2	0.7
HyBRB-B4	4.91	4.99	1.6	13355	12308	7.8	18.0	17.2	4.4

NOTE: Exp = experimentally obtained data, Num = numerically simulated data and Err = error in %.

6.4 Concluding Remarks

This chapter presents an extended Bouc-Wen (BWBN) hysteresis model for simulation of force-displacement hysteretic behaviour of the HyBRB specimens developed in the present study. The parameters of BWBN hysteresis model corresponding to the experimental force-displacement response of the HyBRB specimens are identified using a multi-objective optimization technique which minimizes the error between experimental response of the HyBRBs and their simulated response. The identified BWBN model with the optimized parameters can be utilized to simulate the behaviour of the HyBRB specimens.

Chapter 7

Vulnerability Reduction of Soft-story Building

Contents

7.1 General

Structure with irregular configurations have always been vulnerable to the seismic events. Presence of non-uniform distribution of stiffness, mass and strength due to asymmetry in either plan or elevation in structures result in torsional coupling of responses, thus affecting the stability of the structure. Soft-story problem is one of the frequently observed major irregularity in buildings. Soft-story may be present in any story, however it is most commonly seen in the ground story due to the absence of the infill wall. The vertical discontinuity of infill wall, generally provided to make way to the garage, parking slot, and other amenities in the ground story, results in non-uniform stiffness distribution and thus, soft-story problem arises in the open ground floor. Many earthquakes in India and around the world have taken a toll on such structures with an open ground storey. Fig 7.1 shows severity of seismic effects in buildings during 2001 Bhuj earthquake, which had an open ground floor. In the present study, seismic performance evaluation of a soft-story building (G+3) is carried out. The same building is then considered for seismic retrofitting using HyBRBs developed in the current study. Specifications of the HyBRBs required for retrofitting the soft-story building are finalized to provide sufficient strength, stiffness and energy dissipation capacity. A series of HyBRBs are installed at the ground floor level in the outer frames. The performance of the retrofitted building is then compared with that of the original soft-story building.

Figure 7.1: Damaged soft-story building subjected to Bhuj Earthquake, 2001

7.2 Definition of Soft-story Problems

The Indian Standard Code, IS 1893 (Part 1) (2016) has defined soft-story irregularity cases where lateral stiffness is less than 70 percent of that in the story above or less than 80 percent of the average lateral stiffness of the three stories above.

Soft-story is formed in the bare story without any infill or partial infill because of the abrupt change of load path in frames. In case of open ground story frames (OGS), the shear demand is very high in the columns of the ground story. If the columns are not designed to withstand the stresses or do not have sufficient ductility capacity, these elements can suffer severe damage and the building may collapse, as shown in Fig. 7.2. After the Bhuj earthquake, IS 1893 (Part I) (2002) was revised with new design provisions for OGS frames, which was absent in the code prior to this revision.

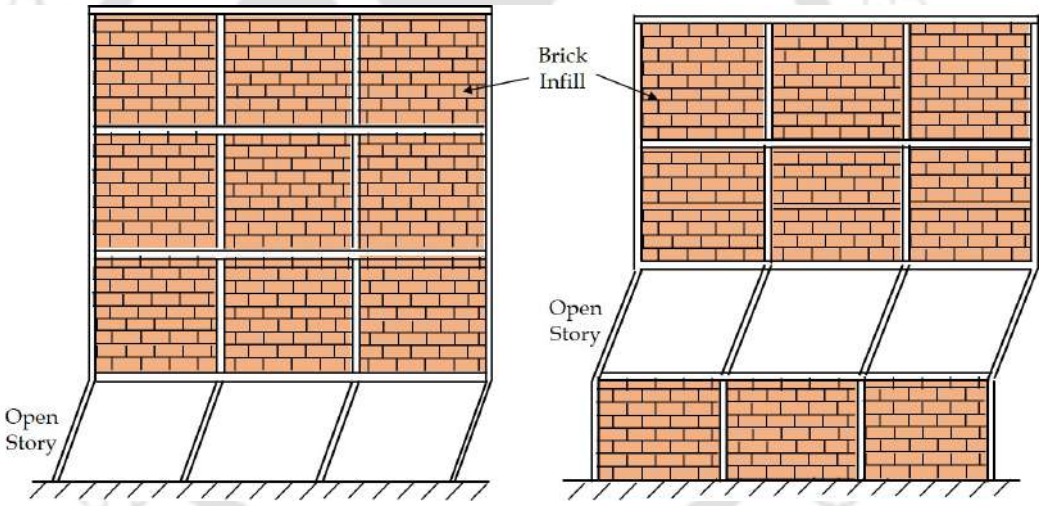

Figure 7.2: Column side-sway mechanism due to open soft story

7.3 Details of Sample Building

A medium rise RC building of height 17.35 m having a soft ground story is considered in the current study for seismic retrofitting using HyBRBs. Plan and elevation of the sample building are shown in Fig 7.3. Infill walls are present in the boundary and at partitions in the upper stories. The irregularity in the form of OGS causes significant change in the strength and stiffness of the ground story from the stories above. It is assumed that the building is situated in zone V of

the seismic hazard map of India. The building is designed against gravity loads following the design recommendations of relevant Indian Standard Code, IS 456 (2000). Gravity loads are applied according to design provisions as outlined in IS 875 (Part I) (1987) and IS 875 (Part II) (1987). Columns are assumed to be fixed at the base. Grades of concrete and rebar are taken as M25 and Fe415 respectively. Elastic modulus of masonry is considered as $550f_m$, where f_m is masonry prism strength in MPa. Fig 7.4 shows the details of reinforcement bars provided in the beams and columns. Spacing of stirrups are assumed as 200 mm in both beams and columns. Geometric details of beams, columns, masonry walls and slab panels are furnished in Table 7.1.

Table 7.1: Details of soft-story building

Element	**Dimensions (mm)**	**Story level**
Beam Cross-sections	150×600, 200×600, 250×600	1-3
	150×600, 250×600	4
Column Cross-sections	300×300	1-4
Masonry Thickness	100	1-4
Slab Thickness	125	1-4

7.4 Soft-story Building Retrofit with HyBRB

Retrofit design of the soft-story building is carried out with implementation of HyBRBs at the selected bays of the open ground story. The design procedure proposed by Della Corte et al. (2015) is considered in this study for calculating the required mechanical characteristics and geometric details of the HyBRBs.

7.4.1 Retrofit Design Procedure

Following steps briefly describe the estimation of strength and stiffness of HyBRB required to retrofit the soft-story building.

- Finalization of performance objective, design drift (θ_d), at ground story under reference level of earthquake intensity.

- Selection of trial values of key design parameters, such as, σ_y or ϵ_y and γ_d,

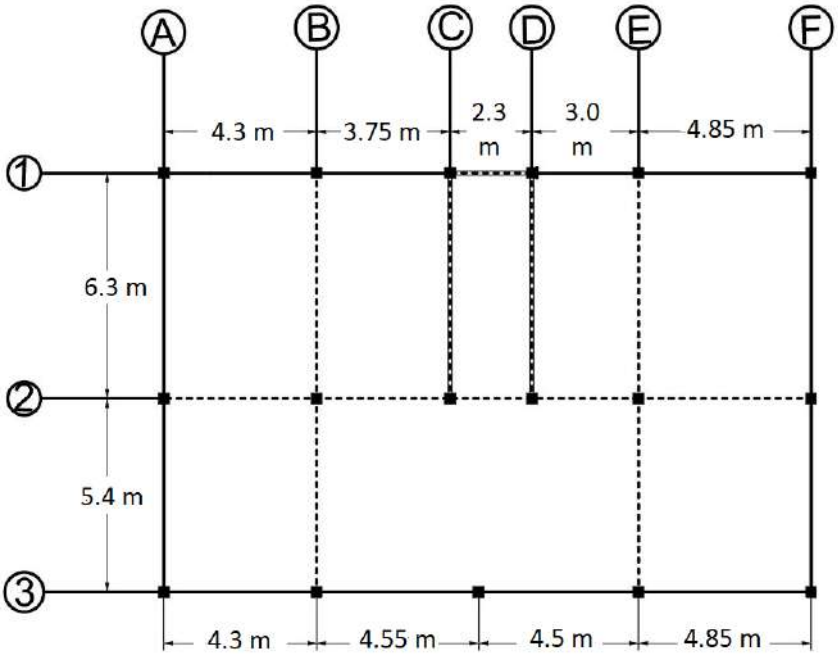

(a)

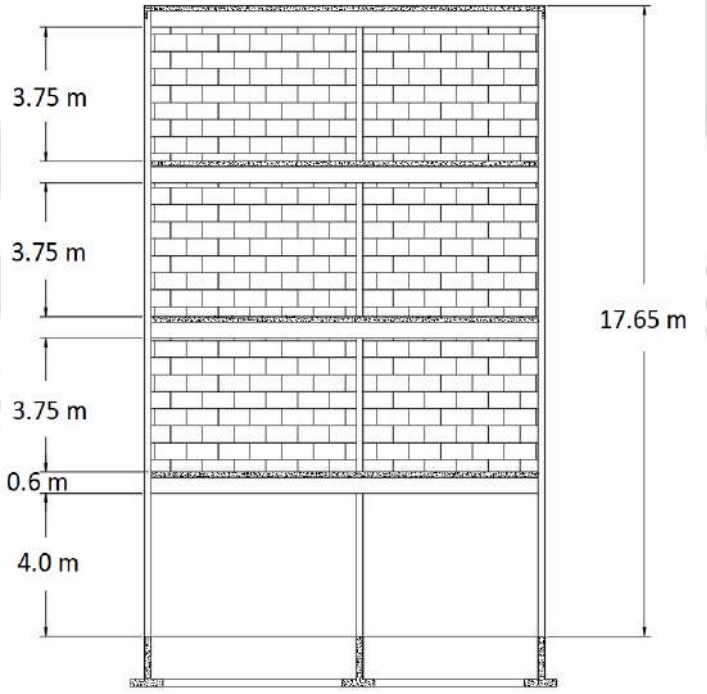

(b)

Figure 7.3: Schematic diagram of sample building: (a) plan, (b) elevation

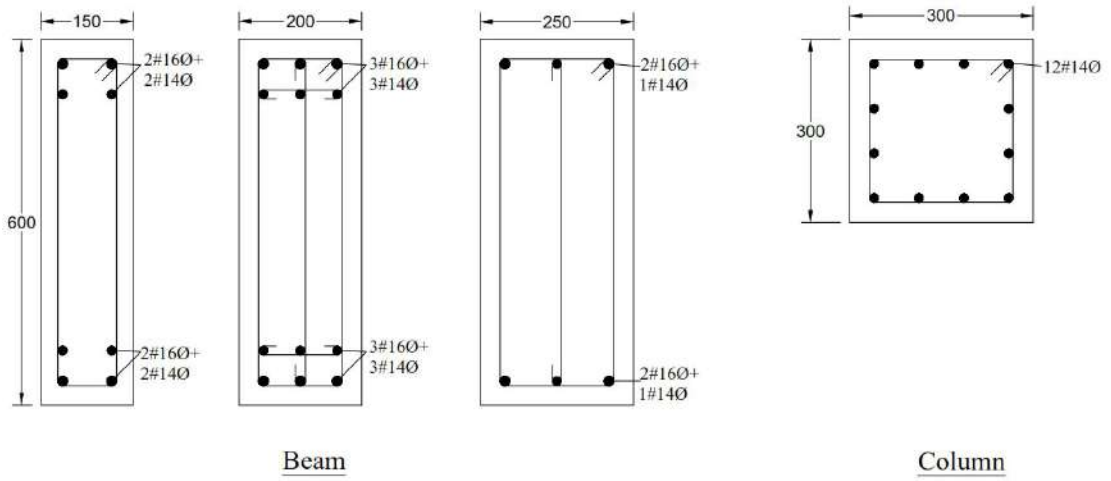

Figure 7.4: Details of reinforcement bars in beams and columns (all dimensions are in mm)

where,

$$\gamma_d = 1 \Big/ (1 + \sum_i L_i A_c / L_c A_i)$$

- Calculation of brace yield axial displacement using following equation,

$$u_y = \epsilon_y L_c \gamma_d$$

- Computation of design yield drift of ground story of the building using,

$$\theta_y = u_y / h. \cos\alpha$$

where, h is height of the ground floor.

- Determination of design ductility demand as:

$$\mu_d = \theta_d / \theta_y$$

- Computation of reduction factor to reduce the elastic demand acceleration (5% critical damping) corresponding to time period T of the equivalent

SDOF system and μ_d, using following equation as:

$$R_\mu = (\mu - 1)T/T_c + 1, T < T_c$$
$$= \mu, T > T_c$$

- Computation of the effective mass, M_e, assuming a target displacement shape profile (Δ_d) of the braced frame system as:

$$M_e = \left(\sum_i m_i \Delta_i\right)^2 \Big/ \sum_i m_i \Delta_i^2$$

where, m_i is the seismic weight of the i^{th} story.

- Computation of the required system resistance using:

$$V_{y,d} = M_e S_{ae}/R_\mu$$

where, S_{ae} is elastic demand acceleration.

- Estimation of the required BRB knowing the shear force contribution from RC frame (V_{RC}) corresponding to ground story drift, θ_y, as:

$$V_{\text{brb},y,d} = V_{y,d} - V_{RC}$$

- Computation of the required BRB stiffness and cross-sectional area as:

$$K_{\text{brb},y} = V_{\text{brb},y,d}/h.\theta_y$$
$$A_c = V_{\text{brb},y,d}/\sigma_y . \cos\alpha_{\text{brb}}$$

7.4.2 Required HyBRB Characteristics

Following the design procedure discussed above, a set of HyBRB parameters are estimated for retrofitting the building. The plan and elevation of bays in the open ground story, identified for retrofitting, are shown in Fig 7.5 and Fig 7.6, respectively. Proposed strategy of HyBRB installation ensures minimum eccentricity between the center of mass and the center of rigidity of the building. The necessary mechanical characteristics and area of the HyBRBs are obtained for bays

in both X and Y directions using the above mentioned retrofit design procedure. Table 7.2 shows the details of the required and provided core areas of the HyBRBs in different bays of the soft ground story.

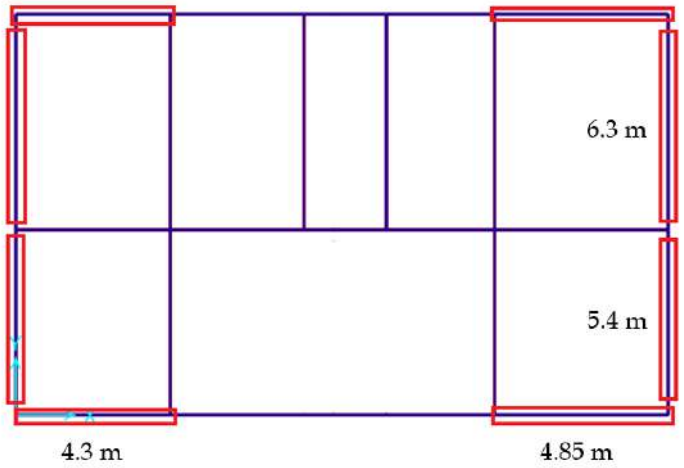

Figure 7.5: Location of HyBRBs in the retrofitted building in plan

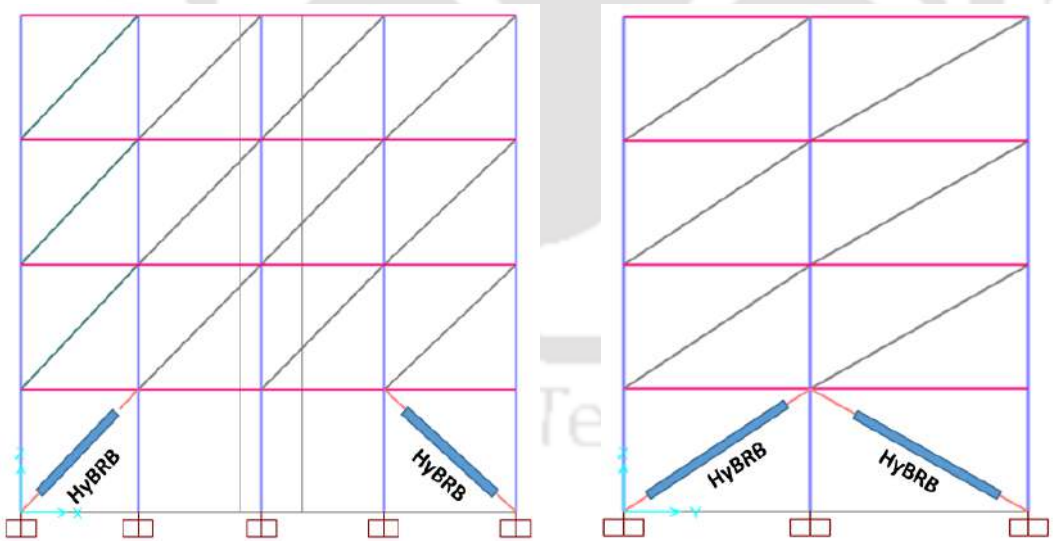

(a) (b)

Figure 7.6: Location of HyBRBs in the retrofitted building in elevation along: (a) X direction, (b) Y direction

Table 7.2: Details of proposed HyBRBs in different bays

Bay width (m)	**Area required (mm^2)**	**Area provided (mm^2)**
5.4	1140	1200
6.3	1143	1200
4.3	1431	1450
4.85	1362	1400

7.5 Numerical Model of Sample Building

A detailed 3D model of the soft-story building is developed in SAP2000 v21.0.2 (2019) to evaluate its seismic performance under nonlinear static and dynamic loading. Beams and columns are modelled using 3D frame elements while infill walls are modelled using diagonal strut elements. Slab panels are considered as rigid diaphragms. Lumped plastic hinges are assigned in the beams and columns to accurately simulate the nonlinear behaviour. Plastic hinges are defined at both ends of the columns considering: a) interaction of axial load-flexure in both directions ($P - M - M$) and b) force-controlled shear-deformation ($V - \Delta$). Plastic hinges at both ends of beams are defined considering flexural moment-rotation behaviour ($M - \theta$). Moreover, the central plastic hinges in the diagonal struts are defined considering axial load-deformation behaviour ($F - \delta$). Strength characteristics of shear hinges are computed considering axial load ratio and reinforcement details, as recommended in ASCE-ACI 426 (1973). In the retrofitted building, HyBRBs are modelled using multi-linear plastic link elements. The axial load-deformation behaviour of the multi-linear plastic links are defined using the backbone curve of the HyBRB specimen, as shown in Fig 7.7.

7.6 Nonlinear Static Analysis

Nonlinear static analysis (NSA) of the sample soft-story building, before and after retrofitting using HyBRBs, is carried out by pushing it along the transverse direction (Y-direction) for evaluation of seismic performance. Prior to NSA, gravity analysis of the soft-story building is carried out for load combinations conforming to IS 1893 (Part-I):2016. Performance along the transverse direction of the soft-story building is examined because the building is more susceptible to damage

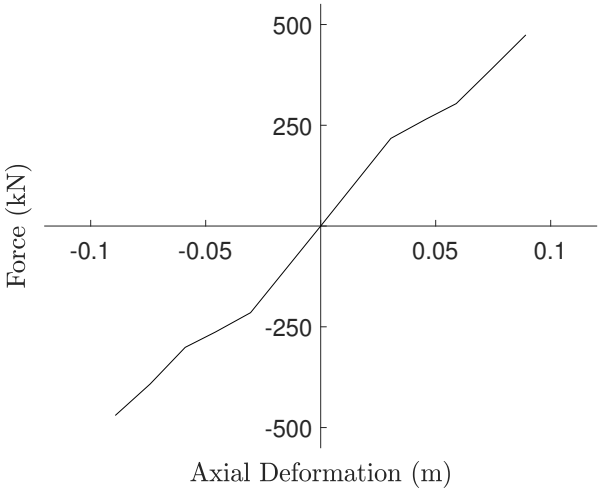

Figure 7.7: Idealized force-displacement behaviour of multi-linear plastic link element

due to seismic action in that direction. Thus, for NSA, lateral forces proportional to mode shapes with higher mass participation ratios are applied to the frames located along the building's transverse direction.

7.7 Results of Nonlinear Static Analysis

Performances of HyBRBs in retrofitting the sample soft-story building are first evaluated using NSA and the capacities of both soft-story and retrofitted buildings are obtained. The results of NSA of both original and soft-story building are first compared in form of pushover or capacity curves. Further, the story displacements and inter-story drifts (%) corresponding to performance points of each buildings are evaluated and compared for performance evaluation of HyBRBs. The distribution of plastic hinges in frame elements of both original and retrofitted building is also investigated. Story displacement and inter-story drift are evaluated at the center of mass of respective story. Details of performance points in pushover curve, corresponding to target capacity spectrum conforming to ATC-40, are presented in Table 7.3.

Fig 7.8 shows the pushover curves obtained from nonlinear static analysis of both the buildings. From the pushover curves, it can be clearly observed that the building retrofitted with HyBRB has a higher base shear capacity as compared to that of the soft-story building. The stiffness of the original building improved

Table 7.3: Performance points of the soft-story and retrofitted building under nonlinear static pushover

Model	Roof displacement (m)	Base shear (kN)
Soft-story Building	0.088	921.26
Retrofitted Building	0.041	1167.73

when retrofitted with HyBRBs, which in turn reduced the roof displacement of the retrofitted building at the performance point. Moreover, in case of the soft-story building, the ultimate lateral deformation capacity reached prior to that observed for the HyBRB retrofitted building. Thus, it is evident that the ductility as well as the energy dissipation capacity in the soft-story building are improved after implementation of the HyBRBs.

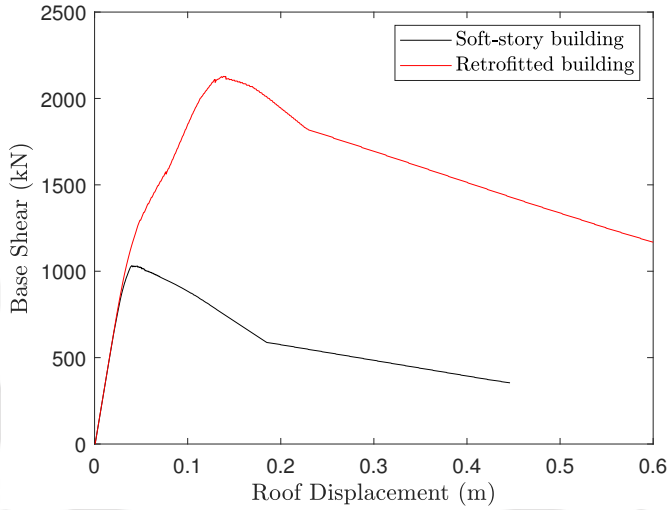

Figure 7.8: Capacity curve of soft-story building before and after retrofit with HyBRBs

Fig 7.9 shows the displacement of each story corresponding to respective performance points of both the soft-story and retrofitted buildings. The displacement demand at the soft ground story of the original building is observed to be much higher than that for the stories above, as shown in Fig 7.9. Retrofitting the soft-story building with HyBRBs reduced the displacement demand at the soft-story level and further maintained uniform demand throughout the height of the building.

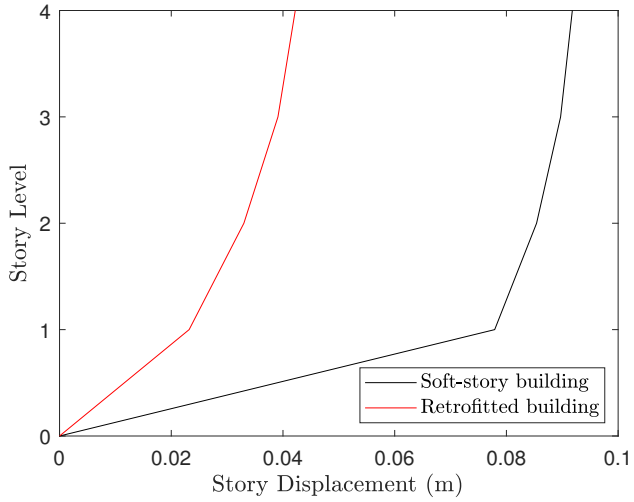

Figure 7.9: Story displacement at performance points of soft-story building before and after retrofit

Fig 7.10 shows the inter-story drifts at each story corresponding to performance points of both the original and retrofitted buildings. Large inter-story drift in the open ground story of the original building indicates that the columns of that story experienced high ductility demands. The use of HyBRBs in the open ground story of the original building reduced inter-story drift and thus ductility demands significantly, as shown in Fig 7.10.

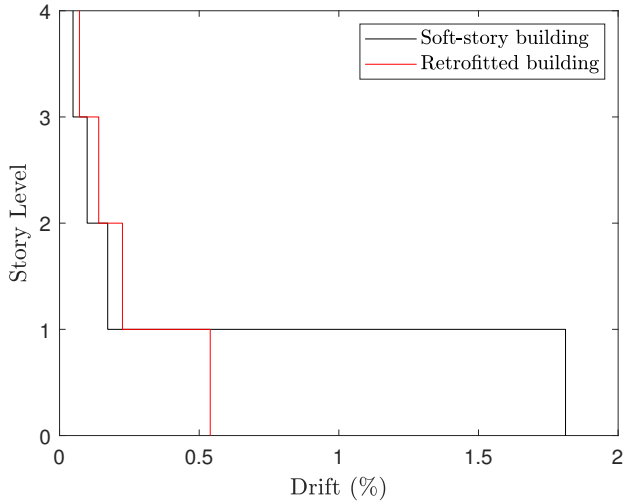

Figure 7.10: Inter-story drift at performance points of soft-story building before and after retrofit

Fig 7.11 shows the distribution of plastic hinges formed in structural elements of the building before and after retrofitting. It can be observed that the plastic hinge distributions in the structural elements of the soft-story building are limited to the ground story level, as shown in Fig 7.11(a). This is consistent with the high displacement demand observed in the ground story columns as shown in Fig 7.9. From Fig 7.11(b), it is observed that the hinges are distributed along the height of the retrofitted building which indicate that the redistribution of moment is better in the retrofitted building. Thus, it can be stated that the problem related to soft-story mechanism is effectively mitigated with the inclusion of HyBRBs.

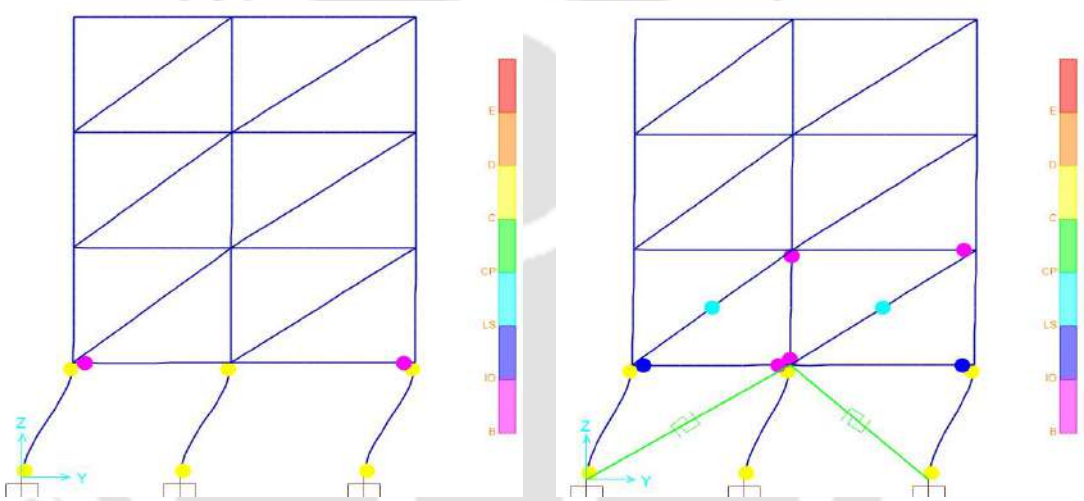

(a) (b)

Figure 7.11: Plastic hinge distribution in (a) soft ground story building, (b) retrofitted building

7.8 Nonlinear Dynamic Analysis for Vulnerability Assessment

Nonlinear dynamic analysis of the soft-story building, subjected to earthquake ground motions of different characteristics, is performed for assessment of the reduction in seismic vulnerability when retrofitted using HyBRBs. Fast nonlinear dynamic analysis method (Wilson, 1996) has been adopted for carrying out eighty numbers of seismic time history analyses of the sample building with and without retrofitting. Considered earthquake ground motion records have different

magnitudes (range of M_w = 4.9-7.40), epicentral distances (6-124 km) and PGA values (0.021-0.812 g). Seismic vulnerability is examined using fragility curves corresponding to different predefined performance limit states of the soft-story building before and after retrofitting.

7.8.1 Fast Nonlinear Dynamic Analysis Method

Response spectrum compatible earthquake ground motion records are used for seismic performance evaluation of the soft-story building before and after retrofitting. A fast nonlinear dynamic analysis algorithm is used for computation of seismic responses of the original and retrofitted building subjected to the prescribed earthquake ground motions. For dynamic problems with limited nonlinear degrees of freedom, a step-by-step numerical integration method has been implemented in SAP2000 v21.0.2 (2019) software. The Fast Nonlinear Analysis (FNA) is a nonlinear modal analysis method useful for the dynamic response evaluation of structural systems, incorporating both material and geometric nonlinearities (Wilson, 1996). FNA is preferred for nonlinear time-history analysis against direct-integration methods because of computationally efficient formulation algorithm used in the FNA method (Wong, 2011; Cancellara and De Angelis, 2017).

7.8.2 Selection of Ground Motions

The selected earthquake records are obtained from PEER-NGA ground motion data base. Following four categories of ground motions are selected for carrying out seismic vulnerability assessment of the sample buildings.

1. LM-SD : large magnitude ($M_w \geq 6.5$) - small distance (D $<$ 35 km)
2. LM-LD : large magnitude ($M_w \geq 6.5$) - large distance (D $>$ 35 km)
3. SM-SD : small magnitude ($M_w < 6.5$) - small distance (D $<$ 35 km)
4. SM-LD : small magnitude ($M_w < 6.5$) - large distance (D $>$ 35 km)

Twenty ground motion records with different characteristics are considered in each of the above mentioned categories. The details of prescribed ground motion data of different categories are presented in Tables B.2, B.3, B.4 and B.5 of Appendix-B. The ground motions are designated with record sequence numbers (RSN) as mentioned in the PEER-NGA database. Prior to nonlinear dynamic

analysis, scaling of the selected records is required to reduce the variability observed in acceleration spectrum for individual ground motions due to different earthquake magnitude, soil type etc. Scaling of the selected ground motion records for the current study is carried out in SeismoMatch (2022) software, corresponding to target response spectrum of the maximum considered earthquake as defined in IS 1893 (Part 1) (2016). Figs 7.12, 7.13, 7.14 and 7.15 show the scaled response spectra of the earthquake records from the respective categories with the target response spectrum. The average response spectrum of the prescribed ground motion records is found to be in close agreement with the target response spectrum.

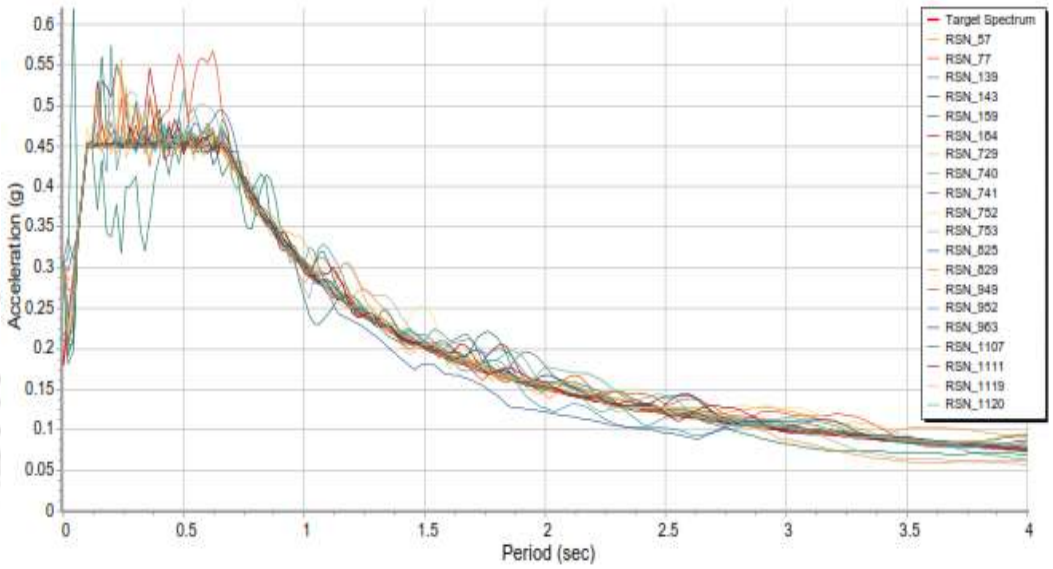

Figure 7.12: Target response spectrum and response spectrum of scaled LM-SD ground motions

7.9 Seismic Vulnerability Assessment

Seismic vulnerability of the soft-story building, with and without retrofitting, is quantified as the probability of exceeding a performance limit state defined in terms of inter-story drift corresponding to PGA (or any other intensity measure) of the prescribed ground motions. Different performance levels corresponding to inter-story drift ratios are adopted following the performance limit states defined in FEMA-356 (2000). Inter-story drift ratios of 1%, 2% and 4% are considered corresponding to immediate occupancy (IO), life safety (LS) and collapse prevention (CP) limit states, respectively. Probability of exceedance corresponding to

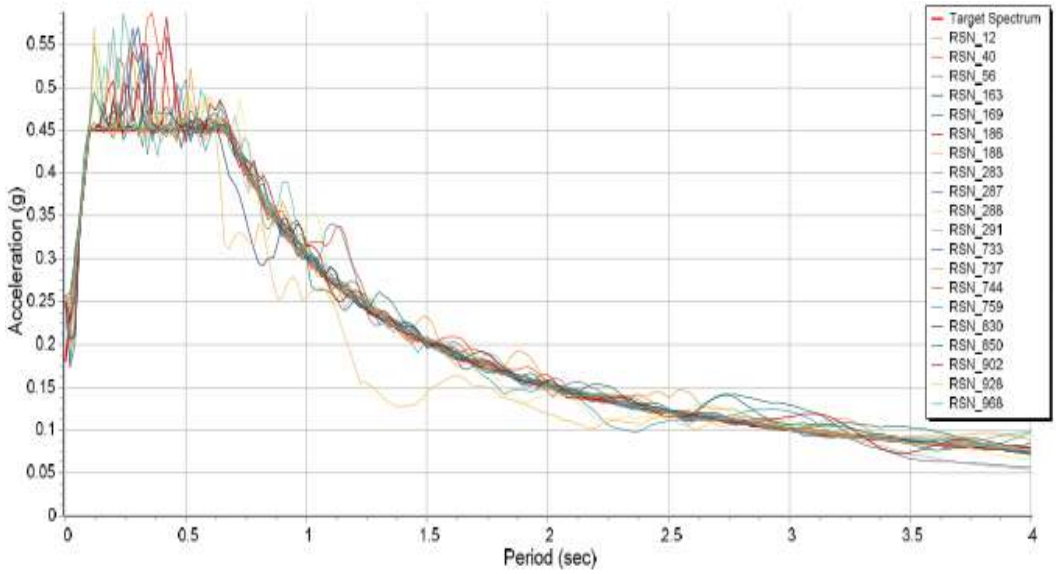

Figure 7.13: Target response spectrum and response spectrum of scaled LM-LD ground motions

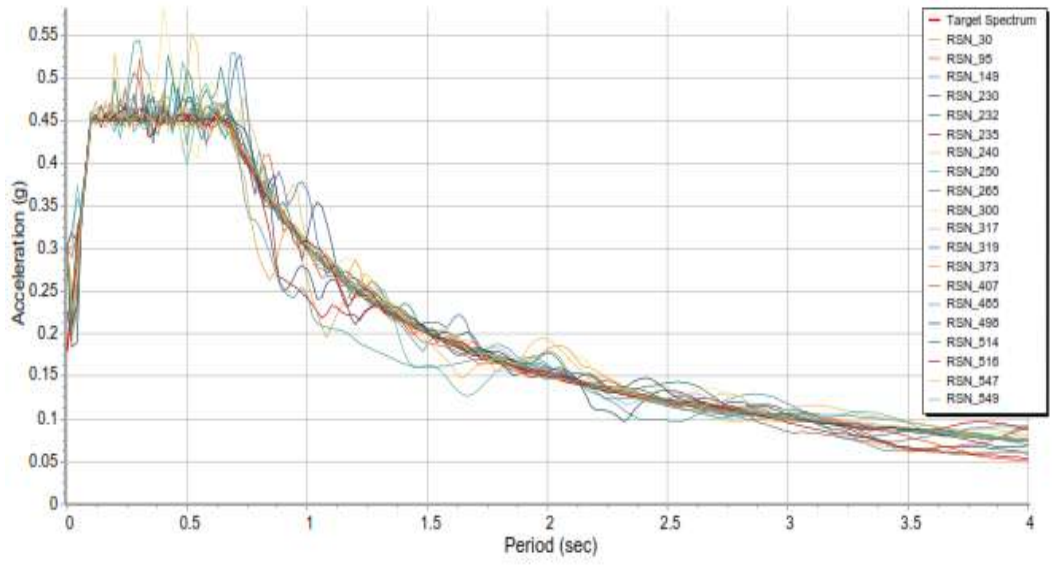

Figure 7.14: Target response spectrum and response spectrum of scaled SM-SD ground motions

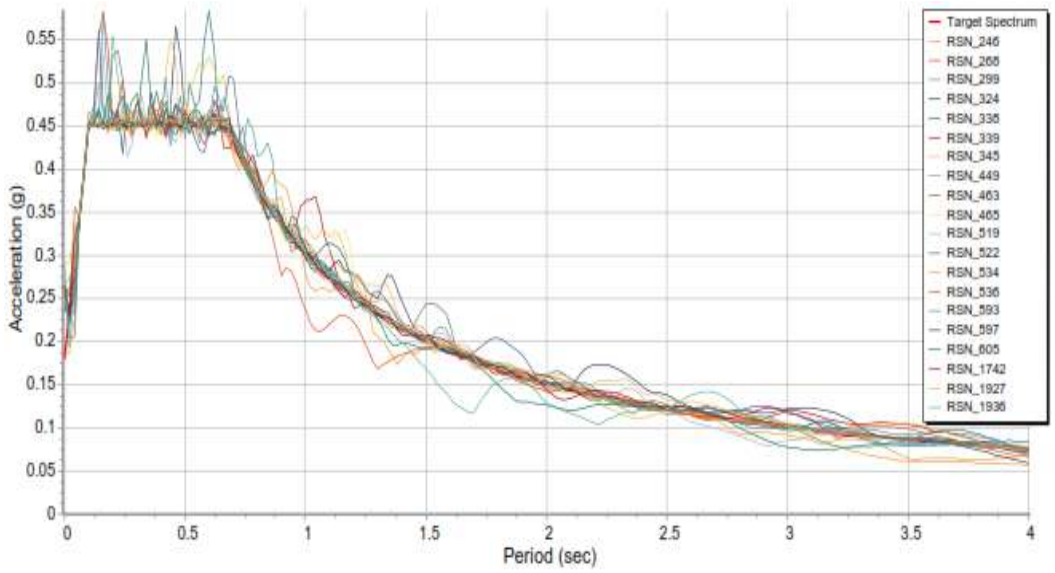

Figure 7.15: Target response spectrum and response spectrum of scaled SM-LD ground motions

these performance limit states w.r.t. PGA values of prescribed ground motions are computed and analytical fragility functions are plotted for both the soft-story and retrofitted buildings.

7.9.1 Development of Fragility Curves

Seismic fragility analysis is carried out for assessment of probability of achieving performance limit state corresponding to a specific earthquake intensity measure. In this study, PGA value of the prescribed earthquake ground motion record is considered as the intensity measure. Fragility function is defined as the probability of exceedance of a certain performance limit state (or damage state), observed in the structure for a certain intensity measure of ground motion and is expressed as follows:

$$P(C|\,IM = x) = \Phi\left(\frac{\ln(x/\theta)}{\beta_{DS}}\right) \tag{7.1}$$

where, C is the predefined performance limit state,
x is the intensity measure of the prescribed ground motion,
θ is the median value of the intensity measure at which the building reaches a certain performance limit state,
and, β_{DS} is the total uncertainty, which includes, material and ground motion

uncertainties.

Material uncertainty is overlooked in this study because suitable material properties are incorporated while modelling the elements of the soft-story building. Therefore, β_{DS} represents only the uncertainty due to variations in different ground motion characteristics. The values of θ and β_{DS} are determined by minimizing error between the estimated probability of exceedance and the observed value, using maximum likelihood fitting procedure.

7.9.2 Results

Analytical fragility curves, for different predefined performance levels, are developed using the above mentioned methods. Figs 7.16, 7.17, 7.18, 7.19 show the plotted fragility functions of the soft-story building, for different categories of prescribed ground motions, before and after retrofit.

It is observed that the probability of exceeding a certain performance level, is significantly lesser in the retrofitted building as compared to that in the soft-story building, for any PGA value. For a realistic PGA range, the probability of exceeding low to moderate level of performance limit state is very low for the retrofitted structure, which clearly indicates the effectiveness of soft-story retrofit with HyBRBs. For the soft-story building, the probability of exceeding collapse prevention limit state is relatively large under moderate to high range of PGA values, irrespective of earthquake magnitude as shown in Figs 7.16(a) and 7.18(a). The high probability of exceeding collapse prevention limit state is effectively reduced by installation of HyBRBs in the retrofitted building, as shown in figures, Fig 7.16(b) and Fig 7.18(b). Similarly, for low to moderate range of PGA values, the probability of exceedance of the soft-story building at collapse prevention limit state is significantly reduced when retrofitted with HyBRBs, as shown in Figs 7.17 and 7.19. Thus, it can be stated that the vulnerability of the soft-story building is effectively reduced by retrofitting the building with HyBRBs at suitable locations.

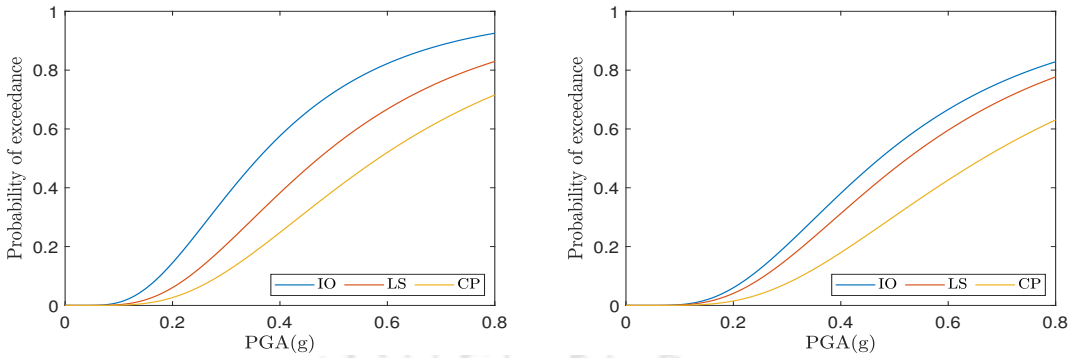

(a) (b)

Figure 7.16: Fragility curves for different limit states in (a) soft ground story building, (b) retrofitted building, under the ground motions of category LM-SD

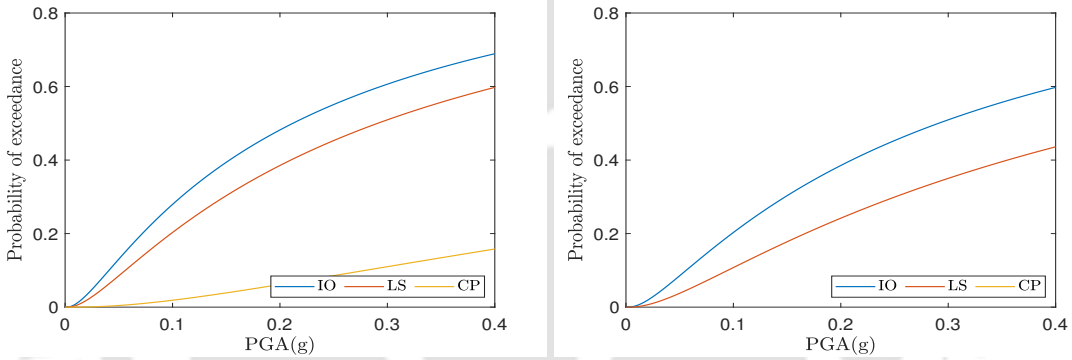

(a) (b)

Figure 7.17: Fragility curves for different limit states in (a) soft ground story building, (b) retrofitted building, under the ground motions of category LM-LD

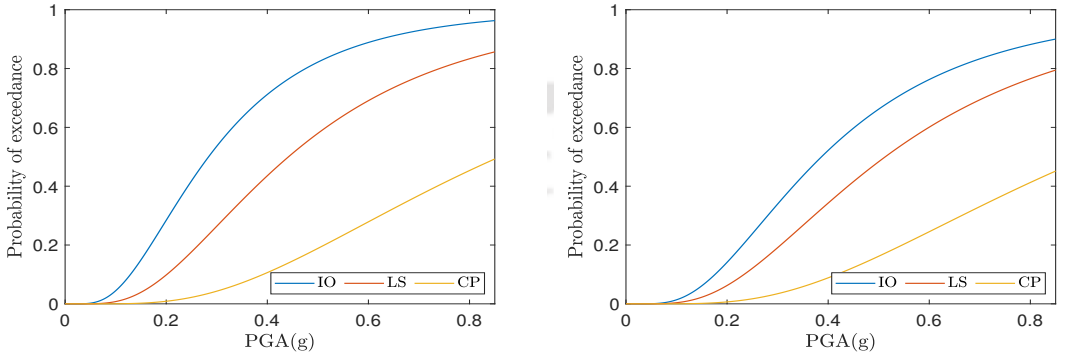

(a) (b)

Figure 7.18: Fragility curves for different limit states in (a) soft ground story building, (b) retrofitted building, under the ground motions of category SM-SD

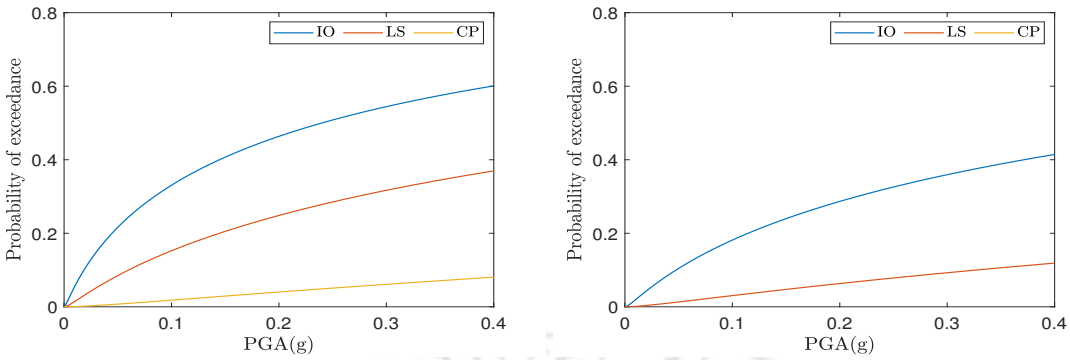

(a) (b)

Figure 7.19: Fragility curves for different limit states in (a) soft ground story building, (b) retrofitted building, under the ground motions of category SM-LD

7.10 Concluding Remarks

This chapter presents a detailed seismic performance assessment of the soft-story building before and after retrofitting. Nonlinear static and dynamic analyses of the soft-story building are carried out and the results are compared with that obtained from the analyses of the retrofitted building. The major conclusions that can be drawn form this study are as follows:

1. Results of the nonlinear static analysis showed that the retrofitted building exhibited a higher base shear capacity than that of the soft-story building, when subjected to monotonic lateral loading.

2. Overall strength and ductility of the original building improved after installation of HyBRBs for its retrofitting. Also, the plastic hinges are widely distributed along the height of the retrofitted building, which otherwise are seen to be limited in the ground story of the soft-story building, before retrofitting.

3. Inter-story drift ratios are much lesser in the retrofitted building than that observed in the soft-story building, which in turn reduced the ductility demand on the ground story columns.

4. Nonlinear dynamic analysis established effectiveness of HyBRBs in reducing seismic vulnerability of the soft-story building when subjected to prescribed ground motions of different characteristics.

5. Significantly low probability of exceedance of different predefined performance limit states is observed in case of the retrofitted building, when subjected to prescribed ground motion records. Thus, problem related to soft story mechanism is effectively mitigated with the installation of HyBRBs.

Chapter 8

Summary, Conclusions and Future Scopes

Contents

8.1 Summary of the Study

In this study, a new hybrid BRB, designated as HyBRB, is developed to address the limitations of conventional BRBs. HyBRB is a combination of steel BRB and highly deformable infill rubber layers. The HyBRB aims to achieve enhanced energy dissipation capacity in a wide range of axial strain levels by combining the contributions of infill layer and steel core through their shear deformation and axial yielding, respectively. The provision of infill layers on both flat sides of the steel core allows restrained local buckling of the steel core initially about its weak axis and subsequently about its strong axis. Thus, successive restrained buckling of the core about both the weak and strong axes improves the performance of HyBRB for a wide range of axial strains. Moreover, addition of infill layers provides additional energy dissipation through shear deformation at lower strain levels.

Experimental investigations are carried out to evaluate the seismic performance of the newly developed HyBRB under cyclic loading. Accordingly, a step-by-step procedure for design of the components of a geometrically scaled HyBRB is presented. Total eight numbers of HyBRB specimens are prepared for their performance assessment. These specimens are classified into two categories: (a) HyBRB-A and (b) HyBRB-B, based on the type of infill material used in their fabrication. HyBRB-A utilizes neoprene rubber, while, HyBRB-B uses butyl rubber as infill material between steel core and restrainer pair. Each category of HyBRB consists of four specimens with different infill geometries, out of which two have continuous infill layers, while, the other two have different discontinuous infill layers. The assembled HyBRB is connected to the test setup diagonally with its one end to a vertical element of the test assembly on top, while, the other end to the strong floor at bottom. A horizontal displacement protocol of increasing amplitudes is applied using a servo-hydraulic actuator. Electrical strain gauges are attached on the sides of the core and outer surface of the restrainer pair to record the strains during experiments. Axial force-displacement responses of the test specimens are recorded using the built-in load cell and tempo-sonic displacement sensor of the servo-hydraulic actuator. Experimental investigation reveals that all the variants of HyBRB exhibited stable hysteretic behavior with comparable tensile and compressive load carrying capacities under the applied displacement loading. The investigation further presents a comparative study on the restrained

buckling behaviour of the cores and overall performances of the tested HyBRB specimens.

Further, analytical study is carried out to optimize the parameters of an extended Bouc-Wen model, known as Bouc-Wen-Baber-Noori (BWBN) model, for simulation of the hysteretic behaviour of the tested HyBRB specimens. The model parameters are adjusted to match the output of the model with the experimental behaviour by minimizing the error between the two. The analytically simulated force-displacement hysteretic behaviour of HyBRBs are found to be in good agreement with that recorded during the experimental investigation. Further, the effective stiffnesses and damping parameters are computed from the simulated force-displacement responses and the same are compared with that obtained from the responses recorded during experimental investigations.

Numerical studies are carried out to investigate the efficacy of HyBRB in reducing seismic vulnerability of a building with asymmetry in elevation. Nonlinear static and dynamic analyses of a sample soft-story building (G+3), located in zone V of the seismic hazard map of India, is carried out using SAP2000 v21.0.2 (2019). The same building is then considered for seismic retrofitting using the HyBRBs developed in this study. Nonlinear static analyses along the transverse direction reveals that the retrofitted building exhibited higher capacity than that of the soft-story building, under monotonic lateral loads. Overall strength and stiffness of the building is improved after retrofitting using HyBRBs.

Finally, nonlinear time history analysis is carried out to assess the seismic vulnerability of the sample building subjected to prescribed earthquake ground motions before and after retrofitting. This study considers eighty ground motions, grouped in four categories, having varying magnitudes (M_w) in the range 4.9-7.4, epicentral distances in the range 6-124 km and PGA values in the range 0.021-0.812g. Seismic performance is assessed using inter-story drift and probability of exceedance of a predefined performance limit state of the building before and after retrofitting, when subjected to the prescribed ground motions. The probabilities of exceedance of different performance limit states corresponding to PGA values of the prescribed ground motions are computed and analytical fragility functions are plotted for both the soft-story and retrofitted buildings. Significantly low probability of exceedance of different predefined performance limit states is observed in case of the retrofitted building, when subjected to the prescribed ground mo-

tion records. Thus, it can be stated that the seismic vulnerability of the soft-story building is effectively mitigated by retrofitting with HyBRBs at suitable locations.

8.2 Major Conclusions

Following are the major conclusions drawn from the present study:

1. Newly designed inspectable and detachable HyBRB would allow visual monitoring and measurement of strains in the core and the restrainers for assessment of the damage state of the steel core. The damaged steel core can be replaced quickly after a seismic event, if needed.

2. Formation of higher order restrained buckling modes of the steel core is observed visually at higher displacement amplitudes with no sign of damages in bolted and welded connection. Further, no appreciable lateral deformation in the restrainer is observed. This establishes that the global buckling of the HyBRB could be restrained effectively.

3. Stable hysteretic behaviour with comparable tensile and compressive load carrying capacities are observed for the newly developed HyBRB specimens with different infill layer geometries. All the mechanical parameters of the HyBRB fulfilled necessary design criteria.

4. The presence of highly deformable infill layers facilitated formation of buckling modes of the steel core about both weak and strong axes. Further, addition of the infill layers contributed in energy dissipation at low axial strain levels through their shear deformation.

5. The deformed shapes of the HyBRB cores at the end of the cyclic tests and the strain distributions in the restrainer wall and core established that restrained buckling of the steel cores occurred first about the weak axis and subsequently about the strong axis at about 1.5-2% axial strain level. This resulted in enhancement of stiffness of the HyBRB and hence increased its energy dissipation capacity in high axial strain levels.

6. The observed residual strain in the steel core is in the range of 0.3-0.4% which is quite low as compared to the maximum applied strain of 3%. This

establishes that the residual deformation in the newly developed HyBRB is insignificant.

7. Effective stiffness of the HyBRB with continuous butyl rubber infill layers is observed to be slightly higher than that of the HyBRB with neoprene infill layers. Effective stiffness values at low axial strains are found to be higher for the specimens with discontinuous infill layers than those of specimens with continuous infill layers. Further, the HyBRBs with shorter discontinuous infill layers, where the area under hard contact is more, exhibited higher axial stiffnesses than that of specimens with longer discontinuous infill layers.

8. HyBRB specimens having neoprene infill layers displayed higher energy dissipation capacities than those of the specimens with butyl rubber of same geometry. HyBRB specimens with continuous infill layers exhibited higher energy dissipation capacities than those of the HyBRBs with discontinuous infill layers. Further, the specimens with longer discontinuous infill layers have higher energy dissipation than that of the specimens with shorter discontinuous infill layers in each category.

9. All variants of the HyBRB provided significantly high equivalent viscous damping factors of the order of 20%, in lower core strain levels. Further, equivalent viscous damping factor of about 22% is achieved in the higher core strain level, which is reasonably high for effective seismic response control of structural systems.

10. Optimization of parameters of extended BWBN model ensured close match of the analytically simulated hysteretic behavior of HyBRB specimens with those obtained from the experimental investigation. The effective stiffness and damping parameters calculated from simulated hysteresis loops were compared with that obtained from the experiments. The computed errors for the above mentioned parameters are found to be in between 0.6 to 8.9%.

11. Nonlinear static analysis reveals the efficacy of HyBRBs in enhancing the load carrying capacity of a building with vertical irregularities. Stiffness and ductility of the retrofitted building, under monotonic lateral loading, are also observed to be much higher than those parameters of the soft-

story building. Displacement demand in the soft ground story columns is significantly reduced after the installation of HyBRBs.

12. Fragility curves exhibit the effectiveness of HyBRBs in reducing seismic vulnerability of the soft-story building when subjected to prescribed ground motions of different characteristics. Installation of HyBRBs reduced the inter-story drift ratios in the retrofitted building than that observed in the soft-story building which in turn reduced the probability of exceedance of a predefined performance limit state. Therefore, it can be stated that the problem related to soft story mechanism is effectively mitigated with the installation of HyBRBs.

8.3 Future Scope

Areas in which this work can be extended through additional research include the following:

- Design of HyBRBs with self-centering ability in order to maximize their effectiveness.
- Modification of the HyBRB with additional self-centering devices like tendon or disc bearings at one or both ends for enhancing the performance of HyBRB.
- Study on the performance of HyBRB with smart core using shape memory alloy (SMA), which regains its original shape once heated to a threshold temperature. This would reduce the cost of repair and maintenance significantly.
- Evaluation of the performance of hybrid structural control system consisting HyBRB and elastomeric isolator for reduction of ground motion transmissibility and enhancement of overall damping of structures.
- Parametric study on influence of key design parameters of HyBRB like thickness of core and infill layer, connection type for optimizing the performance and stability under variety of loading for practical applications.

References

AISC 341-10 (2010). Seismic provisions for structural steel buildings. Standard, American Institute of Steel Construction, Inc. Chicago Illinois, USA.

ASCE-ACI 426 (1973). Task committee 426 on shear and diagonal tension of the committee on masonry and reinforced concrete of the structural division. Standard, American Society of Civil Engineers.

Atlayan, O. and Charney, F. A. (2014). Hybrid buckling-restrained braced frames. *Journal of Constructional Steel Research*, 96:95–105.

Baber, T. T. and Noori, M. N. (1985). Random vibration of degrading, pinching systems. *Journal of Engineering Mechanics*, 111(8):1010–1026.

Bai, J. and Ou, J. (2016). Earthquake-resistant design of buckling-restrained braced rc moment frames using performance-based plastic design method. *Engineering Structures*, 107:66–79.

Bazaez, R. and Dusicka, P. (2016). Cyclic behavior of reinforced concrete bridge bent retrofitted with buckling restrained braces. *Engineering Structures*, 119:34–48.

Black, C. J., Makris, N., and Aiken, I. D. (2004). Component testing, seismic evaluation and characterization of buckling-restrained braces. *Journal of Structural Engineering*, 130(6):880–894.

Bouc, R. (1967). Forced vibrations of mechanical systems with hysteresis. In *Proc. of the Fourth Conference on Nonlinear Oscillations, Prague, 1967*.

Cancellara, D. and De Angelis, F. (2017). Assessment and dynamic nonlinear analysis of different base isolation systems for a multi-storey rc building irregular in plan. *Computers & Structures*, 180:74–88.

Castaldo, P., Tubaldi, E., Selvi, F., and Gioiella, L. (2021). Seismic performance of an existing rc structure retrofitted with buckling restrained braces. *Journal of Building Engineering*, 33:101688.

Chen, Q., Wang, C. L., Meng, S., and Zeng, B. (2016). Effect of the unbonding materials on the mechanic behavior of all-steel buckling-restrained braces. *Engineering Structures*, 111:478–493.

Chen, X., Ge, H., and Usami, T. (2011). Seismic demand of buckling-restrained braces installed in steel arch bridges under repeated earthquakes. *Journal of Earthquake and Tsunami*, 5(02):119–150.

Chou, C. C. and Chen, S. Y. (2010). Subassemblage tests and finite element analyses of sandwiched buckling-restrained braces. *Engineering structures*, 32(8):2108–2121.

Chuang, M. C., Tsai, K. C., Lin, P. C., and Wu, A. C. (2015). Critical limit states in seismic buckling-restrained brace and connection designs. *Earthquake Engineering & Structural Dynamics*, 44(10):1559–1579.

Constantinou, M. C., Soong, T. T., and Dargush, G. F. (1998). *Passive energy dissipation systems for structural design and retrofit*. Multidisciplinary Center for Earthquake Engineering Research Buffalo, NY.

Datta, T. K. (2010). *Seismic analysis of structures*. John Wiley & Sons.

Deb, K., Pratap, A., Agarwal, S., and Meyarivan, T. (2002). A fast and elitist multiobjective genetic algorithm: Nsga-ii. *IEEE transactions on evolutionary computation*, 6(2):182–197.

Della Corte, G., DAniello, M., and Landolfo, R. (2015). Field testing of all-steel buckling-restrained braces applied to a damaged reinforced concrete building. *Journal of structural engineering*, 141(1):D4014004.

Dizaj, E. A., Fanaie, N., and Zarifpour, A. (2018). Probabilistic seismic demand assessment of steel frames braced with reduced yielding segment buckling restrained braces. *Advances in Structural Engineering*, 21(7):1002–1020.

Eatherton, M. R., Fahnestock, L. A., and Miller, D. J. (2014). Computational study of self-centering buckling-restrained braced frame seismic performance. *Earthquake engineering & structural dynamics*, 43(13):1897–1914.

Fahnestock, L. A., Ricles, J. M., and Sause, R. (2007). Experimental evaluation of a large-scale buckling-restrained braced frame. *Journal of structural engineering*, 133(9):1205–1214.

FEMA-356 (2000). Prestandard and commentary for seismic rehabilitation of buildings. Standard, Federal Emergency Management Agency, Washington DC.

Fujimoto, M., Wada, A., Saeki, E., Watanabe, A., and Hitomi, Y. (1988). A study on the unbonded brace encased in bucking-restrained concrete and steel tube. *Journal of Str. Engineering, AIJ*, 34B:249–258.

Ghowsi, A. F. and Sahoo, D. R. (2020). Seismic response of sma-based self-centering buckling-restrained braced frames under near-fault ground motions. *Soil Dynamics and Earthquake Engineering*, 139:106397.

Ghowsi, A. F. and Sahoo, D. R. (2022). Cyclic behavior of all-steel brbs with bolted angle restrainers: Testing and numerical analysis. *Journal of Earthquake Engineering*, pages 1–27.

Guo, Y. l., Zhang, B. H., Jiang, Z. Q., and Chen, H. (2015). Critical load and application of core-separated buckling-restrained braces. *Journal of Constructional Steel Research*, 106:1–10.

Hikino, T., Okazaki, T., Kajiwara, K., and Nakashima, M. (2013). Out-of-plane stability of buckling-restrained braces placed in chevron arrangement. *Journal of Structural Engineering*, 139(11):1812–1822.

Hosseinzadeh, S. and Mohebi, B. (2016). Seismic evaluation of all-steel buckling restrained braces using finite element analysis. *Journal of Constructional Steel Research*, 119:76–84.

Hoveidae, N. and Rafezy, B. (2012). Overall buckling behavior of all-steel buckling restrained braces. *Journal of Constructional Steel Research*, 79:151–158.

Hsiao, P. C., Hayashi, K., Inamasu, H., Luo, Y. B., and Nakashima, M. (2016). Development and testing of naturally buckling steel braces. *Journal of Structural Engineering*, 142(1):04015077.

Huang, F., Duan, H., Cheng, B., and Teng, N. (2021). Hysteretic performance of all-steel assembled double-cores buckling-restrained braces using q195 low-yield core. *Journal of Constructional Steel Research*, 187:106925.

Huang, Y. and Tsai, K. (2002). Experimental responses of large scale buckling restrained brace frames. *Rep. No. CEER/R91-03, Center for Earthquake Engineering Research, National Taiwan Univ., Taiwan (in Chinese)*.

IS 1608 (2005). Metallic materials - tensile testing at ambient temperature. Indian standard, Bureau of Indian Standards, New Delhi, India.

IS 1893 (Part 1) (2016). Criteria for earthquake resistant design of structures, part 1: General provisions and buildings. Indian standard, Bureau of Indian Standards, New Delhi, India.

IS 1893 (Part I) (2002). Criteria for earthquake resistant design of structures, part 1: General provisions and buildings. Indian standard, Bureau of Indian Standards, New Delhi, India.

IS 456 (2000). Plain and reinforced concrete. Indian standard, Bureau of Indian Standards, New Delhi, India.

IS 875 (Part I) (1987). Code of practice for design loads (other than earthquake) for buildings and structures, part 1: Dead loads - unit weights of building material and stored materials. Indian standard, Bureau of Indian Standards, New Delhi, India.

IS 875 (Part II) (1987). Code of practice for design loads (other than earthquake) for buildings and structures, part 1: Dead loads - unit weights of building material and stored materials. Indian standard, Bureau of Indian Standards, New Delhi, India.

Iwata, M. (2004). Applications-design of buckling restrained braces in japan. In *13th World Conference on Earthquake Engineering*. Canadian Association for Earthquake Engineering (CAEE) Vancouver, Canada.

Jia, L. J., Ge, H., Maruyama, R., and Shinohara, K. (2017). Development of a novel high-performance all-steel fish-bone shaped buckling-restrained brace. *Engineering Structures*, 138:105–119.

Jiang, Z., Guo, Y., Zhang, B., and Zhang, X. (2015). Influence of design parameters of buckling-restrained brace on its performance. *Journal of Constructional Steel Research*, 105:139–150.

Jones, S. (2015). Nepal one month after the quake: 'the emotional impact has been devastating'.

Kasai, K. and Ito, H. (2004). Jssi manual for building passive control technology part-8 peak response evaluation and design for elasto-plastically damped system. In *13th World Conference on Earthquake Engineering*.

Kim, J. and Seo, Y. (2004). Seismic design of low-rise steel frames with buckling-restrained braces. *Engineering structures*, 26(5):543–551.

Kimura, K., Yoshioka, K., Takeda, T., Fukuya, Z., and Takemoto, K. (1976). Tests on braces encased by mortar in-filled steel tubes. In *Summaries of technical papers of annual meeting, Architectural Institute of Japan*, volume 1041, pages 1–42.

Koetaka, Y. and Kinoshita, T. (2009). Design criteria of buckling-restrained brace to prevent out-of-plane buckling. *Journal of Structural and Construction Engineering*, 74(641):1371–1378.

Lai, J. W. and Tsai, K. C. (2001). A study of buckling restrained brace frames. Technical report, Report No. CEER/R90-07, Center for Earthquake Engineering Research, National .

Li, G. Q., Sun, Y. Z., Jiang, J., Sun, F. F., and Ji, C. (2019). Experimental study on two-level yielding buckling-restrained braces. *Journal of Constructional Steel Research*, 159:260–269.

Li, H. N., Liu, Y., Li, C., and Zheng, X. W. (2020). Multihazard fragility assessment of steel-concrete composite frame structures with buckling-restrained braces subjected to combined earthquake and wind. *The Structural Design of Tall and Special Buildings*, 29(11):e1746.

Lin, P. C., Tsai, K. C., Chang, C. A., Hsiao, Y. Y., and Wu, A. C. (2016). Seismic design and testing of buckling-restrained braces with a thin profile. *Earthquake Engineering & Structural Dynamics*, 45(3):339–358.

Lin, P. C., Tsai, K. C., Wang, K. J., Yu, Y. J., Wei, C. Y., Wu, A. C., Tsai, C. Y., Lin, C. H., Chen, J. C., and Schellenberg, A. H. (2012). Seismic design and hybrid tests of a full-scale three-story buckling-restrained braced frame using welded end connections and thin profile. *Earthquake Engineering & Structural Dynamics*, 41(5):1001–1020.

Marshall, J. D. and Charney, F. A. (2010a). A hybrid passive control device for steel structures, i: Development and analysis. *Journal of Constructional Steel Research*, 66(10):1278–1286.

Marshall, J. D. and Charney, F. A. (2010b). A hybrid passive control device for steel structures, ii: Physical testing. *Journal of Constructional Steel Research*, 66(10):1287–1294.

Maurya, A., Eatherton, M. R., Matsui, R., and Florig, S. H. (2016). Experimental investigation of miniature buckling restrained braces for use as structural fuses. *Journal of Constructional Steel Research*, 127:54–65.

Mochizuki, N., Murata, Y., Andou, N., and Takahashi, S. (1980). An experimental study on buckling of unbonded braces under centrally applied loads. In *Proc., Annual Meeting of the Architectural Institute of Japan*.

Mochizuki, S., Murata, Y., Andou, N., and Takahashi, S. (1979). Experimental study on buckling of unbonded braces under axial forces: Parts 1 and 2. In *Summaries of technical papers of annual meeting. Architectural Institute of Japan*, pages 1623–1626.

Nishimoto, K., Nakata, Y., Kimura, I., Aiken, I., Yamada, S., and Wada, A. (2004). Sub-assembly testing of large buckling-restrained unbonded braces. In *13th Word Conference on Earthquake Engineering*.

Ortiz, G. A., Alvarez, D. A., and Bedoya-Ruíz, D. (2013). Identification of bouc–wen type models using multi-objective optimization algorithms. *Computers & Structures*, 114:121–132.

Pandikkadavath, M. S. and Sahoo, D. R. (2016). Experimental study on reduced-length buckling restrained braces under slow cyclic loading. *Earthquakes and Structures*, 10(3):699–716.

Pandikkadavatha, M. S. and Sahoo, D. R. (2014). Ductility demand on short-length buckling restrained braces in concentrically braced frames. *Journal of Structural Engineering*, 40(6).

Park, J., Lee, J., and Kim, J. (2012). Cyclic test of buckling restrained braces composed of square steel rods and steel tube. *Steel & Composite Structures*, 13(5):423–436.

Piedrafita, D., Cahis, X., Simon, E., and Comas, J. (2015). A new perforated core buckling restrained brace. *Engineering Structures*, 85:118–126.

Qing, Y., Wang, C.-L., Zhou, Z., and Zeng, B. (2021). Seismic responses of multistory buildings with self-centering buckling-restrained braces: Influence of the pretension force. *Engineering Structures*, 238:112249.

Qu, B., Liu, X., Hou, H., Qiu, C., and Hu, D. (2018). Testing of buckling-restrained braces with replaceable steel angle fuses. *Journal of Structural Engineering*, 144(3):04018001.

Ruiz, S. E., Santos-Santiago, M. A., Orellana, M. A., and Jiménez, R. (2019). Fragility analysis of a soft first story building rehabilitated with buckling restrained braces. In *12th Canadian Conference on Earthquake Engineering*.

SAP2000 v21.0.2 (2019). Computers and Structures Inc.

SeismoMatch (2022). Seismosoft, Earthquake Engineering Solutions.

Sireteanu, T., Giuclea, M., and Mitu, A. M. (2010). Identification of an extended bouc–wen model with application to seismic protection through hysteretic devices. *Computational Mechanics*, 45(5):431–441.

Solomon, F. and Haynes, S. (2018). A look back at asia's most devastating earthquakes.

Soong, T. T. and Dargush, G. F. (1999). Passive energy dissipation and active control. *Structural engineering handbook*, pages 1–28.

Soong, T. T. and Spencer Jr, B. F. (2002). Supplemental energy dissipation: state-of-the-art and state-of-the-practice. *Engineering structures*, 24(3):243–259.

Sun, J., Pan, P., and Wang, H. (2018). Development and experimental validation of an assembled steel double-stage yield buckling restrained brace. *Journal of Constructional Steel Research*, 145:330–340.

Tabatabaei, S. A. R., Mirghaderi, S. R., and Hosseini, A. (2014). Experimental and numerical developing of reduced length buckling-restrained braces. *Engineering Structures*, 77:143–160.

Takeda, T. and Kimura, K. (1979). Experimental study on precast concrete shear walls: Part 6. *Summaries of Technical Papers of Annual Meeting of the Archiectural Instiute of Japan Structural Engineering Section; Tokyo, Japan AU*.

Takeuchi, T., Hajjar, J. F., Matsui, R., Nishimoto, K., and Aiken, I. (2012). Effect of local buckling core plate restraint in buckling restrained braces. *Engineering Structures*, 44:304–311.

Takeuchi, T., Hajjar, J. F., Matsui, R., Nishimoto, K., and Aiken, I. D. (2010). Local buckling restraint condition for core plates in buckling restrained braces. *Journal of Constructional Steel Research*, 66(2):139–149.

Takeuchi, T., Matsui, R., and Mihara, S. (2016). Out-of-plane stability assessment of buckling-restrained braces including connections with chevron configuration. *Earthquake Engineering & Structural Dynamics*, 45(12):1895–1917.

Takeuchi, T., Ozaki, H., Matsui, R., and Sutcu, F. (2014). Out-of-plane stability of buckling-restrained braces including moment transfer capacity. *Earthquake engineering & structural dynamics*, 43(6):851–869.

Torunbalci, N. (2004). Seismic isolation and energy dissipating systems in earthquake resistant design. In *Proc. 13thWorld conference on earthquake engineering, 13WCEE, Vancouver, Canada*. Citeseer.

Tremblay, R., Bolduc, P., Neville, R., and DeVall, R. (2006). Seismic testing and performance of buckling-restrained bracing systems. *Canadian Journal of Civil Engineering*, 33(2):183–198.

Tsai, K. C., Lai, J. W., Hwang, Y. C., Lin, S. L., and Weng, C.-H. (2004). Research and application of double-core buckling restrained braces in taiwan. In *Proceeding of the 13th World Conference on Earthquake Engineering, Paper*, number 2179.

Tsai, K. C., Wu, A. C., Wei, C. Y., Lin, P. C., Chuang, M. C., and Yu, Y. J. (2014). Welded end-slot connection and debonding layers for buckling-restrained braces. *Earthquake engineering & structural dynamics*, 43(12):1785–1807.

Usami, T., Kasai, A., and Kato, M. (2003). Behavior of buckling-restrained brace members. In *Stessa 2003*, pages 211–216. Routledge.

Usami, T., Lu, Z., and Ge, H. (2005). A seismic upgrading method for steel arch bridges using buckling-restrained braces. *Earthquake engineering & structural dynamics*, 34(4-5):471–496.

Wakabayashi, M., Nakamura, T., Katagihara, A., Yogoyama, H., and Morisono, T. (1973a). Experimental study on the elastoplastic behavior of braces enclosed by precast concrete panels under horizontal cyclic loadingparts 1 & 2. In *Summaries of technical papers of annual meeting*, volume 10, pages 1041–1044. Architectural Institute of Japan.

Wakabayashi, M., Nakamura, T., Katagihara, A., Yogoyama, H., and Morisono, T. (1973b). Experimental study on the elastoplastic behavior of braces enclosed by precast concrete panels under horizontal cyclic loadingparts 1 & 2. In *Summaries of technical papers of annual meeting*, volume 6, pages 121–128. Architectural Institute of Japan.

Wang, H., Nie, X., and Pan, P. (2017). Development of a self-centering buckling restrained brace using cross-anchored pre-stressed steel strands. *Journal of Constructional Steel Research*, 138:621–632.

Wang, W. and Liu, Y. (2021). Concept and performance testing of an all-steel miniature dual stiffness damper. *Journal of Constructional Steel Research*, 183:106772.

Wang, Y., Ibarra, L., and Pantelides, C. (2016). Seismic retrofit of a three-span rc bridge with buckling-restrained braces. *Journal of Bridge Engineering*, 21(11):04016073.

Watanabe, A., Hitomi, Y., Saeki, E., Wada, A., and Fujimoto, M. (1988). Properties of brace encased in buckling-restraining concrete and steel tube. In *Proceedings of ninth world conference on earthquake engineering*, volume 4, pages 719–724.

Wen, Y.-K. (1976). Method for random vibration of hysteretic systems. *Journal of the engineering mechanics division*, 102(2):249–263.

Wigle, V. R. and Fahnestock, L. A. (2010). Buckling-restrained braced frame connection performance. *Journal of Constructional Steel Research*, 66(1):65–74.

Wilson, E. L. (1996). Three-dimensional static and dynamic analysis of structures. *Computers and Structures, Inc., Berkeley, CA*.

Wong, K. (2011). Nonlinear dynamic analysis of structures using modal superposition. In *Structures Congress 2011*, pages 770–781.

Wu, A. C., Lin, P. C., and Tsai, K. C. (2014). High-mode buckling responses of buckling-restrained brace core plates. *Earthquake engineering & structural dynamics*, 43(3):375–393.

Wu, B. and Mei, Y. (2015). Buckling mechanism of steel core of buckling-restrained braces. *Journal of Constructional Steel Research*, 107:61–69.

Wu, S., He, H., and Wang, B. (2021). Analytic expression of additional damping ratio based on bouc–wen model and performance evaluation. *The Structural Design of Tall and Special Buildings*, 30(6):e1841.

Xie, Q. (2005). State of the art of buckling-restrained braces in asia. *Journal of constructional steel research*, 61(6):727–748.

Xie, Q., Zhou, Z., and Meng, S. P. (2020). Experimental investigation of the hysteretic performance of self-centering buckling-restrained braces with friction fuses. *Engineering Structures*, 203:109865.

Yoshino, T. and Karino, Y. (1971). Experimental study on shear wall with braces: Part 2. In *Summaries of technical papers of annual meeting*, volume 11, pages 403–404. Architectural Institute of Japan.

Zhao, J., Wu, B., and Ou, J. (2011). A novel type of angle steel buckling-restrained brace: Cyclic behavior and failure mechanism. *Earthquake Engineering & Structural Dynamics*, 40(10):1083–1102.

Zhou, Z., Xie, Q., Lei, X., He, X., and Meng, S. (2015). Experimental investigation of the hysteretic performance of dual-tube self-centering buckling-restrained braces with composite tendons. *Journal of Composites for Construction*, 19(6):04015011.

Publications

List of Patents:

1. Deb, S. K., Das, P. J., (2021). Hybrid buckling restrained brace with high damping capacity and manufacturing method thereof, Application No. 202131007188 (applied for).

List of Publications:

Journal Papers:

1. Das, P. J. and Deb, S. K. (2022), Seismic performance evaluation of a new hybrid buckling restrained brace (HyBRB) under cyclic loading, *Journal of Structural Engineering*, ASCE, doi: https://doi.org/10.1061/(ASCE)ST.1943-541X.0003372
2. Das, P. J. and Deb, S. K. (2022), Experimental study on a new HyBRB with different infill layer geometries. *Engineering Structures* (under review)
3. Das, P. J. and Deb, S. K. (2022), Effect of discontinuous butyl rubber infill layers on seismic performance of HyBRB (to be communicated)

Conference Papers:

1. Das, P. J., Deb, S. K., (2018). Simplified Design of Open-core Buckling Restrained Brace for Enhancement of Damping . *16th Symposium on Earthquake Engineering, IIT Roorkee*, Paper ID: 253

2. Das, P. J., Deb, S. K., (2022). Seismic Fragility Analysis of RC Building with Open Ground Story Retrofitted using HyBRB, *Socio-Technological Aspects of Seismic Disaster and its Mitigation (STASDM), IIT Guwahati*

Appendix A

Design of HyBRB Components

A.1 General

Following geometrical and mechanical characteristics are assumed for design of the HyBRB.

1. Total length of HyBRB = 1785 mm,
2. Length of HyBRB core (elastic length + plastic length) = 1500 mm,
3. Yield stress of steel, $\sigma_y = 250$ MPa,
4. Strain hardening factor, $\Omega_h = 1.5$,
5. Compressive strength adjustment factor, $\beta = 1.1$
6. Nominal yield strength of HyBRB, $P_{ysc} = 125$ kN.

A.2 Maximum HyBRB Axial Force Capacities

The cross-sectional area of the core in yielding region (A_c) is calculated as:

$$A_c = \frac{P_{ysc}}{\sigma_y} = \frac{125 \times 10^3}{250} = 500 \text{ mm}^2$$

Maximum HyBRB compressive force capacity ($P_{\text{max\_c}}$) can be calculated as:

$$P_{\text{max\_c}} = P_y \times R_y \times \Omega_h \times \beta = 125 \times 1.3 \times 1.5 \times 1.1 = 268.2 \text{ kN}$$

The maximum HyBRB tensile force capacity can be computed from $P_{\max\_t}$:

$$P_{\max\_t} = \frac{P_{\max\_c}}{\beta} = 268.2/1.1 = 244 \text{ kN}$$

A.3 Details of HyBRB Core Zones

The HyBRB core is sub-divided into three zones: the yielding zone, the transition zone, and the joint zone. Yielding zone length (L_c) is considered as 0.667 times the HyBRB clear length. Transition zone length (L_t) on each side of HyBRB core is adopted 0.05 times the yielding zone length. Therefore,

$$L_c = 0.667 \times L_{clr} = 0.667 \times 1500 = 1000 \text{ mm}$$
$$L_t = 0.05 \times L_c = 0.05 \times 1000 = 50 \text{ mm}$$
$$L_j = (L_{clr} - L_c - 2 \times L_t)/2 = (1500 - 1000 - 2 \times 50)/2 = 200 \text{ mm}$$

Width of yielding zone is calculated as:

$$B_c = \frac{A_c}{t} = 500/10 = 50 \text{ mm}$$

Joint zone width (B_j) is assumed to be 2.2 times the width of yielding zone. And, width of transition zone (B_t) is tapered from $2.2B_c$ to B_c at both ends.

$$B_j = 2.2 \times B_c = 2.2 \times 50 = 110 \text{ mm}$$

Therefore, cross-sectional area of all zones of the steel core are:

$$A_c = 500 \text{ mm}^2$$
$$A_t = \frac{(B_c + B_j)}{2} t = \frac{(50 + 110)}{2} 10 = 800 \text{ mm}^2$$
$$A_j = B_j \times t = 110 \times 10 = 1100 \text{ mm}^2$$

A.4 Stiffener Weld Requirements

Minimum weld length (L_w) for HyBRB-to-stiffener connection is calculated as:

$$\phi_w \times 0.707 \times t_e \times (4L_w + t_j) \times 0.6 \times F_{exx} \geq P_{\max}$$
$$\Rightarrow 0.75 \times 0.707 \times 3.5 \times (4L_w + 10) \times 0.6 \times 410 \geq 268 \times 10^3$$
$$\Rightarrow L_w \geq 144 \text{ mm}$$

Provide, 2×100+10 = 210 mm long weld on each flat side of the core. Total weld length provided is 420 mm on one end BRB-to-stiffener connection.

Length of slots at each end of core = 100 mm and in stiffener = 150 mm. Total length of weld provided at one end = 2×210 = 420 mm. Considering 5 mm weld size, the capacity of weld is calculated as:

$$P_u = \frac{L_w \times t_e \times F_{uw}}{\sqrt{3} \times \gamma_{mw}} = \frac{420 \times 3.5 \times 410}{\sqrt{3} \times 1.25} = 279 \text{ kN, hence OK.}$$

For stiffened HyBRB to mid-plate (size = 200 × 200) weld design, considering weld of size 6 mm, length of weld required,

$$L_w = \frac{268 \times 1000 \times \sqrt{3} \times 1.25}{4.2 \times 410} = 337 \text{ mm}$$

Therefore provide, 6 mm weld of length 440 mm for stiffened HyBRB-mid plate weld connection on each end.

A.5 Steel Restrainer

To prevent the steel core from global buckling, the Euler buckling strength of the steel restrainer must be greater than maximum HyBRB compressive force capacity ($P_{\text{max\_c}}$). Thus, the moment of inertia of the steel restrainer must satisfy:

$$I_{sc} \geq \frac{P_{\text{max\_c}} L_{sc}^2}{\pi^2 E}$$

For peak compressive force of 268 kN, minimum combined moment of inertia of the restrainer required is 164404 mm^4.

Individual part of the restrainer is made of rectangular base steel plate of

grade Fe250 and size 1100 mm×120 mm×10 mm stiffened longitudinally with two numbers of 1100 mm×20 mm×10 mm steel plates and twelve transverse stiffeners. The combined moment of inertia of restrainer pair is 181675 mm^4.

Weld design: Maximum transverse load acting on each part of restrainer is 250 kN. Therefore single longitudinal stiffener takes 125 KN each. Taking 4 mm size weld of ultimate strength 410 MPa. Therefore, length of weld is calculated as:

$$L_w = \frac{125 \times 1000 \times \sqrt{3} \times 1.25}{2.8 \times 410} = 235 \text{ mm}$$

Provide, weld of size 4 mm throughout the length of both transverse and longitudinal stiffeners.

A.6 Bolts Details

For a target amplitude corresponding to axial strain of 3.5%, higher order buckling wave-length about weak axis is defined as:

$$L_{cw} = \sqrt{\frac{4\pi^2 (EI_w)_{\text{eff}}}{P_y}} = \sqrt{\frac{4\pi^2 \times 0.06 \times EI_w}{\sigma_y B_c t_c}} = 126 \text{ mm}$$

Force acting on the restraining members due to higher order buckling about weak axis is calculated as:

$$N_w = \frac{4s_w + 2\nu\epsilon_c t_c}{L_{cw}}.P_{\max} = \frac{4 \times 4 + 2 \times 0.5 \times 0.035 \times 10}{126}.268 = 34 \text{ kN}$$

During strong axis high mode buckling, buckling wavelength is computed as:

$$L_{cs} = \sqrt{\frac{4\pi^2 (EI_s)_{\text{eff}}}{P_y}} = \sqrt{\frac{4\pi^2 \times 0.02 \times EI_s}{\sigma_y B_c t_c}} = 363 \text{ mm}$$

Force acting on bolts due to strong axis buckling:

$$N_s = \frac{4s_s + 2\nu\epsilon_c B_c}{L_{cs}}.P_{\max} = \frac{4 \times 9 + 2 \times 0.5 \times 0.035 \times 50}{363}.268 = 28 \text{ kN}$$

So, per unit local wave length, bolts must have a minimum tensile strength of 34 kN as well as shear strength of 28 kN. The force calculated above is per

unit buckling wavelength. So for whole length of yielding section, total tensile and shear force is calculated to e 269 kN and 77 kN. Accordingly a total of 30 number of bolts of grade 4.6 is considered for restrainer connection.

A.7 Connection Design

Stiffened HyBRB ends are welded to two 12 mm thick steel plates. Now, two pin strips of thickness 12 mm from each HyBRB end and connector end is adopted to make the pinned connection on both sides. The maximum force calculated, is to be shared by these two strips. Design shear strength of pin strip is calculated considering a safety factor of 2.

Shear strength of each pin strip,

$$V_j = \frac{\sigma_y}{\sqrt{3}} = 145 \text{ MPa}$$

Design shear strength = 145/2 = 72.5 MPa

For a maximum load capacity 400 kN (assumed for conservative design), gross shear area is calculated as:

$$\frac{400 \times 1000}{72.5} = 5517 \ mm^2$$

Dimension of pin strip plate considered as 130×120×12

For the proposed double bolted joint on each end, high strength friction grip bolts (grade 8.8) of diameter 24 mm and length 75 mm are considered. Bolt hole diameter is 26 mm.

Shear capacity of single bolt = 131 kN.

Slip resistance for 1 bolt in single shear is computed as:

$$R = \frac{\mu_f \times K_h \times n_e \times F_0}{\gamma_{mf}}$$

where, $\mu_f = 0.48$

$K_h = 1$

$n_e = 1$

$F_0 = A_{nb} \times 0.7 \times f_{ub}$

$f_{ub} = 800$ MPa

Slip resistance, R = $\frac{0.48 \times 1 \times 1 \times 353 \times 0.7 \times 800}{1.25} = 75.9$ kN

Total strength of joint in single shear = $2 \times 131 + 2 \times 75.9 = 414$ kN

Dimensions of the base plates of connectors 1 & 2 (to connect HyBRB ends with strong floor and actuator) are determined on the basis of strong floor arrangement and actuator swivel head specifications respectively.

Dimensions of the base plate of connectors 1 (strong floor end) = 650 × 650 × 36. Base plate is stiffened in both longitudinal and transverse direction to avoid any damage. Dimensions of the base plate of connectors 2 (actuator end) = 400 × 400 × 25.

Pin to base plate Weld:

Two pin-strip plates together takes maximum axial load. So each one carries 134 kN. Assuming 8 mm size weld, length of weld required:

$$L_w = \frac{134 \times 1000 \times \sqrt{3} \times 1.25}{5.6 \times 410} = 126 \text{ mm}$$

Provide, 240 mm long weld of size 8 mm on both side of 12 mm plate.

Base plate to stiffener weld (Connector 1):

For weld size = 5 mm and maximum load = 268 kN,

Length of weld required,

$$L_w = \frac{268 \times 1000 \times \sqrt{3} \times 1.25}{3.5 \times 410} = 404 \text{ mm}$$

Provide, 5 mm size weld throughout the stiffener length placed along both directions.

A.8 Checks

Following are the results of mandatory checks that are done in order to ensure the stability of the welded and bolted connections:

- For joint connection, considering the bolts strength, bearing strength of plates and bearing strength of bolts, the capacity of the joint is found to be 273 kN.
- Weld strength of connectors is 382 kN.

- Weld strength of mid plate connection section is 292 kN.
- Weld strength for core-stiffener connection is 279 kN.

Appendix B

Details of Design Parameters and Prescribed Ground Motions

B.1 Design Parameters

The step-by step procedure for retrofit design of the sample soft-story building is provided in Chapter 7. Details of design parameters of HyBRBs for retrofitting of the sample building are furnished in the Table B.1.

Table B.1: Details of design parameters

Parameters	**Value**
Yield stress of steel	255 MPa
Young's modulus	210000 MPa
Height of ground floor	4 m
Bay width	5.4 m
	6.3 m
Design drift at ground story	0.0112
Design yield drift at ground story	0.0019
Design ductility demand	5.87
Response reduction factor	4.16

B.2 Details of Prescribed Ground Motions

A set of eighty earthquake data are obtained from PEER-NGA ground motion data base for nonlinear dynamic analysis of the sample soft-story building, before

and after retrofitting. The ground motion data are divided in four categories based on their characteristics, as mentioned in Section 7.8.2. The details of prescribed earthquake data of different categories are presented in the following tables.

Table B.2: Details of ground motion records of category LM-SD

RSN	**Earthquake**	**Year**	**Magnitude**	**Distance (km)**	**PGA (g)**
57	San Fernando	1971	6.6	30.62	0.167
77	San Fernando	1971	6.6	6.72	0.688
139	Tabas, Iran	1978	7.4	27.48	0.191
143	Tabas, Iran	1978	7.4	21.13	0.642
159	Imperial Valley-06	1979	6.5	7.82	0.473
184	Imperial Valley-06	1979	6.5	13.34	0.770
729	Superstition Hills-02	1987	6.5	26.78	0.402
740	Loma Prieta	1989	6.9	28.64	0.053
741	Loma Prieta	1989	6.9	17.46	0.506
752	Loma Prieta	1989	6.9	20.11	0.556
753	Loma Prieta	1989	6.9	13.68	0.458
825	Cape Mendocino	1992	7.0	11.61	0.739
829	Cape Mendocino	1992	7.0	25.1	0.196
949	Northridge-01	1994	6.7	16.88	0.552
952	Northridge-01	1994	6.7	25.58	0.326
963	Northridge-01	1994	6.7	34.16	0.217
1107	Kobe, Japan	1995	6.9	31.8	0.171
1111	Kobe, Japan	1995	6.9	18.59	0.387
1119	Kobe, Japan	1995	6.9	11.16	0.427
1120	Kobe, Japan	1995	6.9	11.88	0.284

Table B.3: Details of ground motion records of category LM-LD

RSN	Earthquake	Year	Magnitude	Distance (km)	PGA (g)
12	Kern County	1952	7.4	124.34	0.021
40	Borrego Mtn	1968	6.6	141.6	0.039
56	San Fernando	1971	6.6	73.62	0.044
163	Imperial Valley-06	1979	6.5	40.49	0.056
169	Imperial Valley-06	1979	6.5	40.51	0.142
186	Imperial Valley-06	1979	6.5	53.81	0.034
188	Imperial Valley-06	1979	6.5	42.71	0.026
283	Irpinia, Italy-01	1980	6.9	73.2	0.022
287	Irpinia, Italy-01	1980	6.9	54.32	0.029
288	Irpinia, Italy-01	1980	6.9	41.13	0.203
291	Irpinia, Italy-01	1980	6.9	35.56	0.070
733	Loma Prieta	1989	6.9	69.4	0.096
737	Loma Prieta	1989	6.9	39.18	0.094
744	Loma Prieta	1989	6.9	69.24	0.093
759	Loma Prieta	1989	6.9	62.17	0.109
830	Cape Mendocino	1992	7.0	38.95	0.054
850	Landers	1992	7.3	47.34	0.167
902	Big Bear-01	1992	6.5	42.15	0.120
928	Big Bear-01	1992	6.5	71.65	0.182
968	Northridge-01	1994	6.7	54.99	0.132

Table B.4: Details of ground motion records of category SM-SD

RSN	Earthquake	Year	Magnitude	Distance (km)	PGA (g)
30	Parkfield	1966	6.2	17.72	0.146
95	Managua, Nicaragua-01	1972	6.2	8.33	0.307
149	Coyote Lake	1979	5.7	9.19	0.422
230	Mammoth Lakes-01	1980	6.1	8.23	0.387
232	Mammoth Lakes-01	1980	6.1	9.21	0.250
235	Mammoth Lakes-02	1980	5.7	12.68	0.265
240	Mammoth Lakes-04	1980	5.7	6.58	0.333
250	Mammoth Lakes-06	1980	5.9	19.06	0.313
265	Victoria, Mexico	1980	6.3	26.84	0.293
300	Irpinia, Italy-02	1980	6.2	11.94	0.158
317	Westmorland	1981	5.9	10.72	0.232
319	Westmorland	1981	5.9	8.82	0.812
373	Coalinga-02	1983	5.1	12.59	0.366
407	Coalinga-05	1983	5.8	8.94	0.503
485	Bishop (Rnd Val)	1984	5.8	23.49	0.107
498	Hollister-04	1986	5.5	15.83	0.105
514	N. Palm Springs	1986	6.1	17.21	0.359
516	N. Palm Springs	1986	6.1	34.68	0.125
547	Chalfant Valley-01	1986	5.8	10.12	0.201
549	Chalfant Valley-02	1986	6.2	22.63	0.145

Table B.5: Details of ground motion records of category SM-LD

RSN	Earthquake	Year	Magnitude	Distance (km)	PGA (g)
246	Mammoth Lakes-06	1980	5.9	48.17	0.065
268	Victoria, Mexico	1980	6.3	52.77	0.047
299	Irpinia, Italy-02	1980	6.2	49.01	0.027
324	Coalinga-01	1983	6.4	52.06	0.060
338	Coalinga-01	1983	6.4	36.03	0.098
339	Coalinga-01	1983	6.4	35.51	0.083
345	Coalinga-01	1983	6.4	38.58	0.056
449	Morgan Hill	1984	6.2	40.85	0.045
463	Morgan Hill	1984	6.2	38.26	0.213
465	Morgan Hill	1984	6.2	38.26	0.283
519	N. Palm Springs	1986	6.1	43.87	0.096
522	N. Palm Springs	1986	6.1	46.26	0.091
534	N. Palm Springs	1986	6.1	32.21	0.209
536	N. Palm Springs	1986	6.1	48.08	0.049
593	Whittier Narrows-01	1987	6.0	41.18	0.085
597	Whittier Narrows-01	1987	6.0	37.46	0.043
605	Whittier Narrows-01	1987	6.0	52.76	0.104
1742	Little Skull Mtn,NV	1992	5.7	48.63	0.034
1927	Anza-02	2001	4.9	39.15	0.041
1936	Anza-02	2001	4.9	55.74	0.061